

2019-01-01

## Exploration And Optimization Of Biomaterials And Cells Required For The Fabrication Of A "Cardiac Patch"

Shweta Anil Kumar  
*University of Texas at El Paso*

Follow this and additional works at: [https://digitalcommons.utep.edu/open\\_etd](https://digitalcommons.utep.edu/open_etd)



Part of the [Materials Science and Engineering Commons](#), and the [Mechanics of Materials Commons](#)

---

### Recommended Citation

Anil Kumar, Shweta, "Exploration And Optimization Of Biomaterials And Cells Required For The Fabrication Of A "Cardiac Patch"" (2019). *Open Access Theses & Dissertations*. 2826.  
[https://digitalcommons.utep.edu/open\\_etd/2826](https://digitalcommons.utep.edu/open_etd/2826)

This is brought to you for free and open access by ScholarWorks@UTEP. It has been accepted for inclusion in Open Access Theses & Dissertations by an authorized administrator of ScholarWorks@UTEP. For more information, please contact [lweber@utep.edu](mailto:lweber@utep.edu).

EXPLORATION AND OPTIMIZATION OF BIOMATERIALS AND CELLS  
REQUIRED FOR THE FABRICATION OF A “CARDIAC PATCH”

SHWETA ANIL KUMAR

Doctoral Program in Materials Science and Engineering

APPROVED:

---

Binata Joddar, Ph.D., Chair

---

David Roberson, Ph.D.

---

Katja Michael, Ph.D.

---

Munmun Chattopadhyay, Ph.D.

---

Stephen L. Crites, Jr., Ph.D.  
Dean of the Graduate School

Copyright ©

by

Shweta Anil Kumar

2019

## **Dedication**

I humbly dedicate this dissertation to my parents and my grandmother for their countless sacrifices and prayers that gave me strength and kept me going even when the odds were stacked against me.

EXPLORATION AND OPTIMIZATION OF BIOMATERIALS AND CELLS  
REQUIRED FOR THE FABRICATION OF A “CARDIAC PATCH”

by

SHWETA ANIL KUMAR, B.Tech

DISSERTATION

Presented to the Faculty of the Graduate School at

The University of Texas at El Paso

in Partial Fulfillment

of the Requirements

for the Degree of

DOCTOR OF PHILOSOPHY

Department of Metallurgical, Materials and Biomedical Engineering

THE UNIVERSITY OF TEXAS AT EL PASO

December 2019

## **Acknowledgements**

Firstly, I would like to express my heartfelt gratitude to my advisor, Dr. Binata Joddar for her infinite patience, unwavering support and constructive criticism that helped me grow, both academically and professionally. I am profoundly grateful to my dissertation committee members, Dr. Munmun Chattopadhyay for her guidance with the experimental work, Dr. Katja Michael for her invaluable suggestions and Dr. David Roberson, for his sincere guidance. I am also indebted to Vikram Thakur for his time and assistance with experiments conducted at Texas Tech University.

I would like to express my sincere thanks to all the past and present members of my research group from the Inspired Materials and Stem Cell based Tissue Engineering Laboratory (IMSTEL) at the University of Texas at El Paso. Their suggestions and inputs have been very helpful in making me achieve my research goals.

I cannot thank our collaborators enough for their prompt response every time I needed their help. I am deeply obliged to the funding sources, facilities and the undoubted support of the faculty, staff and students in the department of Metallurgical, Materials and Biomedical Engineering at the University of Texas at El Paso without whom this would not have been possible.

Last but not the least, I am eternally grateful to my parents who have been my support system during the course of my PhD. None of this would have been possible without their sacrifices and prayers that gave me the strength and the will to keep going till the very end .

## **Abstract**

Cardiac failure induced by myocardial infarction is believed to be one of the primary causes of morbidity and mortality all over the world. Affecting more than 26 million people worldwide, its prevalence has been observed to increase steadily. Myocardial infarction, which initially begins as the occlusion of a coronary artery, results in the death of millions of cardiomyocytes by obstructing blood flow to the serviced regions of the myocardium. The dead myocardium is replaced by a dense, collagenous scar which reduces the contractility of the heart, gradually leading to heart attacks. Most of the existing treatment therapies are palliative in nature and while slowing down the progression of the disease, have not been successful in regenerating the cardiac tissue that has sustained injury following myocardial infarction primarily due to the limited regenerative ability of the cardiac cells. This has become a major cause of concern and has prompted researchers and scientists all over the world to investigate other forms of treatment such as stem cell therapy and tissue engineering to reverse the effects of myocardial infarction-induced cardiac cell death in an effort to restore the functional ability of the heart.

This dissertation explores the feasibility of tissue engineering “cardiac patches” via extrusion based 3D bioprinting technology by combining biomaterials, cells and other soluble factors. This study is novel since we employed furfuryl-gelatin, which is a visible light crosslinkable derivative of porcine gelatin, as the base material for our bioink in tandem with fibrinogen to generate cardiomyocyte-laden scaffolds which exhibited high cell viability and retention, in addition to possessing mechanical properties resembling those of the native myocardium. The outcomes of our experiments show that there is great promise in adopting the fibrin-gelatin based bioinks, specifically for the fabrication of cardiac tissues, and can potentially open up new avenues in the field of regenerative medicine if adopted into clinical trials.

# Table of Contents

Acknowledgements.....	v
Abstract.....	v
Table of Contents.....	viii
List of Tables.....	xi
List of Figures.....	xiii
Chapter 1: Introduction.....	1
1.1 Central Hypothesis, Rationale and Specific Aims.....	6
Chapter 2: Background and Overview.....	9
2.1 The clinical concern caused by cardiac failure.....	9
2.2 The pathophysiology of cardiac failure.....	10
2.3 Current treatment approaches for cardiac failure.....	11
2.4 Stem cell therapy as a treatment strategy.....	12
2.5 Drawbacks of existing stem cell therapy.....	14
2.6 Tissue engineering as an alternative treatment strategy.....	15
Chapter 3: Materials and methods.....	18
3.1 Materials.....	18
3.1.1 Preparation of f-gelatin and its characterization by NMR Spectroscopy.....	18
3.1.1.1 Biocompatibility of f-gelatin.....	20
3.1.1.2 Visible light induced crosslinking of f-gelatin.....	21
3.1.2 Preparation of Fibrinogen.....	22
3.2 Methods.....	22
3.2.1 3D Bioprinting.....	22
3.2.2 Material Characterization.....	25
3.2.2.1 Scanning Electron Microscopy (SEM).....	25
3.2.2.2 Rheology.....	26
3.2.2.3 Fourier Transform Infrared Spectroscopy (FTIR).....	27
3.2.2.4 Swelling and Degradation.....	28
3.2.2.5 Statistical Analysis.....	28



Chapter 4: Development of a novel, visible light crosslinkable f-gelatin based hydrogel for tissue engineering applications .....	29
4.1 Introduction.....	29
4.2 Biofabrication .....	31
4.3 Cell culture, characterization and viability within the printed constructs .....	33
4.3.1 Flow Cytometry (FACS).....	36
4.4 Results .....	36
4.4.1. Material Characterization.....	36
4.4.1.1 Gross morphology and Scanning Electron Microscopy (SEM) .....	36
4.4.1.2 Rheology.....	37
4.4.1.3 Fourier Transform Infrared Spectroscopy (FTIR) .....	38
4.4.1.4 Swelling and Degradation.....	39
4.4.2 Biocompatibility .....	40
4.4.2.1. Flow Cytometry (FACS).....	43
4.5 Conclusion .....	44
Chapter 5: Comparison study to understand the effect of 3D printed scaffold design on tissue engineering.....	45
5.1 Introduction.....	45
5.2 Biofabrication .....	47
5.3 Cell culture, characterization and viability within the printed constructs .....	47
5.3.1 Live/ Dead cytotoxicity assay .....	48
5.3.2 Cell Proliferation.....	49
5.3.2.1 Flow Cytometry (FACS).....	49
5.4 Results .....	50
5.4.1. Material Characterization.....	50
5.4.1.1 Gross morphology and Scanning Electron Microscopy (SEM) .....	49
5.4.1.2 Rheology.....	53
5.4.1.3 Swelling and Degradation.....	54
5.4.2 Biocompatibility .....	56
5.4.2.1. Flow Cytometry (FACS).....	57
5.5 Conclusion .....	59

Chapter 6: Development of a fibrin –gelatin based bioink for the fabrication of “cardiac patches” .....	60
6.1 Introduction.....	60
6.2 Biofabrication .....	61
6.3 Cell culture, characterization and viability within the printed constructs .....	63
6.3.1 Live/ Dead cytotoxicity assay .....	63
6.3.2 Cell viability and orientation within the printed constructs.....	64
6.4 Results .....	65
6.4.1. Material Characterization.....	65
6.4.1.1 Gross morphology and Scanning Electron Microscopy (SEM) .....	66
6.4.1.2 Rheology .....	68
6.4.1.3 Fourier Transform Infrared Spectroscopy (FTIR) .....	69
6.4.1.4 Swelling and Degradation.....	70
6.4.2 Biocompatibility .....	71
6.4.2.1 Live/Dead Toxicity assay .....	71
Chapter 7: Comparison study between f-gelatin- and PEGDA- alginate based bioink systems ...	75
7.1 Introduction.....	75
7.2 Biofabrication .....	75
7.3 Results .....	76
7.3.1 Material Characterization.....	76
7.3.1.1 Gross morphology and Scanning Electron Microscopy (SEM) .....	76
7.3.1.2 Rheology .....	77
7.3.1.3 Biocompatibility .....	77
Chapter 8: Summary and conclusion .....	78
8.1 Cardiac Failure.....	78
8.2 Development of f-gelatin based bioink.....	79
8.3 Significance of scaffold design in tissue engineering .....	80
8.4. Incorporation of fibrin into f-gelatin based bioinks to fabricate cardiac patches .....	80
8.5 Conclusion .....	81

Bibliography .....	83
Appendix.....	102
Vita.....	110

## List of Tables

Table 1.1: Biomaterials in the U.S. Healthcare Market .....	4
Table 3.1: Comparison between inkjet-, extrusion- and laser-based 3D bioprinting .....	24
Table 4.1: Printing parameters used for the f-gelatin based bioink .....	33
Table 6.1: Optimization of the fibrin-gelatin based bioink.....	62

## List of Figures

Figure 1.1: Applications of material science and engineering in the present day .....	2
Figure 1.2: Applications of biomaterials as various implants within the body .....	3
Figure 1.3: A schematic representing how tissue engineering can be employed to replace the diseased myocardial tissue.....	8
Figure 2.1: Mortality resulting from various diseases worldwide,led by ischemic heart disease and stroke.....	9
Figure 2.2: One-year survival of patients after diagnosis of heart failure .....	10
Figure 3.1: NMR spectrum of f-gelatin .....	19
Figure 3.2: Scheme for visible light crosslinking of f-gelatin .....	19
Figure 3.3: Viability of 3T3-L1 fibroblast cells treated with f-gelatin was measured by means of an MTT assay.....	21
Figure 3.4: The three types of 3D bioprinting approaches .....	24
Figure 3.4: Rheological relationship between storage modulus ( $G'$ ), loss modulus ( $G''$ ) and loss factor ( $\tan\delta$ ).....	26
Figure 4.1: (A) Bioink (no cells) showing a viscous mixture prior to crosslinking.(B) Pre- (left) and post-crosslinked (right) hydrogel (sheet) (C) Versatility of patterns being printed (ring: left and sheet: right) (D) Double layered sheet printing feasibility (en-face: top and cross-section: bottom). In B, C and D, yellow corresponds to RF and pink to RB.Scale bar in all images corresponds to 2 cm .....	34
Figure 4.2: Representative image acquired using SEM of a printed sheet sample of f-gelatin after crosslinking.....	37

Figure 4.3: Rheology analysis of f-gelatin based hydrogels. Shown is a characteristic dataset obtained from a disc (8 mm) punched out from a printed crosslinked f-gelatin hydrogel sample. .... 38

Figure 4.4: (A) FTIR spectrum of crosslinked f-gelatin in the presence of RB and HA. (B) FTIR spectra of f-gelatin and (C) of HA respectively..... 39

Figure 4.5: Degree of swelling of a printed sheet sample of f-gelatin after crosslinking..... 40

Figure 4.6: (A) Viability of the mouse MSC stained with Hoechst (blue), post printing after 24 hr being demonstrated. (B) Retention of mouse MSC, pre-stained with PKH67 (green), within the bioprinted construct after 5 days of culture. .... 41

Figure 4.7: In A and B, shown are bright field z-scans of STO fibroblasts (elongated spindle shaped) co-cultured with C2C12 myoblasts cells (rounded enlarged, confirmed in C and in E). Scale bar is 150  $\mu\text{m}$  in A, B and 200  $\mu\text{m}$  in C and E. In C, a single plane (cross section) was imaged whereas in E, a Z-scan was run spanning several planes as indicated with the arrow (right hand side). In D, shown is a single slice of z-stack section showing top layer (fluorescent green: C2C12) and bottom layer (non-fluorescent: STO)..... 42

Figure 4.8: FACS analysis to show cell proliferation and biocompatibility of the printed sheet structures of f-gelatin after crosslinking. Cells pre-stained with cell trace violet (CTV) were cultured upto (A) 24 hr and (B) 72 hr within printed constructs. The positive controls for 24 hr and 72 hr are depicted by (C) and (D)..... 44

Figure 5.1: Gross Morphology of lattice and rectangular-sheet structures printed using pluronic and gelatin. (AI, BI) depict the stl. file image for the lattice and rectangular structures, respectively. (AII, BII) represent the en-face images for the same structures printed using Pluronic F-127. (AIII,

BIII) are representations of the en-face images for lattice and rectangular patterns printed using the f-gelatin-based bioink, respectively. .... 50

Figure 5.2: Representative SEM surface images of lattice and rectangular-sheet structures deposited using pluronic and gelatin. (AI, II) show the en-face images for the lattice structures printed with Pluronic-F127 and the f-gelatin-based bioink, respectively. (BI, II) depict the en face images for the rectangular structures printed using the same materials, respectively. .... 51

Figure 5.3: A representative SEM cross-section image of a gelatin lattice structure that was acquired in order to determine the apparent porosity and average pore size (A). The cross-sectional SEM image for the rectangular-sheet structure printed using f-gelatin was previously reported (B). The scale bars represent 5  $\mu\text{m}$  and 500  $\mu\text{m}$  in A and B respectively..... 52

Figure 5.4: Rheology analysis of f-gelatin-based lattice structures obtained from a disc-shaped (8 mm) sample..... 53

Figure 5.5: (A) Swelling analysis for both the f-gelatin-based lattice and rectangular-sheets over a period of three days after being subjected to visible light crosslinking. (B) Shown above in (BI, II) is cell-laden lattice constructs. In (BIII, IV) is cell-laden rectangular-sheet constructs. (BI, III) was acquired after 24 hr of culture. (BII, IV) was acquired after 72 hr of culture. No significant differences in the degradation rates of both structures were evident at 72 hr of incubation. .... 55

Figure 5.6: Live/Dead assay performed 15 min after printing and crosslinking. Shown in (A) are Calcein AM stained live cells and in (B) are Ethidium homodimer stained dead cells, respectively. In (C), a phase-contrast image of cells cultured for this experiment is shown. .... 56

Figure 5.7: Shown in (A, B) are characteristic images of mouse MSC printed in lattice structures. Elongated cell morphologies and the extensive coverage area by the cells both confirm the

biocompatibility of the lattice design and the bioink used. White arrows point to the extracellular matrix deposited by the cells cultured. .... 57

Figure 5.8: FACS analysis to show cell proliferation and biocompatibility of the printed and crosslinked lattice and rectangular-sheet structures, respectively. Cells pre-stained with CTV were cultured up to 24- and 72- hr within printed constructs, respectively. Gated X-A mean values indicate the average intensity of the dye exhibited during that particular sample run. .... 58

Figure 6.1:Gross Morphology of the structure printed using the fibrin-gelatin based bioink. (A) Depicts a representative SEM en face image of a characteristic 3D printed pattern. (B) Depicts bioprinted herringbone construct ..... 66

Figure 6.2: SEM analysis for pore size estimation. (A) A representative SEM image of the edge of a characteristic fibrin-gelatin film. At least 5 representative images were acquired per sample and used to determine the average pore size depicted in (C), in comparison with the f-gelatin structures as depicted in (B). (C) Depicts a plot comparing the average pore diameters for the fibrin-gelatin (current study) and f-gelatin (gel-fu) based constructs. In (A) scale bar corresponds to 50  $\mu\text{m}$  and in (B) corresponds to 20  $\mu\text{m}$ . .... 67

Figure 6.3: Rheology analysis of fibrin-gelatin based square structures. (A) Representative storage-, loss-moduli and complex viscosity from one characteristic gel-sample. Therefore, it does not have error bars. Shown in inset (B) is the average storage and loss moduli for similar sample patterns (#1 and #2, n=2) analyzed during rheological characterization..... 68

Figure 6.4: FTIR spectra for the fibrin-gelatin based sample. .... 70

Figure 6.5: Swelling behavior of the fibrin-gelatin based hydrogel samples with respect to the f-gelatin samples used in a previous study ..... 71



Figure 6.6: Cell retention, viability and proliferation. (A) Shows characteristic images of human CM cell lines, that were bioprinted within fibrin-gelatin patterns and imaged using Live (Green)/Dead (Red) assay, and (B) quantification of cell viability estimated by Live-Dead assay after 5 days of culture. Statistically significant differences are denoted by  $*(p<0.05)$  ..... 72

Figure 6.7: (A) Characteristic image of human CM cell lines stained with Troponin I antibody (red) and DAPI (blue) after 5 days of culture. (B) PKH26 (red) prestained cells bioprinted using a herringbone design were seen to align along this pattern after 24 hr of culture, in a maximum intensity projection of a Z-stack of confocal microscope images.(C) Extent of cell proliferation in both 3D gels and 2D controls after 5 days of culture is depicted ..... 72

Figure 7.1: En face SEM image of the crosslinked PEGDA-alginate printed sample ..... 76

Figure 7.2: A representative confocal microscopy image obtained after Live/Dead assay performed on human CM cell lines encapsulated within casted PEGDA based gels 24 hr following cell culture ..... 78

Appendix A.1.1: Retention of cells in mono- and bi-layered f-gelatin printed constructs ..... 102

Appendix A.1.2: Confocal microscopy to observe the cellular crosstalk between STO (bottom layer) and C2C12 (top layer) cells in the f-gelatin based bi-layered sheets ..... 102

Appendix A.1.3: FACS analysis on CTV stained cells culture on plastic for 24- and 72- hr .... 103

Appendix A.1.4: (A) Bright-field images of cells cultured in TCPS (Control) or in the presence of Rose Bengal (+RB) at days 1, 3 and 5. (B) Confirmation of cell viability after addition of Rose Bengal using (continued from the previous page) Calcein AM, which only stains for viable cells after 24 hr of in vitro culture. (C) Absorbance assay conducted at days 1, 3 and 5 depict an increase in cell growth while viability was also maintained across samples at different time points. .... 104

Appendix A.1.5: FTIR spectra for controls ..... 105

Appendix A.1.6: Live/Dead and Troponin-T/DAPI staining of human iPS-CM bioprinted within fibrin-gelatin patterns.....	106
Appendix A.1.6: Live/Dead and Troponin-T/DAPI staining of human CM cell lines cultured in tissue culture wells and images as controls.....	107
Appendix A.2.1: Image permits for Chapter 4 .....	108
Appendix A.2.2: Image Permits for Chapter 5 .....	109
Appendix A.2.2: Image Permits for Chapter 6 .....	109

## Chapter 1: Introduction

Materials science, the study of the properties of materials and their applications to various areas of science and engineering (Figure 1.1), has been a topic of great fascination for scientists and researchers all over the world since the 1940s. Most of the pressing scientific problems around the world are due to the limits of materials that are available and the manner in which they are used. For the same reason, breakthroughs in the field of material science can significantly alter the future of technology. Material scientists endeavor to understand how the processing of a material can affect its structure and thus, influence its properties and performance. The knowledge of the processing-structure-properties-performance relationship is known as the “*Materials Paradigm*”. Although the knowledge of the Materials Paradigm has been extensively used to acquire a deeper understanding in various areas of research such as metallurgy and nanotechnology, its impact on the field of biomaterial research for applications in regenerative medicine and medical therapeutics has been astounding. The need for improved medicine for the amelioration, correction, and prevention of dysfunction in health does not seem likely to ever disappear [1]. The field of biomaterial research encompasses two closely related areas of interest, namely the application of engineering principles to understand how living organisms function and utilization of engineering technologies for designing and developing diagnostic or therapeutic instruments or for formulating novel biomaterials for medical applications [2] in the form of prosthetic implants or tissue engineering scaffolds for the replacing damaged or diseased hard and soft tissues within the body (Figure 1.2) respectively or for developing high fidelity models to study disease morphology and progression, and for drug screening and cytotoxicity tests. Some of the important criteria that govern the selection of biomaterials include host response, biocompatibility, biofunctionality, toxicology, appropriate design and manufacturability, functional tissue structure and pathobiology, mechanical properties, high corrosion and wear resistance [3].

Many notable advances and breakthroughs in the healthcare industry have been made possible by biomaterials research. Some of the healthcare areas in which biomaterials have been successfully employed primarily for cardiovascular and orthopedic applications, besides other fields such as dentistry, plastic medical procedures, wound repair, ophthalmology and neurology. Additionally, they have also been extensively utilized in advanced healthcare technologies such as cosmetic surgeries, tissue engineering, medical implants and advanced drug delivery. The largest share in biomaterials in the global market has been held by North America since 2017, from a geographical standpoint (Table 1.1). This growth maybe an outcome of various technological and mechanical progressions, high utility of medical services, growing geriatric population, and higher medical insurance coverage.

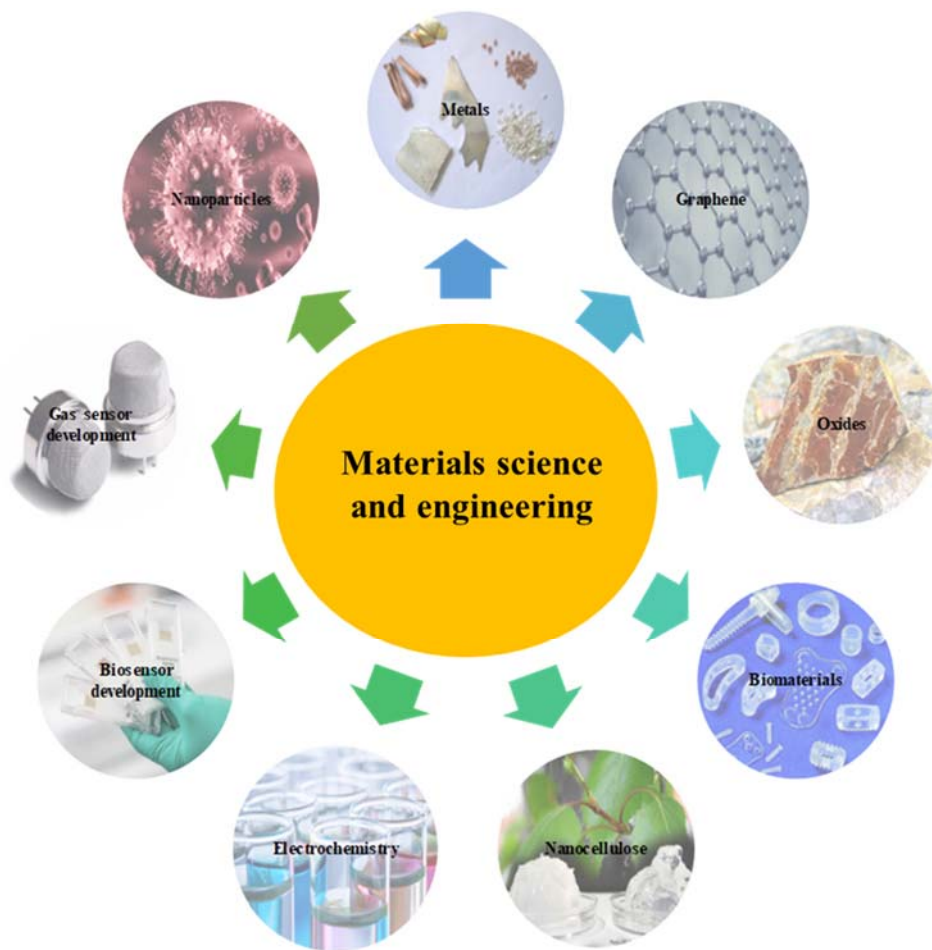


Figure 1.1: Applications of materials science and engineering in the present day

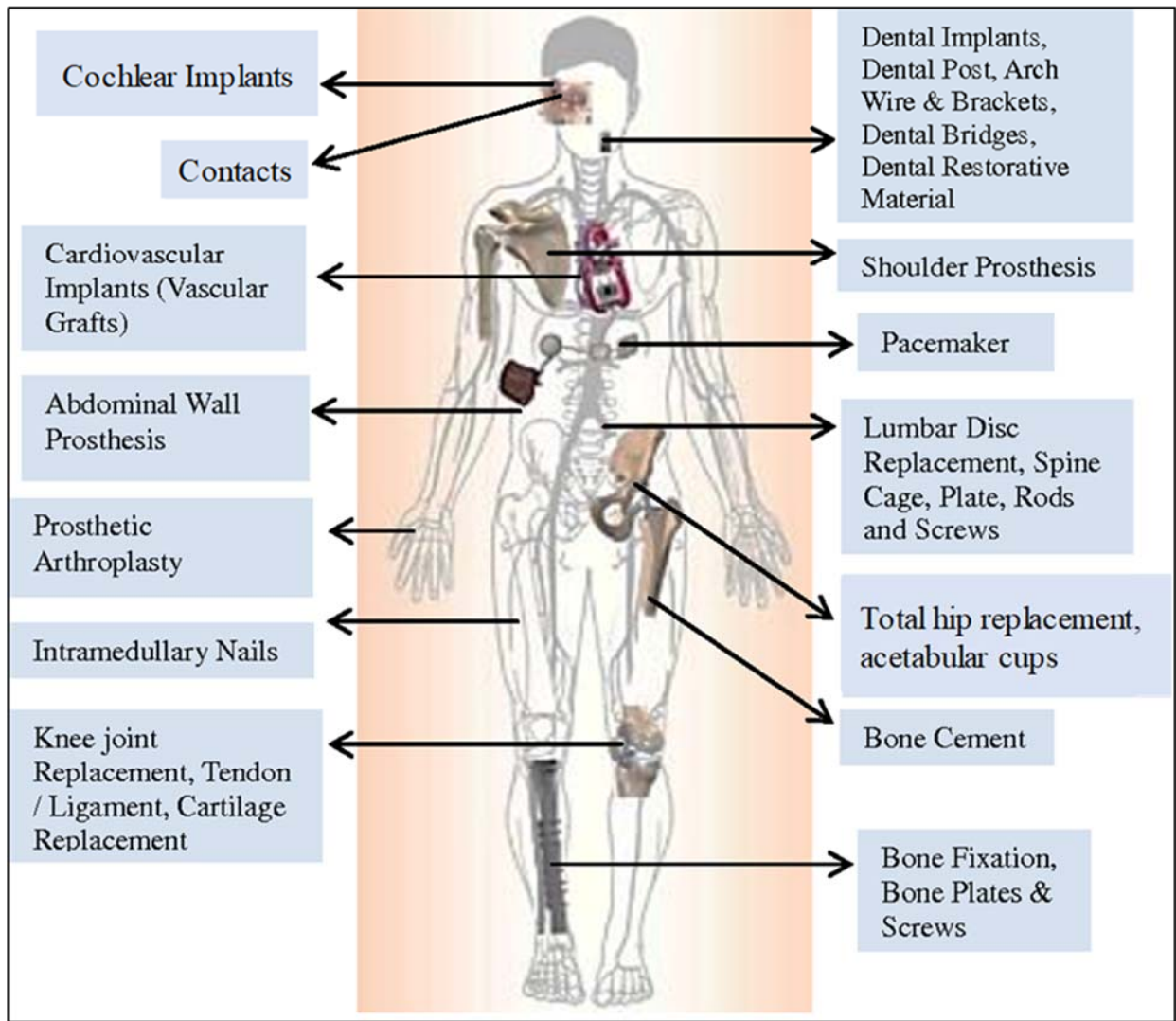


Figure 1.2: Applications of biomaterials as various implants within the body [3]

Table 1.1: Biomaterials in the U.S. Healthcare Market [4]

Total U.S. healthcare expenditure (2000)	\$ 1,400,000,000,000
Total U.S. health research and development (2001)	\$ 82,000,000,000
Number of employees in the medical device industry (2003)	300,000
Registered U.S. medical device manufacturers (2003)	13,000
Total U.S. medical device market (2002)	\$ 77,000,000,000
U.S. market for disposable medical supplies (2003)	\$ 48,600,000,000
U.S. market for biomaterials (2000)	\$ 9,000,000,000
Individual medical device sales:	
Diabetes management products (1999)	\$ 4,000,000,000
Cardiovascular devices (2002)	\$ 6,000,000,000
Orthopedic-muskoloskeletal surgery US market (1998)	\$ 4,700,000,000
Wound care U.S. market (1998)	\$ 3,700,000,000
In vitro diagnostics (1998)	\$ 10,000,000,000
Number of devices (U.S.):	
Intraocular devices (2003)	2,500,000
Contact lenses (2000)	30,000,000
Vascular grafts	300,000
Heart valves	100,000
Pacemakers	400,000
Blood bags	40,000,000
Breast prostheses	250,000
Catheters	200,000,000
Heart-lung (Oxygenators)	300,000
Coronoary stents	1,500,000
Renal dialysis (number of patients,2001)	320,000
Hip prostheses (2002)	250,000
Knee prostheses (2002)	250,000
Dental implants (2000)	910,000

The past few decades have witnessed an increased incidence of cardiac failure-related deaths all over the world. Although there are numerous factors that have been found to be responsible for cardiac failure, myocardial infarction has been hailed as the primary reason for inducing cardiac failure leading to coronary thrombosis [5]. A myocardial infarction begins with the occlusion of a coronary artery, obstructing blood flow to the serviced regions of the myocardium [6]. The hypoxic environment leads to a loss of cardiomyocytes, further triggering an immune response. Fibroblasts that are recruited to the injury site, deposit extracellular matrix leading to the formation of a non-contractile scar. As the heart adapts to the changes in its altered mechanical load, it undergoes maladaptive chronic remodelling that leads to decreased function and heart failure. In a clinical setting, coronary angioplasty restores blood flow to the myocardium, acutely resulting in the generation of reactive oxygen species and causing additional damage. Numerous advances in surgical techniques, better knowledge of pharmacological agents and a deeper understanding of the risk factors involved have been very helpful in controlling the disease [7]. However, most of the existing treatment therapies are palliative in nature and while slowing down the progression of the disease, have not been successful in regenerating the cardiac tissue that has sustained injury following myocardial infarction. The diseased cardiac tissue is replaced by a collagenous scar tissue which in turn hampers the contractile ability of the heart triggering cardiac arrests over a gradual passage of time [8]. This has become a major cause of concern and has prompted researchers and scientists all over the world to investigate other forms of treatment such as stem cell therapy and tissue engineering to reverse the effects of myocardial infarction-induced cardiac cell death in an effort to restore the functional ability of the heart.

To this effect, several clinical trials are underway to assess the safety and efficacy of these alternate treatment strategies following infarction. Notable among these trials are Cardiac Stem Cell Infusion in Patients with Ischaemic Cardiomyopathy (SCIPIO), Cardiosphere-Derived Autologous Stem Cells, to reverse Ventricular Dysfunction (CADUCEUS) and Autologous Human Cardiac-Derived Stem Cell to treat Ischemic Cardiomyopathy (ALCADIA), all of which demonstrated how unique cardiac stem cell populations could be safely utilized to induce

functional improvements in patients who were suffering from severe heart failure [9]. The primary challenge associated with stem cell therapy is to ensure the adequate retention and survival of the implanted stem cells [10]. The significance of biomaterials comes into prominence in this regard as they can be used as scaffolds that could house the cells by providing them with a controlled environment that would facilitate their growth and proliferation while shielding them from the harmful environment of the diseased myocardium, following implantation. Numerous studies have been conducted to develop biomaterial systems that could be fabricated into scaffolds that are ideal for cardiac tissue engineering by being cytocompatible and tuned to resemble the native myocardium tissue, both structurally and mechanically.

### 1.1 Central Hypothesis, Rationale and Specific Aims

The **central hypothesis** of this dissertation is that *3D bioprinting can be employed to create a cardiac patch using a combination of various biocompatible materials in optimised quantities, followed by the addition of cardiomyocytes, resulting in a solution (bioink) that can be extruded onto a template in a user-specified design (Figure 1.3).*

The extensive use of gelatin in the past, as a tissue engineering scaffold on account of its biocompatibility [11] and low immunogenicity [12], coupled with its easy availability [13] and low cost [14], prompted the usage of furfuryl-gelatin, which is a chemically-derivatized form of porcine gelatin, in this research. Using such a novel bioink to engineer cardiac tissue on a dish, our **rationale** behind bioprinting is *to provide a hierarchical mechanical support to cells during tissue regeneration, while simultaneously engineering the properties of the materials with which the cells come into contact so that the biological response of the cells themselves can be improved.*

The specific aims for each of the studies that were conducted as part of this dissertation have been enumerated as follows:

- **AIM I:** To optimize the material composition of a visible light cross-linkable gelatin-based hydrogel material for bioprinting cells in monolayer and bilayer sheets.



- **AIM II:** To explore the ability of this gelatin-based hydrogel towards the printing of a complex lattice structure infused with cells to compare and contrast with simple rectangular-sheets printed in the first study.
- **AIM III:** To extend the application of this gelatin-based bioink to incorporate fibrin (as it is a naturally derived blood protein) to develop a novel dual crosslinkable bioink that could be 3D printed into scaffolds for cardiac tissue engineering.
- **AIM IV:** To validate the superiority of the fibrin based bioink as a cardiac tissue engineering scaffold by comparing it with a synthetic dual crosslinkable PEGDA-based bioink with similar mechanical properties.

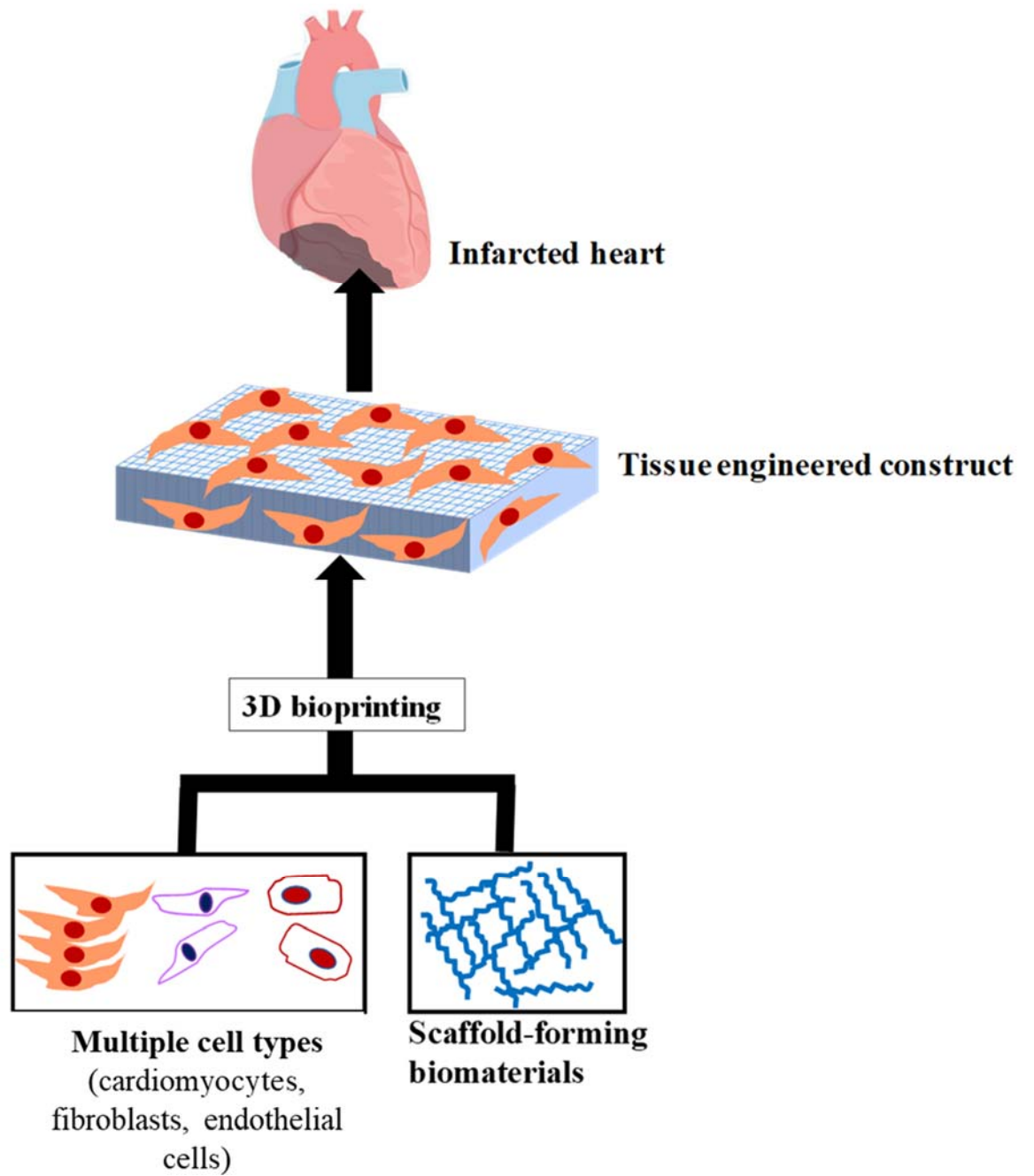


Figure 1.3: A schematic representing how tissue engineering can be employed to replace the diseased myocardial tissue

## Chapter 2: Background and overview

### 2.1 The clinical concern posed by cardiac failure

Cardiac failure remains one of the leading causes of morbidity and mortality in countries all over the world and its prevalence has been observed to be on a steady rise (Figure 2.1) [15]. Statistical estimates show that over 26 million people have been diagnosed with cardiac failure worldwide [16], with more than 5.7 million cases being reported in the United States alone [17]. Approximately 50% of the patients were deceased within two years (Figure 2.2) after they were diagnosed with failure of the heart indicating poor prognosis, despite the numerous advances and breakthroughs in medical science [17-19].

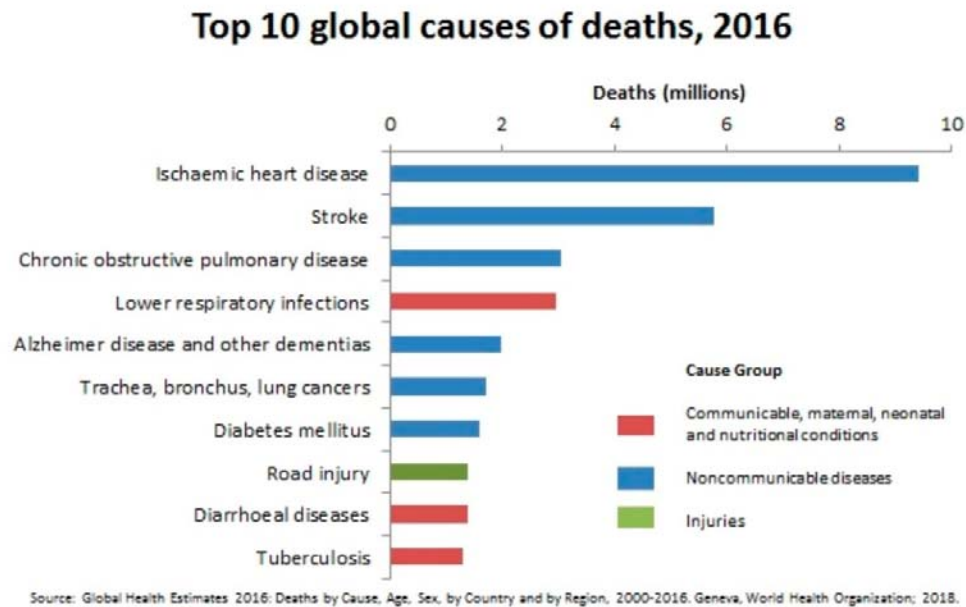


Figure 2.1: Mortality resulting from various diseases worldwide, led by ischemic heart disease and stroke (Source: Global health estimates 2016: deaths by cause, age, sex, by country and by region, 2000-2016. Geneva, World Health Organization; 2018)

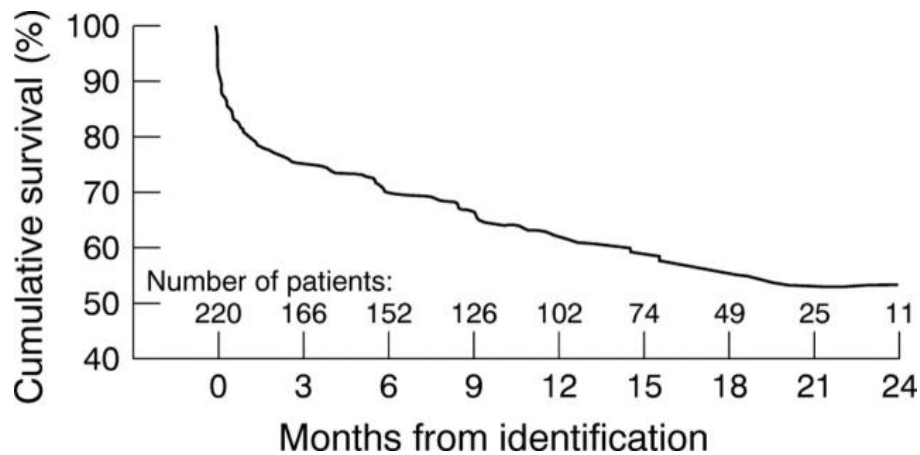


Figure 2.2: One-year survival of patients after diagnosis of heart failure [20]

Cardiac failure also poses an undeniable financial liability to the healthcare industry and accounts for about 2% of the total health care expenditure [21]. It has been deemed responsible for more than 3 million visits to a primary care physician and over 600,000 emergency room visits per year. Immediate hospital admission is necessary for about 83% of the people who are diagnosed with cardiac failure with more than 43% of them requiring multiple admissions [17]. Since heart failure has largely known to be affecting the elderly [22], the ageing population worldwide is likely to experience medical and financial demands in the future.

## 2.2 The pathophysiology of cardiac failure

Cardiac failure has been defined as a complex clinical syndrome that is a result of any structural or functional disorder that can impede the ability of the ventricle to fill with or eject blood [23]. This eventually triggers classical clinical symptoms such as shortness of breath (dyspnoea) upon exertion and fluid retention, that are characteristic of cardiac failure, which in turn can have an adverse effect on the functional ability and quality of life of the patients, with the latter being significantly impaired by heart failure to a greater extent than any other chronic disease

[20, 21]. Cardiac failure has been described as a progressive disease accompanied by a tendency of deterioration in symptoms over time.

Although cardiac failure can stem as a result of any disease that can negatively impact the blood vessels or the pericardium, myocardium or the endocardium, it has been largely associated with myocardial infarction that causes the functional failure of the left ventricle (LV). Myocardial infarction results due to the generation and rupture of atheromatous plaques within the coronary artery wall, completely interrupting the blood supply to the highly metabolically active myocardial tissue. This paves the way for tissue ischemia and consequently, the irreversible necrosis of millions of cardiac muscle cells or cardiomyocytes. The dead myocytes are gradually replaced by a stiffer collagenous scar tissue comprised of myofibroblasts, which reduces the contractile ability of the heart and eventually leads to cardiac arrests.

### **2.3 Current treatment approaches for cardiac failure**

The currently employed approaches to treat cardiac failure consider all aspects of the disease, beginning with the primary prevention by controlling risk factors like hypertension, obesity, diabetes and coronary disease. The impact of heart disease on public health can be significantly lowered by identifying the people who are at a higher risk of cardiac failure [23]. The past decade has witnessed great improvement in revascularization techniques employing thrombolytic therapy and percutaneous coronary intervention (PCI) with angioplasty and stenting that promote revascularization and reduce the infarct size, for people who suffer from myocardial infarction [24]. This has in turn reduced the mortality rate and the possibility of subsequent cardiac failure. Most patients with established heart failure are administered a combination of medications involving diuretics, beta blockers, aldosterone-receptor-blockers (ARB) and angiotensin-converting-enzyme inhibitors (ACEi). Cardiac resynchronization therapy and exercise training

have also been found to be beneficial for cardiac patients [23]. Cardiac transplantation is the only available surgical strategy for treating end stage refractory heart failure. However, one of the biggest challenges of cardiac transplants is the limited availability of donors, with only about 2500 people receiving healthier hearts per year in the US and the negative side effects of long-term immunosuppression are not to be ignored. Left ventricular assist devices (LVADs) also gained wide recognition for their ability to serve as a bridge to transplantation by the provision of long-term hemodynamic support to patients suffering from end stage cardiac failure. However, the use of LVADs can increase the occurrence of strokes, excessive bleeding, infections and other thromboembolic events in addition to suffering device failure [25].

Although there have been many advances and scientific breakthroughs in the field of cardiac research, a treatment strategy that has the potential to address the underlying issue encountered in most cases of cardiac failure, irreversible loss of functional cardiac cells remains to be discovered. Therapies that are targeted towards the reversal of the effects of myocardial injury can significantly save millions of lives worldwide, if harnessed effectively.

#### **2.4 Stem cell therapy as a treatment strategy**

Over recent years, stem cell therapy has garnered widespread interest among the scientific communities as a mode of treatment for cardiac repair and regeneration to ultimately reverse the damage caused by myocardial injury. Stem cells are considered ideal sources for cardiac regenerative techniques owing to their infinite potential to self-renew and also differentiate into other cell-types. The growth of stem cells can be amplified in tissue culture although they are strictly regulated within the body, making them extremely useful for stem-cell therapy [26].

Stem cells are classified into the following categories based on their cell potency or their varying ability to differentiate into specialized cell-types:

- Totipotency – the ability of stem-cells to differentiate into all the cell-types that constitute an organism and is restricted to a zygote/fertilized egg.
- Pluripotency – the ability of stem-cells to differentiate into any of the three germ layers, namely the endoderm (inner lining of the stomach, the gastrointestinal tract and the lungs), the mesoderm (muscle, bone, blood and the urogenital tract) and the ectoderm (epidermal tissues and the nervous system).
- Multipotency- the ability of stem-cells to differentiate into discrete cell-types.
- Oligopotency – the ability of stem-cells to differentiate into only a few cell-types.
- Unipotency – the ability of stem-cells to differentiate into only one type of cells.

Stem-cells exhibiting pluripotency or totipotency are the most ideal cell-sources for regenerative therapies since they are theoretically able to replace any damaged tissue within the body. ESC cardiomyocytes were successfully employed to form human myocardial tissue within infarcted rat hearts as per studies conducted by Laflamme et al. [27, 28]. Despite the significant improvements that have been noted in the cardiac function, perfusion and metabolism in experimental studies, there are multiple challenges such as stem-cell retention and viability post-implantation, the possibility of teratoma formations and the ethical and immunological issues associated with the use of ESCs that have restricted their use in human clinical trials for cardiac research.

However, adult stem cells have been shown to have great promise for cardiac tissue repair by avoiding the problems of immunosuppression without the complication of ethical concerns. Numerous types of adult stem cells have been investigated such as cardiac progenitor cells (CPC) [29, 30], cardiospheres [31, 32], skeletal myoblasts (SkM) [33], adipose derived stem cells (ADSC) [34, 35], induced pluripotent stem cells (iPSC) [36] and mesenchymal stem cells (MSC) [37, 38] among others. The evidence collected from investigations with adult stem cells paved the

way for numerous human clinical trials employing adult stem cells to treat cardiac failures [39]. There have been multiple experiments conducted to study the effects of adult bone marrow-derived cells (BMC) in stem cell therapy involving acute myocardial infarction and ischemic heart failure [33, 40-42]. The results obtained from these studies were mostly inconsistent thereby necessitating the need for further investigations that standardize aspects like stem-cell processing, timing of therapy, dosage and route of stem cell administration [43]. There is also the need to examine clinical end points like mortality and recurrent cardiac events in contrast with radiographical indices of cardiac function. Although skeletal myoblasts have been widely used in clinical trials, the limited efficacy and the uncertainty associated with the occurrence of arrhythmias have restricted their usage.

In spite of the numerous caveats, the trials have been able to provide substantial evidence suggesting that there is great promise with stem cell therapy for the treatment of myocardial injury. The safety of these approaches on BMC therapy, with a follow-up time of up to 10 years, has also been demonstrated [43].

## **2.5 Drawbacks of existing stem cell therapies**

The reparative potential of adult cells like BMC is widely believed to stem from the paracrine effects rather than direct regeneration of the transplanted cells themselves [39]. Cardiomyocytes have been known to have a very limited capacity for self-renewal and their true replacement can be possible only by employing pluripotent cells. Scientists have been successful in reverting adult cells back to their pluripotent state [44] and this could eventually be helpful in establishing a patient specific cell source that could be employed without the various ethical and immunological constraints that accompany other pluripotent cell sources.



However, there are various other issues that are associated with cell therapy that need to be addressed even if the pluripotent cells are established as a safe and consistent cell source. One of the primary challenges of stem cell therapy involves problems related to cell-engraftment, retention and survival. Studies have shown that cells have the tendency to drift away from the target locations as they are injected in liquid solutions and have no matrix to which they can adhere to. According to MRI studies of radiolabelled BMC conducted by Hofmann et al., the uptake of cells into the myocardium after an intracoronary transfer procedure was found to be merely 2.6%, with negligible retention of cells in the myocardium post-peripheral transfer [45]. A separate study involving the injection of fluorescent microspheres into the myocardium in animal models, the retention rates were only found to be about 11% which could be possibly due to the effect of myocardial infarction [46]. A study performed by Zhang et al. involving neonatal cardiomyocytes demonstrated that the survival rates were as low as 1 to 33% of the cells surviving 7 days, for the cells retained within the myocardium [47]. It was also observed that patients who were injected with a larger dose of cells exhibited better outcomes with respect to those who were given smaller doses [33]. The success of stem cell therapy is governed by the issues of cell retention and survival, irrespective of the cell type employed. Hence, there is a need for a multimodal strategy in order to overcome the issues associated with stem cell therapy.

## **2.6 Tissue engineering as an alternative treatment strategy**

The term “tissue engineering” was first introduced to the scientific community by Langer and Vacanti in 1993 and has been defined as “an interdisciplinary field that applies the principles of engineering and life sciences toward the development of biological substitutes that restore, maintain, or improve tissue function or a whole organ” [48].

Tissue engineering has been successfully employed ever since its inception and has been developed into a strategy involving a triad of cells, biomaterial scaffolds and growth factors. Cardiac regeneration can be best achieved through tissue engineering by applying the right combination of the appropriate biomaterials, cells and soluble growth factors. It is also imperative to design the most ideal biomaterial scaffold in order to fabricate a cardiac-tissue-on-a-chip.

A biomaterial has been described as a substance that can be engineered to take a form that can be used wholly or as part of a complex system, to direct the course of any therapeutic or diagnostic procedure in humans or animals by controlling the interactions with components of living systems [49]. New scientific advancements have made it possible for the complex design of biomaterial scaffolds on a molecular level to direct specific cellular responses to external signals and stimuli [50], in addition to utilising the bulk properties of biomaterials to facilitate the healing of body tissues. It is possible to induce and direct the differentiation of proliferating cells by tuning properties of the biomaterial such as its surface chemistry, topography and other physical attributes. Further, cell survival is prompted by other cues such as growth factors and signalling molecules which can be incorporated into the biomaterial scaffold, enhancing the success of the tissue engineering strategy.

Literature provides ample evidence of multiple ways in which biomaterials have been successfully employed for the treatment of myocardial infarction [51-54]. Cellular cardiomyoplasty which can be described as a therapeutic modality involving the injection of biomaterials that have been loaded with cells and growth factors directly into the damaged myocardial tissue allowing the in-situ regeneration of the tissue has also been widely practised [55]. Despite its success, there is always the risk of arrhythmogenesis or the erratic beating of the heart in addition to the possibility of limited cell retention and survival with this method. In other instances, the biomaterial scaffolds are employed as “patches”, which forms the basis of this thesis.

These “patches” can be transplanted atop the damaged myocardium to facilitate the transfer of healthy cells that can replace the diseased cells, in addition to providing mechanical support by infarct restraint, which can address the issues that limit the efficacy of cellular cardiomyoplasty.

Cardiac patches have been investigated extensively and numerous research groups succeeded in engineering tissue constructs that could mimic the cardiac tissue. Chen et al. designed a polyglycerol sebacate based “patch” that could match the mechanical properties of the native heart tissue and also able to support stem-cell derived cardiomyocytes for upto a period of 3 months with no adverse effect on the cardiac function [56]. Numerous other studies have also demonstrated the success of cardiac patches for the treatment of myocardial infarction-induced heart failure [57, 58].

## Chapter 3: Materials and Methods

### 3.1 Materials

Furfuryl-gelatin (f-gelatin) and fibrinogen (60 mg/mL) were prepared as described below and were kindly contributed by our collaborators Drs. Park and Ito from RIKEN, Japan and Dr. Willerth from the University of Victoria, Canada, respectively. Sodium salt of hyaluronic acid (HA; mol wt  $\sim 1.5\text{-}1.8 \times 10^6$  Da) was procured from Sigma-Aldrich (St. Louis, MO, USA). Rose Bengal (RB) and Riboflavin (RF) were purchased from Thermo Fisher Scientific (Waltham, MA, USA). Dimethyl Sulfoxide (DMSO) was obtained from Sigma-Aldrich (St. Louis, MO, USA).

#### *3.1.1 Preparation of f-gelatin and its characterization by NMR spectroscopy*

Porcine gelatin powder, furfuryl glycidyl ether (96%) were obtained from Sigma-Aldrich. Dimethylsulfoxide (DMSO) was acquired from Duchefa Biochemie (Haarlem, The Netherlands). Sodium hydroxide (NaOH), hydrochloric acid (HCl), acetone and ether were products of Duksan Pure Chemical Co., Ltd (South Korea). Porcine gelatin (2 g) was dissolved in d.d water (80 mL) and the pH was adjusted to 11 by the addition of 1 N NaOH solution. Furfuryl glycidyl ether (250  $\mu\text{L}$ ) was dissolved in DMSO (20 mL) and added to the gelatin solution at room temperature and stirred for 30 hr at 65°C. 1N HCl solution was added to the resulting mixture to adjust its pH to 7 and dialyzed in DI water for 48 hr, using a dialysis membrane with a molecular weight cut-off of 1,000 Da (Spectrum Laboratories Inc., Rancho Dominguez, CA, USA), for the purification of the f-gelatin. After dialysis, the solution was evaporated, and the purified f-gelatin was first washed four times with acetone, once with ether and then dried.  $^1\text{H}$  NMR Measurement using an NMR spectrometer (Gemini 2000, 300 MHz, Varian Inc., Palo Alto, CA, USA) was employed for the characterization of the dried f-gelatin. For the analysis, porcine gelatin (control) and f-gelatin were dissolved in deuterium oxide ( $\text{D}_2\text{O}$ , Sigma) and then used. The NMR spectra obtained was

analysed to confirm the derivatization of the f-gelatin from gelatin by the integration of the furan ring to the gelatin (Figure 3.1).

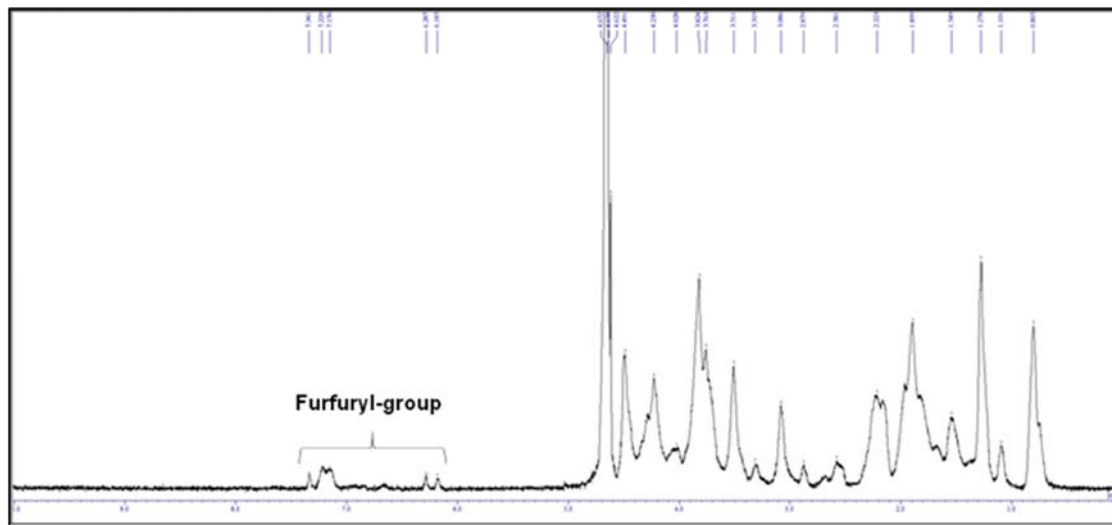


Figure 3.1: The  $^1\text{H}$  NMR spectrum of f-gelatin showed a distinct peak at 6-8 ppm representing the aromatic furan ring. During synthesis, the  $\text{NH}_2$  group of gelatin was substituted with a furan ring.

The  $^1\text{H}$  NMR spectrum of f-gelatin showed a distinct peak at 6-8 ppm representing the aromatic furan ring. The  $\text{NH}_2$  group of porcine-gelatin was substituted with the furan ring during the synthesis of the f-gelatin. Upon visible light irradiation, f-gelatin undergoes crosslinking and

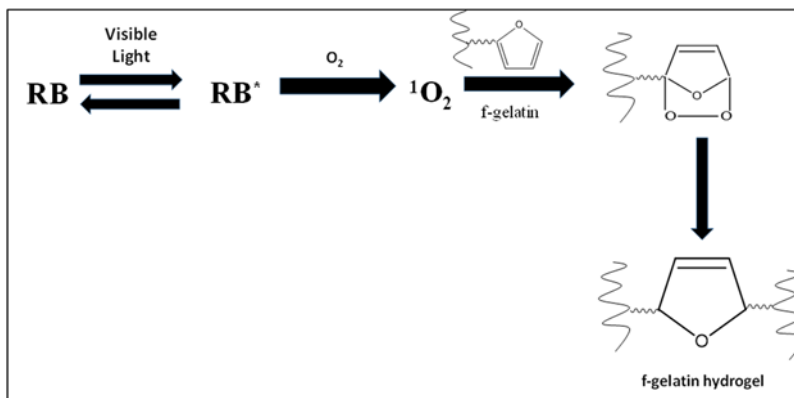


Figure 3.2: Scheme for visible light crosslinking of f-gelatin.

changes into a film. The crosslinking of the f-gelatin is facilitated by the  $^1\text{O}_2$  (singlet-oxygen) generated by the photosensitizer dye (Rose Bengal) when it absorbs energy from the visible light (Figure 3.2).

#### *3.1.1.1 Biocompatibility of f-gelatin*

The f-gelatin was analysed to test its cell-compatibility. Dulbecco's Modified Eagle's Medium (DMEM), fetal bovine serum (FBS) and penicillin streptomycin (PS) were obtained from GIBCO (Eggenstein, Germany). The 3T3-L1 cell line (originating from Swiss mouse fibroblasts) was used for the cytotoxicity test. The MTT assay was performed to study cytotoxicity. 3T3-L1 cells were cultured in DMEM media that contained 5% FBS and 0.2% PS at 37°C with 5% CO<sub>2</sub>. Cells were seeded at a density of 10<sup>4</sup> cells/well in 96-well plates (DK-4000 Roskilde, Kamstrup Vej 90, Nunc A/S, Denmark) and incubated for a period of 24 hr. The f-gelatin solutions were prepared at a concentration of 10% and 10 µL of this solution was added to 96-well plates. The plates were then incubated for 5 days at 37°C with 5% CO<sub>2</sub>. Following incubation, the culture media was removed, and 100 µL of MTT solution (1 mg/mL) was added to the plates. After 4 hr of incubation, the MTT solution was replaced with 150 µL of DMSO, and the plates were incubated for 10 min to dissolve the formazan crystals. A microplate reader (Sepctramax190, Molecular Device, Sunnyvale, California, USA) was used to measure the plates for absorbance at 595 nm. The OD<sub>595</sub> (sample), optical density, was measured in wells treated with f-gelatin, and OD<sub>595</sub> (control) was measured in non-treated wells. Cell viability (%) was calculated according to a previously used formula. The estimated viability (% absorbance) of 3T3-L1 fibroblast cells that were treated with f-gelatin and measured using the MTT assay showed no significant difference from the values estimated from cells treated with controls. This was confirmation that the f-gelatin solution was not cytotoxic, in agreement with previously published results.

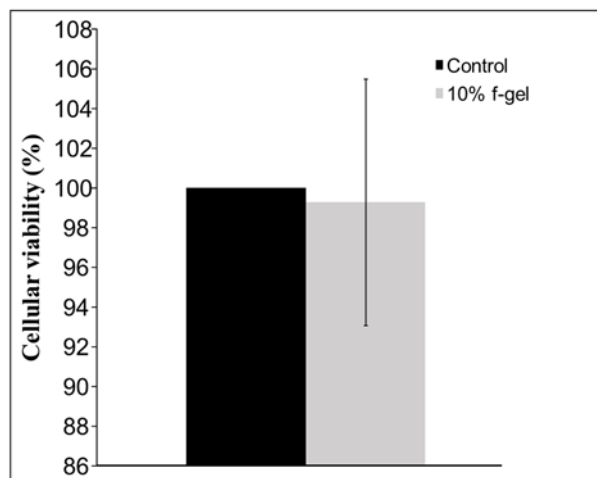


Figure 3.3: Viability of 3T3-L1 fibroblast cells treated with f-gelatin was measured by means of an MTT assay. Controls were non-treated cells, and samples were cells treated with 10% f-gelatin solution. Cells treated with f-gelatin solution were similar to controls in terms of the measured absorbance values as shown.

### 3.1.1.2 Visible light induced crosslinking of the f-gelatin:

Two different concentrations of f-gelatin solutions (1%, 10% w/v) were prepared and mixed with RB or RF (0.5% w/v) and spread onto empty petri plates with a pipette tip, in order to ascertain the amounts of the f-gelatin required for subsequent experiments. Visible light (100 ~ 150 W) was then used to irradiate the samples for 5 min, following which they were incubated (RT) for up to 14 days in DI water. Samples that were not exposed to visible light for the photo-curing served as controls for this study. The observations showed that the controls dispersed readily in water, whereas 10% f-gelatin treated with either RB or RF, retained their structures for 8 days, while the 1% f-gelatin structures dissolved in the interim. After 14 days, the photo-cured f-gelatin samples could still be recovered from the bottom of the petri dishes. This confirmed the visible light induced crosslinking and stability of the 10% photo-cured f-gelatin constructs.

### ***3.1.2 Preparation of fibrinogen***

Approximately 1300 mg of lyophilised fibrinogen was dissolved in 20 mL of Tris-buffered Saline (pH 7.4) as explained in prior studies [59]. The solution was incubated at 37°C for about an hour and then dialyzed overnight in 4 L of Tris-Buffered Salin, following which it was sterile filtered with a 0.2 mm syringe filter. The concentration of the solution was measured using a NanoVue Plus spectrophotometer (Biochrom, Holliston, MA) using the Protein A280 assay. The solution was then diluted to the required concentration of 60 mg/mL with sterile Tris-Buffered Saline.

## **3.2. Methods**

### ***3.2.1. 3D bioprinting***

3D bioprinting is a form of additive manufacturing (AM) employed to print structures using viable cells, biomaterials and biological molecules [60]. Bioprinting must generate scaffolds possessing a suitable microarchitecture so as to provide mechanical stability and promote cell ingrowth while ensuring that the manufacture process does not compromise the cell viability; for instance, chemical cytotoxicity resulting from the use of solvents or pressure-induced apoptotic effect produced during the extrusion of material [60]. An important benefit of bioprinting is that it prevents homogeneity issues that accompany post-fabrication cell seeding, as proper cell placement is included during fabrication. Homogenously distributed cell-laden scaffolds have been demonstrated to exhibit lower risk of rejection, faster integration with the host tissue and uniform tissue growth in vivo [60].



Bioprinting can be applied in a clinical setting, where it can be used to create regenerative scaffolds in accordance with patient specific requirements [61]. To begin with, imaging modalities such as CT, MRI and ultrasound are employed create a digital 3D model of the tissue defect. The internal and external architecture of the scaffold, such as porosity and pore sizes, can be incorporated into the 3D model of the tissue defect with the help of computer aided design (CAD) [62]. A selection of materials, cell types and bioactive molecules, can be used to fabricate a bioink for printing by considering factors like the nature, type and the location of the defect. Cell laden structures are then manufactured by applying the bioprinting technology and are then placed either in cell culture or directly implanted into the patient. The primary objective behind bioprinting is to provide an alternative to autologous and allogeneic tissue implants, and to replace animal testing for the study of disease and development of treatments.

The three main 3D bioprinting methods that have been used extensively are inkjet-, extrusion- and laser assisted-bioprinting [63] (Figure 3.4, Table 3.1). Inkjet bioprinters, also known as drop-on-demand printers, utilize a non-contact technique that may involve thermal, piezoelectric, or electromagnetic forces to expel successive drops of bioink onto a substrate, replicating a CAD design with a printed tissue [63]. Extrusion based models use mechanical or pneumatic forces to dispense a bioink in continuous streams as opposed to the discrete droplets deposited by inkjet printers, onto a substrate [63]. Laser assisted 3D bioprinting technology directs laser pulses through a “ribbon” containing bioink, which is supported by a titanium or gold layer capable of absorbing and subsequently transferring energy to the ribbon [63]. The bioink and cells, suspended on the bottom of the ribbon, create a high-pressure bubble that eventually propels discrete droplets to the receiving substrate that lies just beyond the ribbon, when vaporized by the laser pulse. This step is repeatedly performed to functionally create the 3D structures [63].

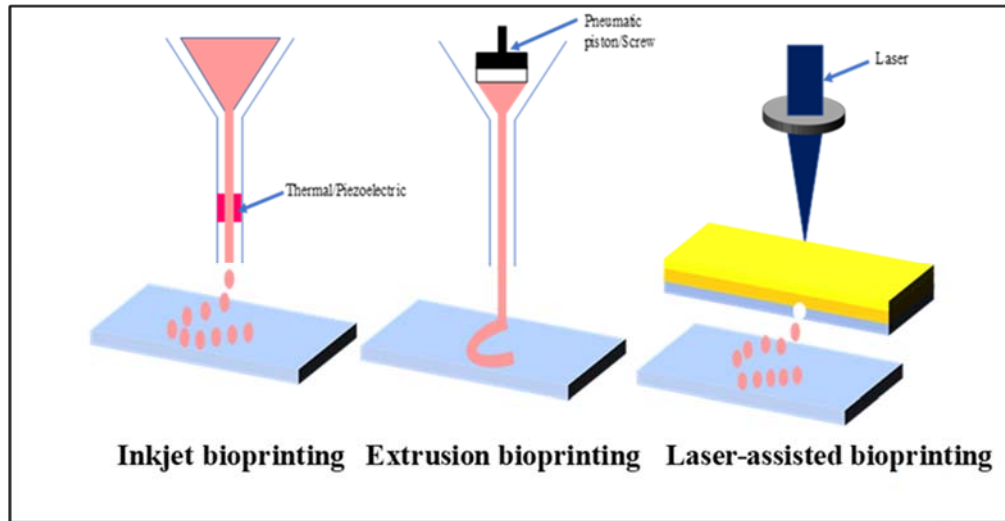


Figure 3.4: The three types of 3D bioprinting approaches

Table 3.1: Comparison between inkjet-, extrusion- and laser-based bioprinting [56]

Category	Inkjet	Extrusion	Laser
Material viscosity (mPa/s)	Low (3-12)	High (30-6 x 10 <sup>7</sup> )	1-300
Method of crosslinking	Chemical-/Photo-crosslinking, Temperature	Chemical-/Photo-crosslinking, Temperature	Chemical-/Photo-crosslinking
Print speed	1-10,000 droplet/s	10-50 μm/s	200-1600 mm/s
Resolution	50-300 μm wide droplets	100 μm to 1 mm wide	50 μm
Accuracy	Medium	Medium-low	High
Cell viability	>85%	40-80%	>85%
Cell density	10 <sup>6</sup> -10 <sup>7</sup> cells/mL	High: cell spheroids	10 <sup>6</sup> -10 <sup>7</sup> cells/mL
Structural integrity	Low	High	Low
Fabrication time	Medium	Short	Long
Scalability	Yes	Yes	Limited
Cost	Low	Medium	High

### **3.2.2 Material characterization**

#### **3.2.2.1 Scanning Electron Microscopy (SEM)**

Scanning Electron Microscopy (SEM) is a technique that generates images of a sample by scanning its surface with a beam of electrons. These electrons interact with the atoms that make up the sample and produce various signals that contain information about the surface topography and composition of the sample under study. The electron beam is scanned in a raster scan pattern, and the beam position coupled with the intensity of the detected signal to generate an image. The most common SEM mode utilises the secondary electrons, which are emitted by atoms excited by the electron beam, are captured by the detector.

SEM has been extensively used for the characterization of biological scaffolds to study their morphologies and pores [64]. The 3D printed f-gelatin samples were fabricated as explained later, lyophilised overnight and sputter-coated with gold in a sputter coater (Gatan Model 682 Precision etching coating system, Pleasantown, CA, USA). The samples were then used to obtain both en-face and cross-sectional images using SEM (S-4800, Hitachi, Japan) at a voltage of 5-13 kV. The fibrin-gelatin based 3D printed constructs were visualised using a table top SEM (TM-1000, Hitachi, Japan) at a voltage of 15kV. The cross-sectional images acquired for all samples were analysed using ImageJ and the apparent porosity and average pore diameters were estimated using the formula given below.

$$\text{App. porosity} = \frac{\text{total area covered by pores (sq. } \mu\text{m)}}{\text{total sample area of the cross section (sq. } \mu\text{m)}} * 100$$

### 3.2.2.2 Rheology

Rheology is defined as the study of flow of matter and is employed to determine the viscoelastic properties of the hydrogel material that is used as the tissue engineering scaffold. Viscoelasticity refers to the property of materials to exhibit both viscous and elastic behaviour when they undergo deformation. Rheology is studied with the help of a rheometer that performs small deformation experiments, typically in the form of small amplitude oscillatory shear measurements, on the sample. Small deformations are used in order to ensure that the experiment is carried out within the linear viscoelastic region of the material. This implies that the properties of the hydrogel are independent of the magnitude of the applied stress or strain and the results are solely based on the material tested and are not influenced by the experimental variables.

The key parameters that can be determined by rheology are the storage ( $G'$ ) and the loss ( $G''$ ) moduli and the loss factor ( $\tan\delta$ ) (Figure 3.5). The storage modulus  $G'$  measures the stored deformation energy or the stiffness component of the material and the loss modulus  $G''$  measures the energy dissipated or the flowability of the material during the shear process. The ratio of the loss to storage moduli indicates the loss factor  $\tan\delta$ .

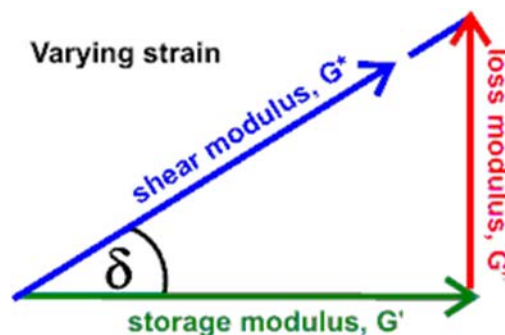


Figure 3.5: Rheological relationship between storage modulus ( $G'$ ), loss modulus ( $G''$ ) and loss factor ( $\tan\delta$ ). If  $G' > G''$ , the material is predominantly elastic and if  $G'' > G'$ , the material is predominantly viscous.

It was established that if  $G' > G''$  ( $\tan\delta > 1$ ), the sample behaves more like an elastic solid and if  $G'' > G'$  ( $\tan\delta < 1$ ), the sample behaves like a viscous liquid. The complex modulus  $G^*$  gives a measure of the overall resistance to the deformation of the material regardless of whether it is elastic or viscous and is calculated using the equation given below:

$$G^* = \sqrt{(G')^2 + (G'')^2}$$

To perform the rheometric analysis, the hydrogels were made as described in the succeeding chapters and cut out with the aid of biopsy punches (~1mm deep and 8mm in diameter) and allowed to swell in 1X PBS for an hour prior to testing. An Anton-Paar MCR 101 rheometer (Anton-Paar, Graz, Austria) was employed to carry out oscillatory shear stress rheometry (1% strain, 0.5-50 Hz). The complex modulus was calculated as a function of the storage and loss moduli and measured at 1.99 Hz for all samples. Although, the viscoelastic behaviour of the gels was evaluated from 0.5 to 500 Hz, the elastic modulus was determined through a shorter sweep from 0.5 to 50 Hz as done in published studies [65].

### 3.2.2.3 Fourier Transform Infrared Spectroscopy (FTIR)

The Fourier Transform Infrared Spectroscopy (FTIR) is a highly sensitive and non-destructive technique used for the characterization and identification of organic molecules. The interaction of infrared radiation with the sample molecules results in the stretching, contraction or bending of chemical bonds resulting in the absorption of infrared radiation in a specific wavenumber range independent of the structure of the rest of the molecule. An FTIR spectrometer obtains the infrared spectra by collecting an interferogram of a sample signal with an interferometer, which measures all the infrared frequencies simultaneously. The spectrometer then acquires and digitizes the interferogram, performs the Fourier Transform function and generates the spectrum. Since every functional group has a characteristic vibrational frequency and

wavenumber, the analysis of the IR spectrum will aid in identifying the different functional groups present in the sample.

The Attenuated Total Reflectance (ATR)-FTIR spectra for the f-gelatin- and fibrin-based samples were acquired using a Perkin-Elmer, Spectrum 100, Universal ATR Sampling Accessory within the range of 650-3650  $\text{cm}^{-1}$  in the transmittance mode. Spectral manipulations were carried out using the spectral analysis software GRAMS/32 (Galactic Industries Corp., Salem, NH, USA). A Specac grazing angle accessory using an s-polarized beam at an angle of incidence of 40° and a mercury cadmium telluride (MCT/A) detector, was used to record the external reflection FTIR. A piranha-treated silicon carbide wafer served as the background.

#### *3.2.2.4 Swelling and degradation*

Swelling assay is a technique used to study the hydration parameters of crosslinked hydrogel structures. Prior to testing, the samples were lyophilised and their dry weights ( $W_0$ ) taken following which they are immersed in DMEM and their swollen weights ( $W_t$ ) recorded after every 24 hr upto 5 days as done in previous studies [66]. The swelling ratio ( $D_s$ ) is calculated using the formula given below:

$$D_s = (W_t - W_0) / W_0$$

#### *3.2.2.5 Statistical analysis*

Sample datasets under study were all in triplicates unless otherwise stated. Data are expressed as the Mean  $\pm$  Std. deviation. Student's t-test was performed to determine if the averages of any two sample datasets compared were significantly different.  $p$ -values less than 0.05 were considered statistically significant wherever reported.

## **Chapter 4: Development of a novel, visible-light crosslinkable f-gelatin based hydrogel for tissue engineering applications**

### **4.1 Introduction**

3D bioprinting has revolutionized the field of regenerative medicine with its ability to create cell patterns within confined spaces, while also ensuring that the cellular function and viability are preserved [67]. A 3D bioprinter employs “bioinks” which are materials capable of mimicking an extracellular matrix environment in order to facilitate the adhesion, growth, proliferation and differentiation of mammalian cells [67]. Bioinks can be deposited in the form of filaments during additive manufacturing unlike traditional biomaterials such as polymer networks and foam scaffolds. However, it is essential that they are processed under milder conditions than those employed for thermoplastic polymers, ceramics and metals, in order to preserve cell viability and to prevent the bioactive molecules from degrading [68]. The properties that need to be considered in order to formulate an ideal bioink include viscosity, biocompatibility, gelation kinetics, hydration ability, viscoelasticity and shear thinning ability (printability) [69]. Hydrogels are usually adopted from existing literature and are derived from natural polymers such as fibrin, gelatin and alginate [69].

Hydrogels belong to a class of water swollen polymer-based materials produced by reactions of monomers or hydrogen bonding and can form and maintain distinct 3D structures [70]. They have gained immense popularity as the material of choice for the creation of scaffolds for use in cell culture and tissue engineering over recent years [71]. They provide a remarkable environment for cell culture as they contain more than 70% of water [5]. Hydrogels are also biodegradable, absorbable, erodible and most importantly, biocompatible giving them an edge over other biomaterials [72]. Gelatin, a collagen-derived translucent, flavourless food additive obtained from various animal body parts is one of the most extensively used hydrogels. It is chiefly

composed of peptides and proteins generated by the partial hydrolysis of collagen extracted from the skin, bones and connective tissues of pigs and fish [71-73]. Gelatin is ideal for cell-culture as it is biodegradable, biocompatible due to the presence of an R-G-D (Arg-Gly-Asp) sequence [74] and is economically feasible [75]. Studies have also shown that it has superior properties as compared to its parent protein such as reduced immunogenicity, greater solubility in aqueous systems and a sol-gel transition at 30°C [75]. Additionally, the biochemical properties of gelatin can be crosslinked and modified by adding other materials that significantly alter its biochemical properties [76-79] and also enhance its mechanical properties [80] in vitro. Gelatin has been crosslinked in prior studies by means of disulphide crosslinking [81], photo crosslinking [82, 83] and enzymatic crosslinking [84, 85] to name a few. Prior studies have shown that chemical modifications of gelatin can render the resultant compound cytotoxic and limit its applications to in vitro studies [86, 87].

However, f-gelatin that was generated by the incorporation of furfuryl groups into porcine gelatin and mixed with RB and crosslinked by irradiating with visible light by a photo-oxidation induced crosslinking mechanism, did not exhibit any signs of toxicity but also enhanced cell migration and adhesion in vitro [88]. Further, f-gelatin was also found to be capable of protein immobilization for the modification of existing implant surfaces [89] and for in-vivo tissue repair applications [81]. In this study, our motive was to test the applicability of an f-gelatin based hydrogel as a bioink for bioprinting [90] and fabricating single and double layered cell sheets for tissue engineering [91]. Our hypothesis was that the f-gelatin based solutions could exhibit all properties that are characteristic of an ideal bioink, such as high print fidelity, optimized shear-thinning characteristics, the ability to generate crosslinked scaffolds with high mechanical strength, high cytocompatibility and be feasible for modulation of cellular functions [92]. It was



expected that f-gelatin would serve as a novel bioink for the fabrication of 3D structures infused with cells, while simultaneously preserving the functions and viability of the cells encapsulated within. To make the f-gelatin based bioink, hyaluronic acid (HA) was added as a viscosity enhancer [93] and Rose Bengal [94] or Riboflavin [95] was added to the f-gelatin solution to act as a photo sensitizer. The resultant mixture was homogenously mixed with cells and bioprinted into single and double layered rectangular sheet structures with the aid of a pneumatic extrusion 3D printer, following which they were irradiated with visible light to enhance their structural fidelity through photocrosslinking.

3D bioprinting presents numerous difficulties like the choice of materials, cell types, growth and differentiation factors, and issues related to the sensitivities of living cells encapsulated within the bioprinted constructs [67]. The addressal of these challenges will enable the integration of concepts from the fields of biology and engineering, and will significantly advance our knowledge regarding in vitro construction of complex tissues [67]. With the possibility of multi-layered tissue fabrication, this work may eventually open up new vistas in the field of 3D bioprinting of implantable organs by providing a cost effective and rapid prototyping technique for biofabrication of tissues mimicking complex organs in a dish.

## **4.2 Biofabrication**


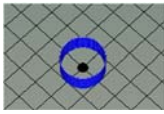
BIOBOT 1 (BioBots, Philadelphia, PA, USA), an extrusion-based bioprinter was used for biofabrication, with the bioink we formulated as described below. The bioink was primarily composed of a mixture of f-gelatin and HA to which either RB or RF was added for crosslinking the bioprinted structure through a visible light induced crosslinking mechanism [83, 88]. In order to make 1 mL of this bioink solution, HA (10 mg) was dissolved in DI water (900  $\mu$ l, 25°C), followed by the addition and mixing of f-gelatin (100 mg) at 25°C. The resulting mixture was then

heated at 37°C for 1 hr with stirring to form a homogenous viscous mixture. The ratio of HA to f-gelatin was maintained at 1:10 and RB (100 µl) or RF (100 µl) was added to serve as a photo sensitizer, to induce the crosslinking after the bioprinting. Experiments were also done by adding the cells to the mixture were added to this mixture as described later.

This bioink mixture was then loaded into a 10 mL plastic syringe (BD, Franklin lakes, NJ, USA), fitted with a stainless steel blunt-tip dispensing needle (Huaha, Amazon, USA) and extruded using a low extrusion pressure (Table 4.1). Patterns printed using this bioink were designed using SolidWorks and saved as .stl files. The versatility of the f-gel bioink was tested by printing structures having two different patterns, rectangular and circular respectively, were printed on 100 mm x 15 mm petri-dishes (Thermo Fisher Scientific, Waltham, MA, USA). The .stl files were converted into a g-code using the Repetier Host program available via BIOBOT server. These g-code files were uploaded and used for printing using parameters in Table 4.1.

The printed structures were immediately exposed to visible light for 2.5 min for crosslinking (at 100% intensity, Intelli-Ray 600, Uvitron International, West Springfield, MA, USA). The rectangular sheet structure, initially printed as a monolayer, was further expanded by printing a secondary layer to demonstrate the feasibility of fabricating a bi-layer structure using the f-gelatin based bioink (Figure 4.1). Particularly for printing bi-layer sheet structures, the bottom layer was first printed using bioink with added RB and crosslinked for 2.5 min. Cells were added to this mixture for printing the bottom layer, as described later in section 2.5. A second layer was printed atop the former, using bioink with added RF, and crosslinked similarly for an additional 2.5 min. The necessity for the addition of two different dyes, RB and RF was to highlight a distinct two layered structure that could be printed easily.

Table 4.1: Printing parameters used for the f-gelatin based bioink

Structure	Printing method	Needle diameter (mm)/ Gauge (G)	Extrusion speed (mm/s)	Extruder temperature (°C)	Bed temperature (°C)	Extrusion Pressure (psi)
Rectangular structure* 	Traditional	0.34-0.43/ 23-25	5	Room temperature	Room temperature	4.5±1.9
Circular structure 	Traditional	0.34/ 23	5	Room temperature	Room temperature	2.8

### 4.3 Cell culture, characterization and viability within the printed constructs

Strain C57BL/6 Mouse MSC (catalog #: MUBMX-01001) and Growth Medium (complete growth medium, catalog #: MUXMX-90011) were obtained from Cyagen (Santa Clara, CA, USA). The cells were cultured, passaged and stabilized for at least 6 passages prior to their use in bioprinting. For bioprinting with cells, bioink was prepared as described earlier (section 4.2) and cells were added to it. Prior to their addition in the bioink mixture, the mouse MSCs were labelled with PKH67 green fluorescent dye (Sigma-Aldrich, St. Louis, MO, USA), or PKH26 red fluorescent dye (Sigma-Aldrich, St. Louis, MO, USA) as per manufacturer's protocols. Both dyes are used for cell tracking purposes in vitro or in vivo [96].

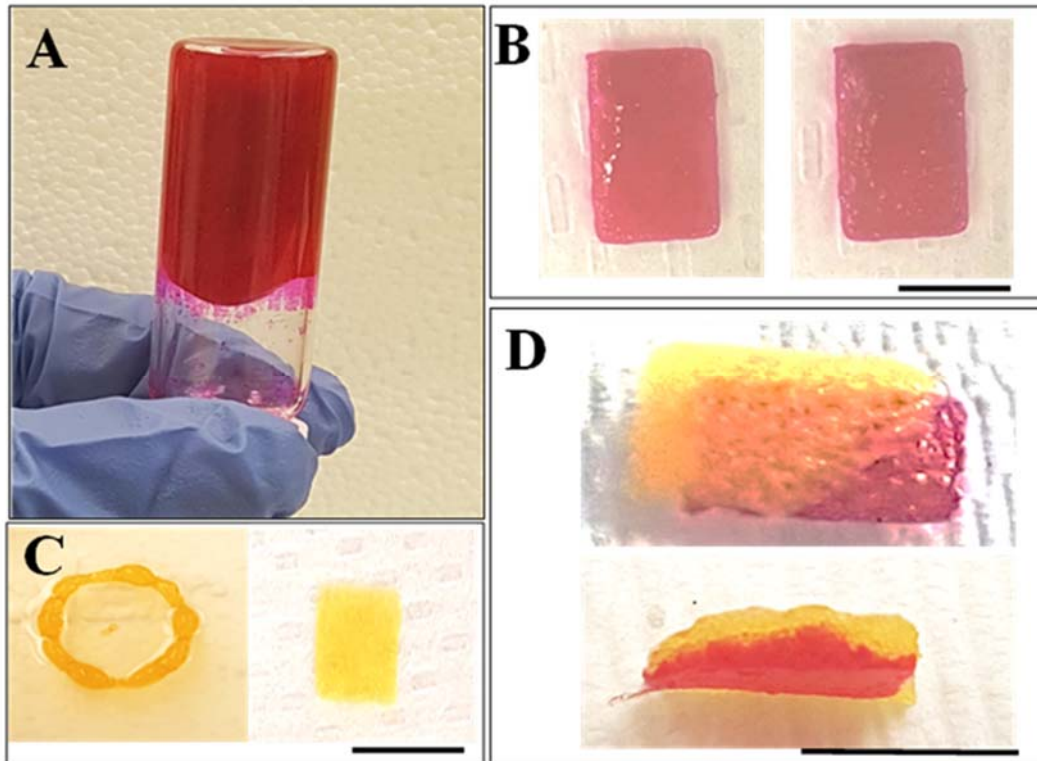


Figure 4.1 (A) Bioink (no cells) showing a viscous mixture prior to crosslinking. (B) Pre- (left) and post-crosslinked (right) hydrogel (sheet) (C) Versatility of patterns being printed (ring: left and sheet: right) (D) Double layered sheet printing feasibility (en-face: top and cross-section: bottom). In B, C and D, yellow corresponds to RF and pink to RB. Scale bar in all images corresponds to 2 cm.

These labelled mouse MSCs were mixed with bioink ( $1 \times 10^7$  cells/mL) and loaded into a 10 mL syringe for extrusion and printing. The printed, crosslinked, cell-laden gel structures were then incubated with 5 mL of complete growth medium for mouse MSC and incubated ( $37^\circ\text{C}$ , 5%  $\text{CO}_2$ ) for a period of up to 72 hr. The cell-laden bioprinted structures, both mono- and bi-layered sheets were analysed using inverted confocal fluorescence microscopy (ZEISS LSM 700 confocal, Oberkochen, Germany) following 5 days of culture, to confirm cell retention and density. To confirm that the printing process did not adversely affect cellular viability, Hoechst 33342

(Thermo Scientific Pierce, Waltham, MA, USA), a 20 mM aqueous stock solution of a fluorescent stain was used to detect and image cells, immediately after printing (within 24 hr).

Additionally, as a means to check the capability of this method for co-layering, two different cell types namely, STO fibroblasts (STO, ATCC® CRL-1503™) and C2C12 myoblasts (C2C12, ATCC® CRL-1772™), both from American Type Culture Collection (ATCC) (Manassas, VA, USA) were used. Both cells were cultured and stabilized for at least 6 passages using DMEM/F12 medium supplemented with 5% foetal bovine serum (FBS, Invitrogen, Carlsbad, CA, USA) before being used in bioprinting. For bioprinting of a bi-layer structure with STO (bottom) and C2C12 (top), two separate bioinks were prepared by adding  $1 \times 10^7$  cells/mL of STO or C2C12 respectively, to the f-gelatin mixture and loaded into two separate 10 mL syringes for extrusion and printing. First, the STO encapsulated layer was printed, and crosslinked, atop which the C2C12 layer was deposited and crosslinked to generate a composite bi-cellular construct. These structures were then incubated with 5 mL of DMEM/F12 and incubated (37 °C, 5% CO<sub>2</sub>) for a duration of about 48 hr, following which they were fixed with paraformaldehyde (Sigma-Aldrich, St. Louis, MO, USA) for 30 min (25°C) and then permeabilized with 0.2% Triton X-100/phosphate buffered saline (PBS) for 15 min. After blocking with 1% bovine serum albumin (BSA/PBS, Sigma-Aldrich, St. Louis, MO, USA) for 30 min at room temperature, the samples were incubated with a mouse monoclonal antibody against Anti-MyoD1 antibody [5.2F] followed by a goat polyclonal secondary antibody to mouse IgG1 - heavy chain (FITC) (Abcam, Cambridge, UK). The STO cells were not labelled with any dye. The cells were then imaged using a confocal fluorescence microscopy (Olympus IX81 inverted fluorescence motorised microscope, Shinjuku, Tokyo, Japan) to confirm the retention of both cell types and their possible co-localization in a single plane of view, within the printed structure.

### ***4.3.1 Flow Cytometry (FACS)***

To estimate cell proliferation and overall biocompatibility of the printed construct, the cells were pre-stained with Cell Trace Violet (CTV), proliferation kit (Invitrogen, Carlsbad, CA, USA) in accordance with manufacturer's protocols. These pre-stained cells were mixed with the bioink ( $1 \times 10^7$  cells/mL) and printed into monolayer sheets and cultured for 24- and 72- hr respectively ( $37^\circ\text{C}$ , 5%  $\text{CO}_2$ ). After 24- and 72-hr, cell-gel samples were treated using Trypsin-EDTA (0.25%, phenol red) (Thermo Fisher Scientific, Waltham, MA, USA), following which cells were detached, extracted and processed for flow cytometry, by fluorescence assorted cell sorting (FACS). Flow cytometry works on the principle that greater dilution of the dye used to pre-stain the cells, implies that there are successive generations of proliferating cells. Extracted cells were fixed and processed further for FACS (Beckman Coulter Gallios Flow Cytometer, Brea, CA, USA) using excitation and emission wavelengths of 405 and 450 nm respectively. Pre-stained cells grown on plastic petri dishes for 72 hr were used as positive controls, while non-stained cells grown on plastic petri dishes for the same duration were used as negative controls.

## **4.4 Results**

### ***4.4.1 Material characterization***

#### ***4.4.1.1 Gross Morphology and Scanning Electron Microscopy (SEM)***

The en face images obtained by SEM revealed a striated, highly organized structure with repeating units. The cross-sectional images demonstrated a highly porous structure with an average apparent porosity of  $21 \pm 0.45$  %. The pores were observed to be homogeneously distributed and well interconnected and the average pore size was calculated to be  $142.20 \pm 1.08$   $\mu\text{m}$  (Figure 4.2).

The porosity measurements imply that the structure possesses significant porosity that would enable the effective intake of oxygen, nutrients and water during cell culture.

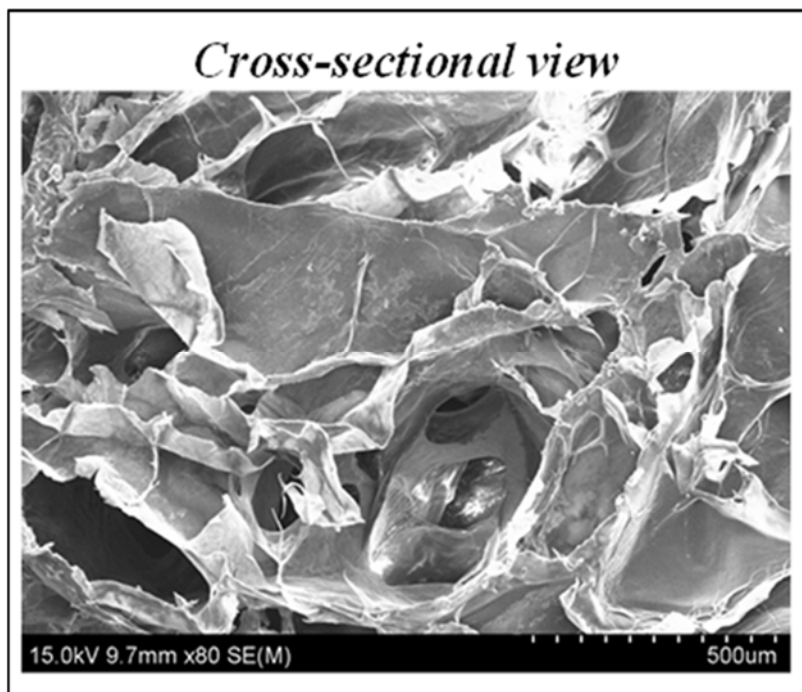


Figure 4.2: Representative image acquired using SEM of a printed sheet sample of f-gelatin after crosslinking

#### 4.4.1.2 Rheology

Rheology measurements revealed that the elastic modulus of the irradiated hydrogel was  $\sim 1.7$  kPa while that of the non-irradiated hydrogel was found to be  $\sim 1.4$  kPa (Figure 4.3). Additionally, the complex viscosity of the hydrogels was found to increase from 206.25 Pa-s to 319.7 Pa-s upon exposure to visible light validating the occurrence of the visible-light induced crosslinking mechanism. Elastic modulus and complex viscosity values are influenced by the additives present in the bioink and the time of exposure of crosslinking. These variables will be

investigated further in future studies to understand if stiffer hydrogels can be formulated by altering them.

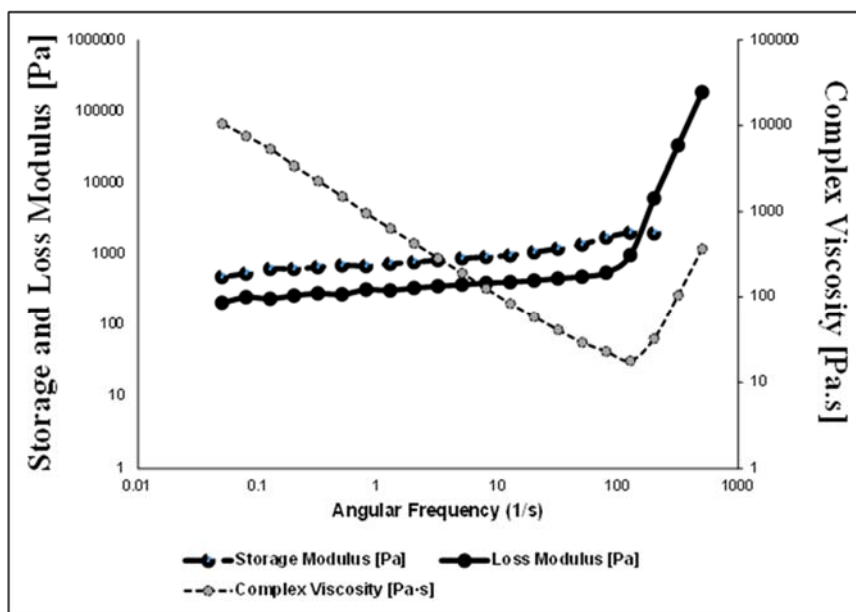


Figure 4.3: Rheology analysis of f-gelatin based hydrogels. Shown is a characteristic dataset obtained from a disc (8 mm diameter) punched out from a printed crosslinked f-gelatin hydrogel sample.

#### 4.4.1.3 Fourier Transform Infrared Spectroscopy (FTIR)

FTIR spectroscopy was performed to validate the formation of the crosslinked structure of f-gelatin, HA and RB upon irradiation with visible light. The FTIR spectra obtained is represented (Figure 4.4). As has been described in the reaction mechanism (Figure 3.2), the single double-bond formed within the furan ring of the crosslinked product corresponds to the band of C=C at  $1447\text{ cm}^{-1}$ . Other functional groups were also detected in the spectrum at different bands. The C-N stretching peak was found at  $2942\text{ cm}^{-1}$  and the C-O-C peak of the aryl ether was observed at  $1234\text{ cm}^{-1}$  in the crosslinked hydrogel and at  $1215\text{ cm}^{-1}$  in the non-crosslinked f-gelatin indicating a shift due to the formation of a new bond [97]. The aryl ether peak is depicted by bands at  $1039\text{ cm}^{-1}$  and  $1075\text{ cm}^{-1}$ . The broad peak at  $3000\text{-}3400\text{ cm}^{-1}$



represents the vibrational -OH stretching peak of the -COOH group present in HA. The absence of oxy-HA peak around  $1697\text{ cm}^{-1}$  in the crosslinked sample indicated that HA was not oxidized during the irradiation of the hydrogel with visible light [98]. The C-N stretching peak was present at  $1363\text{ cm}^{-1}$  in both pure HA and the crosslinked f-gelatin gel.

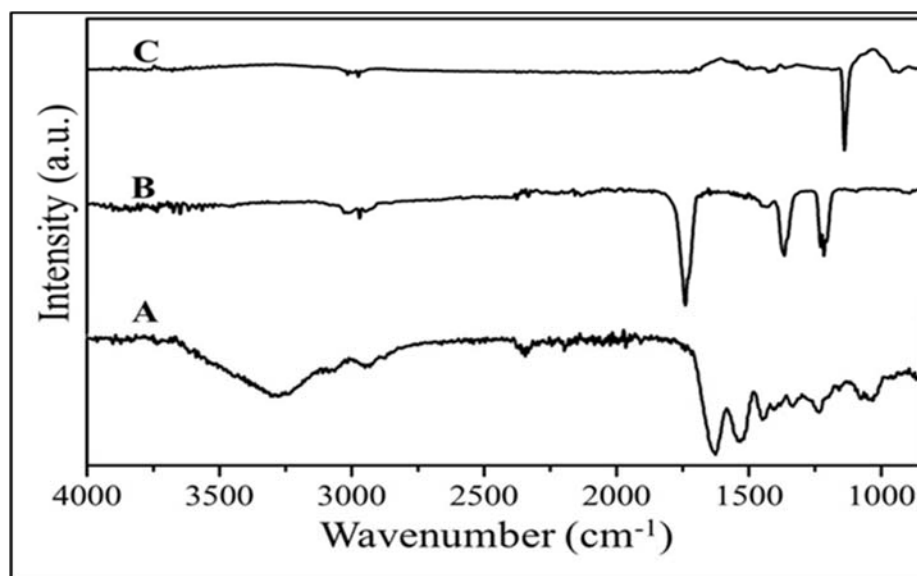


Figure 4.4: (A) FTIR spectrum of crosslinked f-gelatin in the presence of RB and HA. (B) FTIR spectra of f-gelatin and (C) of HA respectively.

#### 4.4.1.4 Swelling and degradation

The swelling behaviour of the f-gelatin based hydrogels has been depicted (Figure 4.5). As shown, the maximum swelling for all the samples tested was observed at 24 hr of incubation following which the swelling ratios remained relatively stable throughout the remaining incubation period of 5 days. Although the data reported only accounts for 5 days, the stored gels did not exhibit any visible signs of degradation for upto 21 days in culture. The results imply that the bioprinted crosslinked constructs can maintain their structural fidelity when implanted *in vivo* for a considerably long duration of time.

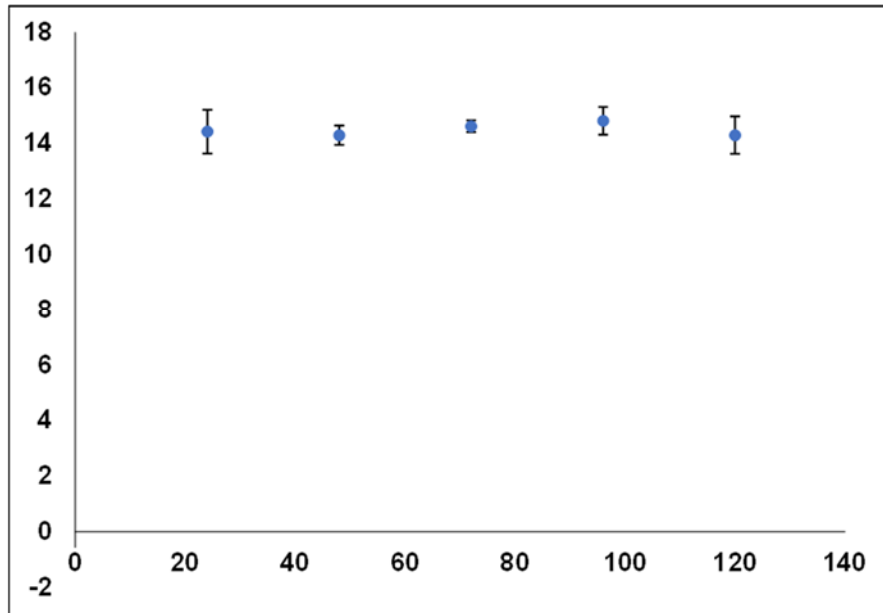


Figure 4.5: Degree of swelling of a printed sheet sample of f-gelatin after crosslinking.

#### 4.4.2 Biocompatibility

Densely packed Hoechst-dye stained cells (image not included) confirmed the viability of cells post printing thereby affirming that neither the printing process, the bioink mixture nor the crosslinking had adversely affected cell viability, post printing. This cell density appeared slightly reduced when samples were imaged after 5 days (Figure 4.6). This may be attributed to the swelling of the gels which allowed cells to migrate out of the structure into other areas of the tissue culture petri dish.

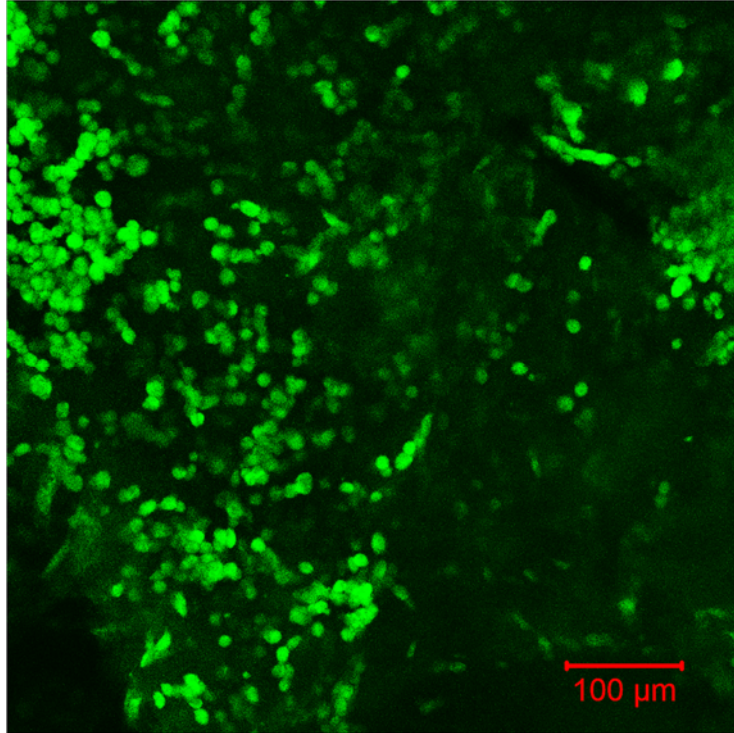


Figure 4.6: Retention of mouse MSC, pre-stained with PKH67 (green), within the bioprinted construct after 5 days of culture.

Pre-stained mouse MSC when printed within monolayer sheets, showed the evidence of cell retention after 5 days of culture (Figure 4.6, A.1.1) when stained with either PKH67 or PKH26. Similar results were also observed when the labelled mouse MSC (PKH26:red) were printed within bi-layer sheets and cultured for the same duration (A.1.1). There were no apparent differences in the cell density in both cases (A.1.1) even though cells in the bi-layer (bottom) were subjected to photo crosslinking by visible light for a longer duration (5 min) compared to the mono-layer (2.5 min). PKH67 labelled cells could not be used for visualization within the bi-layers, as the dye was also absorbed by the gels exhibiting high background fluorescence (images not included). The average area occupied by the cells was estimated to be  $33.8 \pm 9.91\%$  of the total area. The presence of a large number of viable cells, even after 5 days of incubation, proved that cells could survive the process of extrusion-based 3D printing, crosslinking and culture.

Confocal microscopy performed on bi-layered structures with STO fibroblasts (bottom layer) and the C2C12 myoblasts (top layer) showed evidence that the two cell-types were encapsulated within the same layer (Figure 4.7 (C, E)). It was observed that the STO cells were in the same plane as the C2C12 cells, although they were confined to their respective layers during

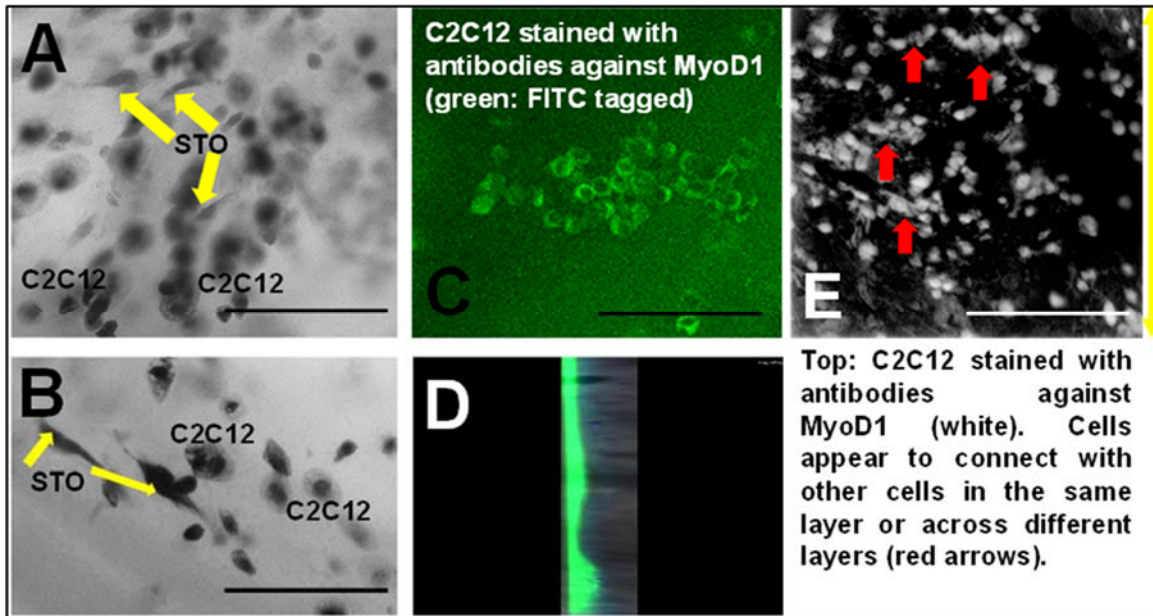


Figure 4.7: In A and B, shown are bright field z-scans of STO fibroblasts (elongated spindle shaped) co-cultured with C2C12 myoblasts cells (rounded enlarged, confirmed in C and in E). Scale bar is 150  $\mu\text{m}$  in A and B, and 200  $\mu\text{m}$  in C and E. In C, a single plane (cross section) was imaged whereas in E, a Z-scan was run spanning several planes as indicated with the arrow (right hand side). In D, shown is a single slice of z-stack section showing top layer (fluorescent green: C2C12) and bottom layer (non-fluorescent: STO)

the bioprinting process (Figure 4.7 (A, B), A.1.2). This probably was due to their interaction at the junction of the two layers containing two different cell types respectively.

The morphologies exhibited by both the C2C12 [99] and the STO [100] cells were in accordance with the images that have been reported in other published works. This data validated the feasibility of culturing two different cell-types separately within two different layers of the same bioprinted construct, that unified through cellular-crosstalk to form a single compact structure which did not break apart into two separate layers during culture and incubation.

#### *4.4.2.1 Flow cytometry*

Flow cytometric analysis was performed employing single parameter histograms depicting the percentage of proliferating cells as a function of dye intensity. The percentage cell proliferation was obtained by setting a gate within the histogram. Based on the results obtained from the flow cytometric analysis, it was observed that after 24 hr of culture, 9.1% (Figure 4.8 (A)), of the total number of cells which were encapsulated within the bioprinted construct had proliferated with respect to the unstained controls (0.3%) (Figure 4.8 (C)). Following 72 hr of culture, the number of proliferating cells was found to be 48.6% (Figure 4.8 (B)) when compared to the positive controls in which 32% of the total number of cells had proliferated (Figure 4.8 (D)), further validating the viability of the cells within the printed constructs and hence, the biocompatibility of the f-gelatin based bioink. Further, the occurrence of multiple peaks indicated the presence of successive generations of proliferating cells, within the bioprinted constructs. The reduction in the cell count from 24- to 72- hr could have been a result of them migrating away from the scaffolds, preventing their complete extraction from the printed constructs.

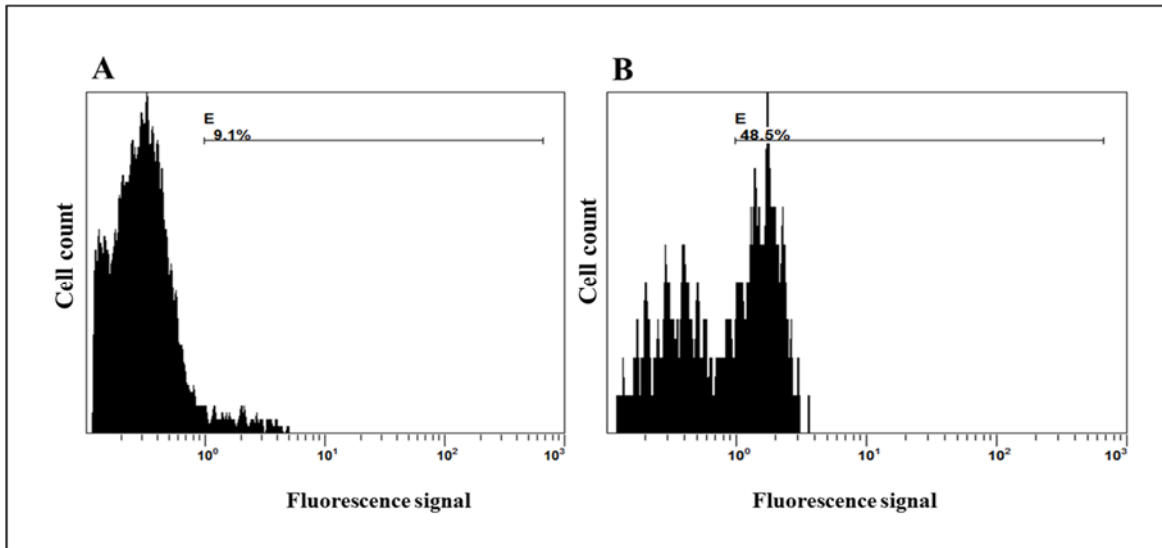


Figure 4.8: FACS analysis to show cell proliferation and biocompatibility of the printed sheet structures of f-gelatin after crosslinking. Cells pre-stained with CTV were cultured upto (A) 24 hr and (B) 72 hr within printed constructs. Positive controls were also used for both 24- and 72-hr.

#### 4.5 Conclusions

In conclusion, the applicability of f-gelatin as a novel, biocompatible bioink for biofabrication of cell-gel constructs with enhanced fidelity was demonstrated by this study. Although both synthetic and natural materials have been proposed to generate suitable tissue engineering grafts, the ideal material or scaffold for repair and regeneration of cardiac tissue is yet to be discovered [101]. The f-gelatin-based bioink optimized in this study could potentially be used for mimicking myocardial tissue, by printing layer-by-layer with the actual cardiac cells, namely cardiomyocytes, fibroblasts and endothelial cells [102]. This will aid in the generation of a functional cardiac patch that can be used for drug cytotoxicity screening [103], or exploring triggers for heart diseases in vitro [104].

## **Chapter 5: Comparison study to understand the effect of 3D bioprinted scaffold design on tissue engineering**

### **5.1 Introduction**

Scaffolds are materials that are engineered to stimulate desirable cellular interactions that can contribute to the formation of new functional tissues for medical purposes [105]. These structures are capable of supporting three-dimensional tissue formation and serve as templates onto which cells can be seeded. Scaffolds can mimic the extracellular matrix of biological tissues by recapitulating the in vivo milieu and allowing the cells to influence their own microenvironments [105]. Scaffolds are required to perform numerous functions such as allowing cell attachment and migration, delivery and retention of cells and biochemical factors, enabling the diffusion of vital cell nutrients and other expressed products and exertion of biological and mechanical influences to modify the behaviour of the cell phase, in addition to providing a structural framework and support to the cells seeded in them [106]. It is imperative that scaffolds meet some specific criteria in order for them to be able to achieve the goal of regenerating tissues effectively. High porosity and adequate pore size are essential in order to facilitate cell seeding and diffusion throughout the whole structures of both cells and nutrients [107]. Biodegradability is an important aspect since scaffolds should be preferably absorbed by the surrounding tissues without being surgically removed [108]. This necessitates the need for the rate of degradation of the scaffold to coincide with the rate of formation of the new tissue implying that while the cells fabricate their own extracellular matrix around themselves, the scaffold can provide structural integrity within the body and will eventually degrade allowing the newly formed tissue to take over the mechanical load [109]. Scaffolds also require to be injectable for clinical purposes.

In a prior study, f-gelatin, a furan-group incorporated derivative of porcine gelatin, was used in tandem with HA and RB to formulate a novel visible light crosslinkable bioink, that was successfully fabricated into bi-layered rectangular scaffolds infused with STO fibroblasts and C2C12 myoblasts [110]. As has been explained earlier, the crosslinking of the f-gelatin is facilitated by visible light irradiation during which molecular oxygen is converted into singlet oxygen species leading to the formation of a stable, cured f-gelatin structure after bioprinting and deposition [110]. These bioprinted cell-sheets were found to exhibit high fidelity during sustained in vitro culture and the encapsulated cells retained viability and exhibited heterocellular coupling [110]. Despite the favorable outcomes of the previous study, the versatility of the f-gelatin based bioink to create complex structures such as a lattice, which may serve as an enhanced physical scaffold and provide microarchitectural cues necessary for mimicking the native architecture of the myocardium remained unassessed. This served as a motive behind exploring the feasibility of 3D bioprinting a lattice mesh structure with the same f-gelatin based bioink and comparing it with the rectangular structure developed previously based on careful considerations of criteria like structural integrity, rheological properties, porosity and biocompatibility. It was hypothesized that the experiments performed as a part of this study would help highlight considerable differences between the two structures, i.e., lattice and rectangle, and also open up the possibility of significantly enhancing the design of a 3D bioprinted construct for engineering cardiac tissue-on-a-chip, using bioprinting.



## **5.2 Biofabrication**

The f-gelatin based bioink was made as has been described previously and loaded into 10 mL plastic syringes (Becton Dickinson, Franklin lakes, NJ, USA), with stainless steel blunt-tip dispensing needles (Huaha, Amazon, USA) for bioprinting. The printing parameters used were the same as described before. The .stl files for both the rectangular and lattice structures designed using SolidWorks, were converted into the g-code format using the Repetier Host program as done before and used to print on 100 mm x 15 mm petridishes (Thermo Fisher Scientific, Waltham, MA, USA). The dimensions of the lattice were 1.5 cm x 1.5 cm and the rectangular-sheet, 1.5 cm x 1 cm. Both structures were printed up to a thickness of 1 mm. After printing, the structures were irradiated with visible light for 2.5 min to facilitate chemical crosslinking at 100% intensity (Intelli-Ray 600, Uvitron International, West Springfield, MA, USA). Pluronic F127 was used to print complex structures which serve as positive control for structural comparison. For printing, pluronic was maintained at room temperature (25°C) until it freely flowed and then loaded into the syringe fitted with a 23G (0.34 mm ID) stainless steel blunt-tip dispensing needle and extruded using a high extrusion pressure in the range of 25.9–29 psi, following recommendations from Allevi.

## **5.3 Cell culture, characterization and viability within printed constructs**

Strain C57BL/6 Mouse Mesenchymal Stem Cells (mouse MSC, catalogue #: MUBMX-01001) were used to disperse in the “bioink” and printed into structures. For their culture, growth, and maintenance, Mouse Mesenchymal Stem Cell Growth Medium (complete growth medium, catalogue #: MUXMX-90011) was obtained from Cyagen (Santa Clara, CA, USA). Cells were

cultured and passaged according to the manufacturer's recommendations before they were mixed with the bioink and used to print as described earlier (Section 5.2).

The cell-laden, bioprinted, and crosslinked constructs of both lattice and rectangular-sheets were overlaid with complete growth medium for mouse MSC and cultured in an incubator (37 °C, 5% CO<sub>2</sub> and 95% RH) up to 72 hr. During this time, the culture medium was changed by removing the spent medium and by adding fresh growth medium after every 24 hr interval. From our previous study [110], it was shown that culturing the cell-laden constructs in this manner did not affect cell viability nor proliferation, even in the interior parts of the construct, as it was reasonably porous, allowing nutrient uptake and oxygenation [110]. Moreover, 3D cell printing has been shown to allow the effective generation of a cell-laden porous architecture that enables a sufficient supply of cellular nutrition and oxygen [111]. In addition, others have shown that porous 3D cell-printed patches exhibit a higher cell viability [111] than their non-3D printed counterparts.

### ***5.3.1 Live/Dead cytotoxicity assay***

The cytotoxicity assay was performed using a Live/Dead assay kit, to assess the biocompatibility of the f-gelatin bioink and the printing method [112]. Mouse MSC after being subjected to extrusion-based bioprinting and visible light crosslinking were subjected to the Live/Dead assay after about 15 min. First, the cell-laden structures were rinsed with 1X PBS thrice and supplemented with pre-warmed complete growth medium for an additional 15 min. Next, the growth medium was removed, and the samples were incubated with pre-warmed cytotoxicity reagent (Live/Dead Cytotoxicity Assay Kit Green/Red Staining). A sufficient amount of the reagent was added to cover the samples during the incubation process, for which the samples were placed back into the incubator for 45 min. After incubation, the samples were washed using 1X PBS and imaged using light and confocal microscopy (ZEISS LSM 700 Confocal, Oberkochen,

Germany). Acquired images were analyzed using Image J (NIH, Bethesda, MD, USA) and the number of live or dead cells per unit area was reported as the Mean  $\pm$  Std. deviation.

### **5.3.2. Cell Proliferation**

For an estimation of the actual cell numbers in a sample at different time points, lattice structures printed with cells and cultured as described earlier were carefully rinsed with PBS, overlaid with a generous amount of 0.25% trypsin-EDTA, and incubated at 37 °C for 10 min in an orbital shaker (45 rpm). Cells extracted from the first-trypsinization cycle were pelleted by centrifugation, added with other cells that were removed in a second cycle of trypsinization, and counted using a haemocytometer throughout the entire culture period after 24- and 48-hr of culture. Absolute cell densities extracted from samples at 24- and 48-hr are reported.

#### *5.3.2.1 Flow Cytometry Analysis (FACS)*

For the estimation of cell proliferation in the bioprinted lattice and rectangular-sheet structures, the cells were pre-stained with the Cell Trace Violet (CTV) proliferation kit as per the manufacturer's protocols [66, 110]. Briefly, 1:5000 dilutions were used for the CTV dye in this study, for pre-staining cells. These pre-stained cells were mixed with the bioink ( $2 \times 10^5$  cells/mL) and printed into a lattice or rectangular-sheets and cultured for 24- and 72-hr, respectively (37 °C, 5% CO<sub>2</sub>). After 24 and 72-hr, cell-gel samples were treated using Trypsin-EDTA (0.25%, phenol red), after which the cells were detached, extracted, and processed for flow cytometry (FACS). Extracted cells were fixed and processed further for FACS (Beckman Coulter Gallios Flow Cytometer, Brea, CA, USA) using excitation and emission wavelengths of 405 and 450 nm, respectively. Positive controls comprised of pre-stained cells ( $1 \times 10^5$  cells/mL) grown on plastic

petri dishes for 24- and 72-hr, respectively. Negative controls included non-stained cells grown on plastic petri dishes for 24- and 72-hr, respectively.

## 5.4 Results

### 5.4.1 Material Characterization

#### 5.4.1.1 Gross Morphology and Scanning Electron Microscopy (SEM)

Digital images of the printed rectangular and lattice sheet structures printed using both f-gelatin and pluronic were acquired using an upright Leica M205C microscope (Microsystems, Buffalo Grove, IL, USA) to compare and contrast the overall morphology and to identify the essential dissimilarities in the two structures.

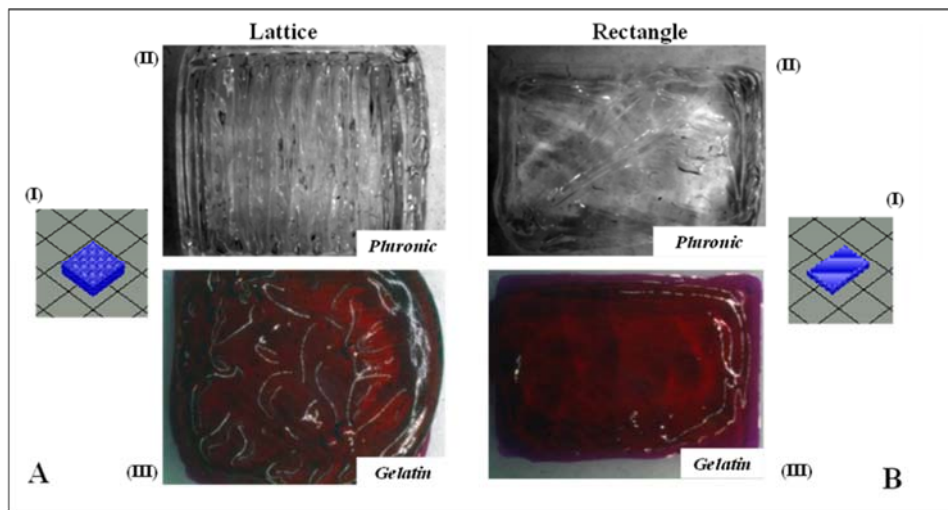


Figure 5.1: Gross Morphology of lattice (1.5 cm x 1.5 cm) and rectangular-sheet (1.5 cm x 1 cm) structures printed using pluronic and gelatin. (AI, BI) depict the stl. file image for the lattice and rectangular structures, respectively. (AII, BII) represent the en-face images for the same structures printed using Pluronic F-127. (AIII, BIII) are representations of the en face images for lattice and rectangular patterns printed using the f-gelatin-based bioink, respectively.

The images revealed that the rectangular sheets printed using both f-gelatin and and pluronic appeared similar in terms of dimensions and morphology (Figure 5.1 (BII, III)). However, there were significant differences between the lattice structures printed using the two gels as depicted (Figure 5.1 (AII, III)). The stereolithography (stl.) designs used for printing are shown in Figure 5.1 (AI, BI), respectively. The pluronic lattice structure retained the structural complexity and fidelity of the lattice to a greater extent, when compared to the f-gelatin-based structure (Figure 5.1 (AII, III)).

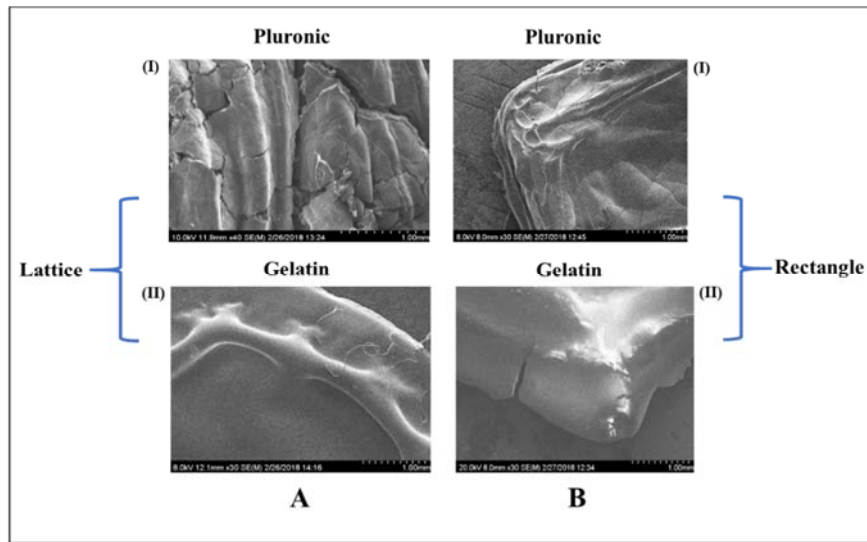


Figure 5.2: Representative SEM surface images of lattice and rectangular-sheet structures deposited using pluronic and gelatin. (AI, II) show the en-face images for the lattice structures printed with Pluronic-F127 and the f-gelatin-based bioink, respectively. (BI, II) depict the en face images for the rectangular structures printed using the same materials, respectively.

En face images of both the lattice and rectangular sheet structures printed using both f-gelatin and pluronic showed significant differences in the lattice structures only (Figure 5. 2 (AI, II) while the rectangular sheets bore structural resemblance (Figure 5.2 (BI, II)).

The SEM cross-sectional image of the gelatin lattice exhibited a highly organized, striated, patterned, and networked structure (Figure 5.3 (A)) in comparison to the loosely networked and largely porous rectangular-sheet cross-sectional SEM (Figure 5.3 (B)), as has been reported.

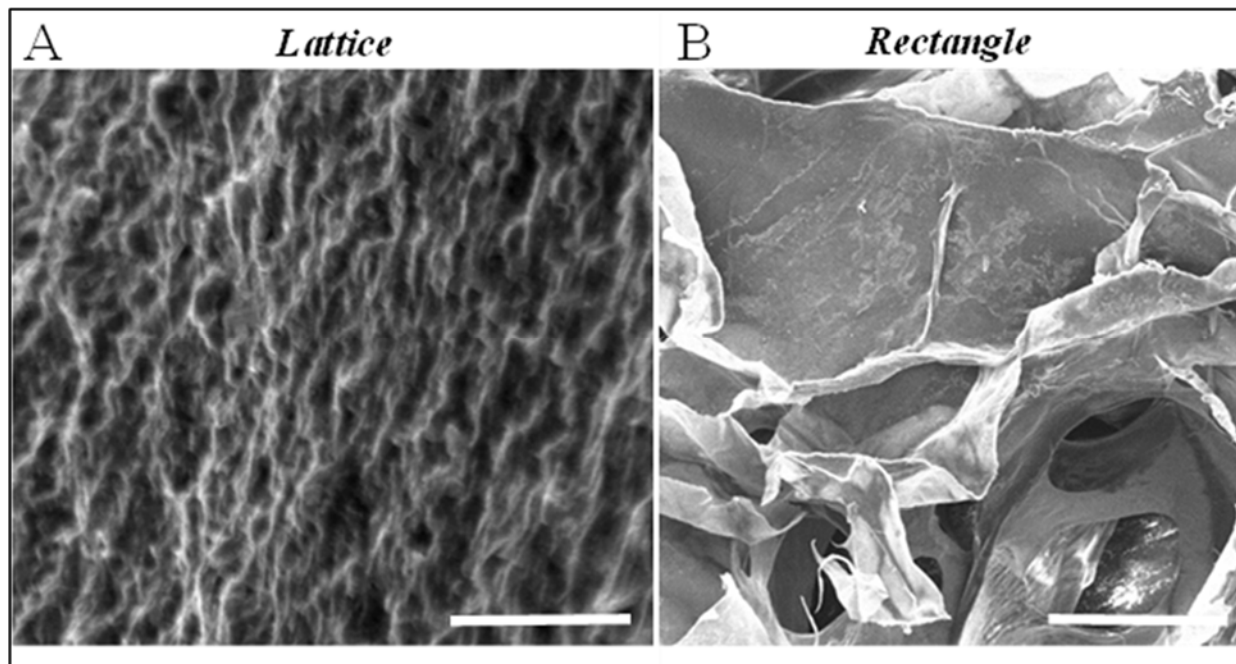


Figure 5.3: A representative SEM cross-section image of a gelatin lattice structure that was acquired in order to determine the apparent porosity and average pore size (A). The cross-sectional SEM image for the rectangular-sheet structure printed using f-gelatin was previously reported (B) [110]. The scale bars represent 5  $\mu\text{m}$  and 500  $\mu\text{m}$  in A and B respectively.

previously [110]. Porosity and pore-size are crucial to ensure cell colonization of the scaffold, deposited using bioprinting. Likewise, SEM micrographs showed a homogeneous distribution of equal sized pores within the entire area scanned and imaged (Figure 5.3 (A)). Furthermore, the cross-sectional SEM image also depicted highly interconnected pores with a mean value of  $\sim 1 \mu\text{m}$  (Figure 5.3). This was significantly smaller compared to the average pore size of the rectangular-sheet structures that was reported previously (Figure 5.3 (B)) [110]. The average apparent porosity of this lattice structure was estimated to be about 50% compared to 21% for the rectangular-sheet

[110]. The results led to the conclusion that although the mean pore size was significantly reduced by printing in the form of lattice, the inherent design of the lattice allowed pores to be uniformly sized and to be homogeneously distributed throughout the entire structure, with respect to the rectangular structure.

#### 5.4.1.2 Rheology

As per the data obtained from the rheology analysis, the lattice structures exhibited an elastic modulus of  $5.5 \pm 2.4$  kPa and complex viscosity of  $920 \pm 400$  Pa.s (Figure 5.4), both of which were significantly higher,  $\sim 5$  times, than the respective values of the rectangular sheet structure as reported in a previous study [110].

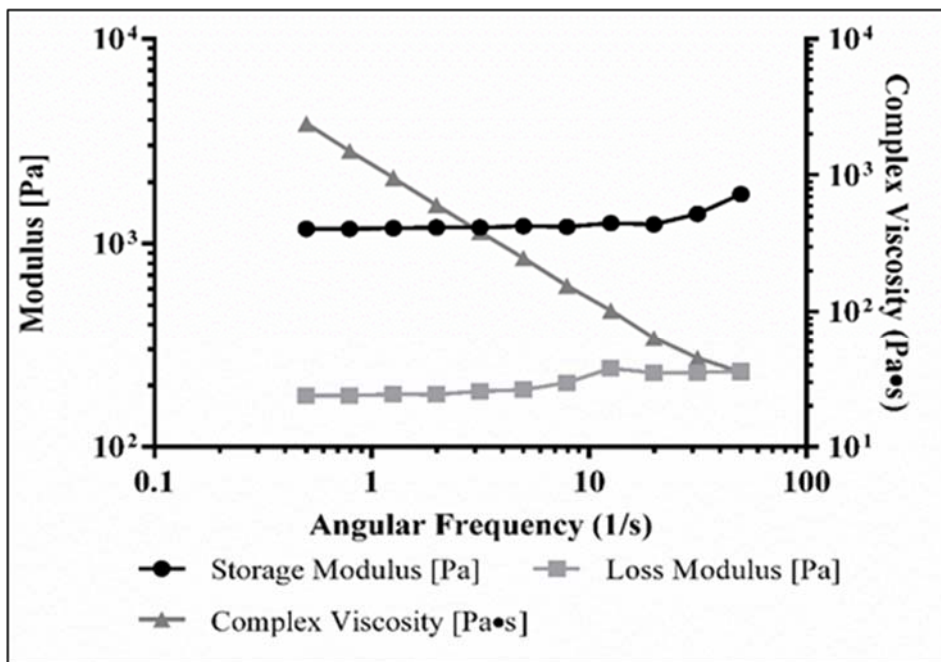


Figure 5.4: Rheology analysis of f-gelatin-based lattice structures obtained from a disc-shaped (8 mm diameter) sample.

These results implied that although the bioink material composition and the crosslinking mechanism were kept unchanged, the lattice geometry actually enhanced the stiffness and mechanical properties of the printed structures. However, the larger error is due to the fact that the lattice structures were macroporous and hence, more difficult to measure with shear.

#### *5.4.1.3 Swelling and Degradation*

The swelling behavior of the bioprinted lattice and rectangular crosslinked hydrogels is shown in Figure 5.5. The maximum swelling was observed at 24 hr for all the samples tested as has been reported previously [110]. After 24 hr of incubation, the structures showed signs of slight degradation, as evidenced by 48 hr (Figure 5.5 (A)).

However, the lattice structure seemed to have reached an equilibrium point after 48 hr as it did not exhibit any further degradation beyond 48 hr, when analyzed at 72 hr (Figure 5.5 (A, B)). On the other hand, the rectangular-sheet continued to degrade beyond 48 hr, when analyzed at 72 hr (Figure 5.5 (A, B)).

These observations confirmed indicated that the lattice structures exhibited a lower degree of swelling compared to the rectangular-sheets and these results indicated that the lattice possessed a more stable structure compared to the latter (Figure 5.5 (A, B)). No significant differences in trends between both structures were noted. Although the data reported was from three days of observation and analysis, the stored gels did not degrade until six days in culture following this observation.



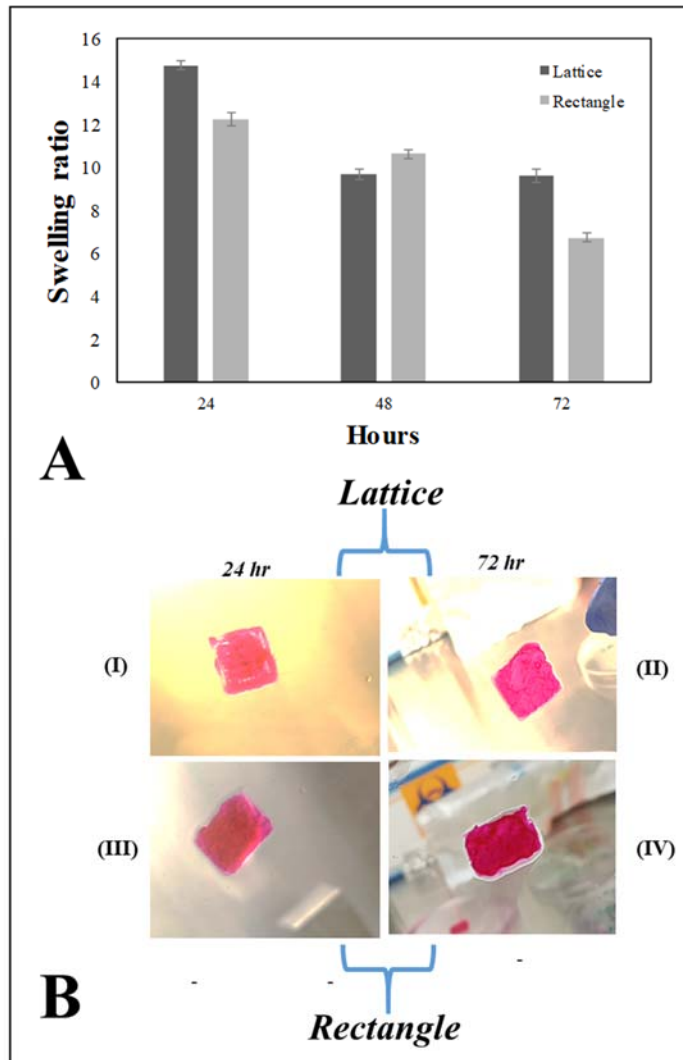


Figure 5.5: (A) Swelling analysis for both the f-gelatin-based lattice (1.5 cm x 1.5 cm) and rectangular-sheets (1.5 cm x 1 cm) over a period of three days after being subjected to visible light crosslinking. (B) Shown above in (BI,II) is cell-laden lattice constructs. In (BIII,IV) is cell-laden rectangular-sheet constructs. (BI,III) was acquired after 24 hr of culture. (BII,IV) was acquired after 72 hr of culture. No significant differences in the degradation rates of both structures were evident at 72 hr of incubation.

### 5.4.2 Biocompatibility

As per the Live/Dead assay results, there were fewer dead cells when compared to the live cells, encapsulated within the lattice structure after it was printed and crosslinked (Figure 5.6). The number of viable cells was significantly more ( $p = 0.03$ ) at  $22 \pm 5$  per unit area ( $12 \times 10^4$  sq. microns) as opposed to the number of dead cells that was estimated to be about  $6 \pm 2$  per unit area. The average percentage cell-viability was calculated to be about 81.48% in comparison to a low percentage of cell death, averaging only 22%. These results were in accordance with the findings of others during extrusion-based cell bioprinting [113].

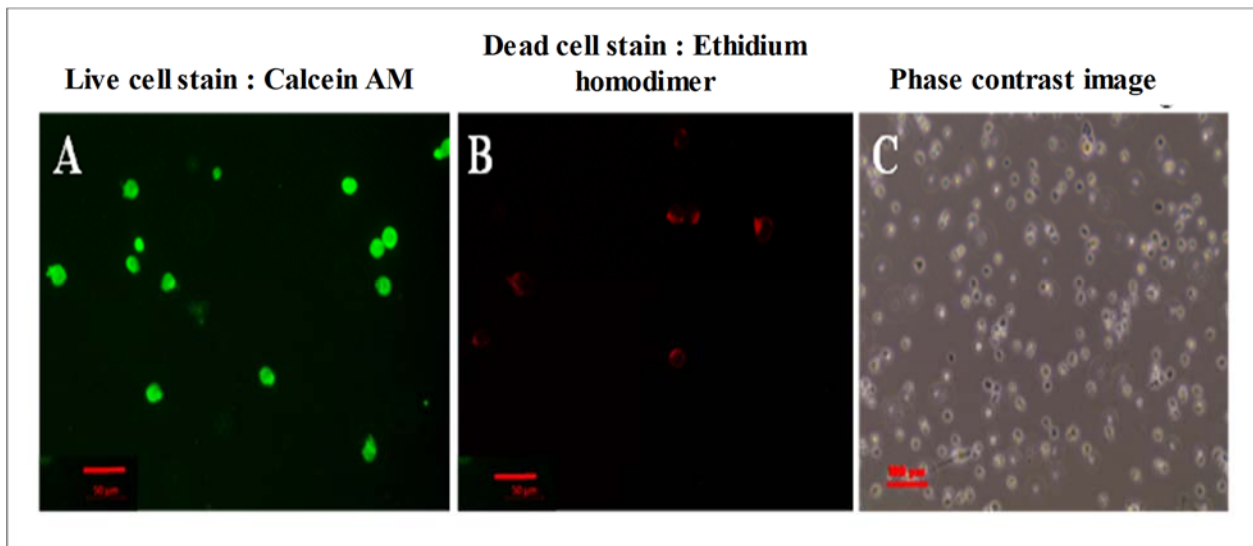


Figure 5.6: Live/Dead assay performed 15 min after printing and crosslinking. Shown in (A) are calcein stained live cells and in (B) are ethidium homodimer stained dead cells, respectively. In (C), a phase-contrast image of cells cultured for this experiment is shown.

SEM images of cells in lattice structures revealed confluent cell populated surfaces as depicted in Figure 5.7 (A, B). Moreover, there was also a significant amount of extracellular matrix (pointed using white block arrows) deposited by cells, that was noted in all representative images

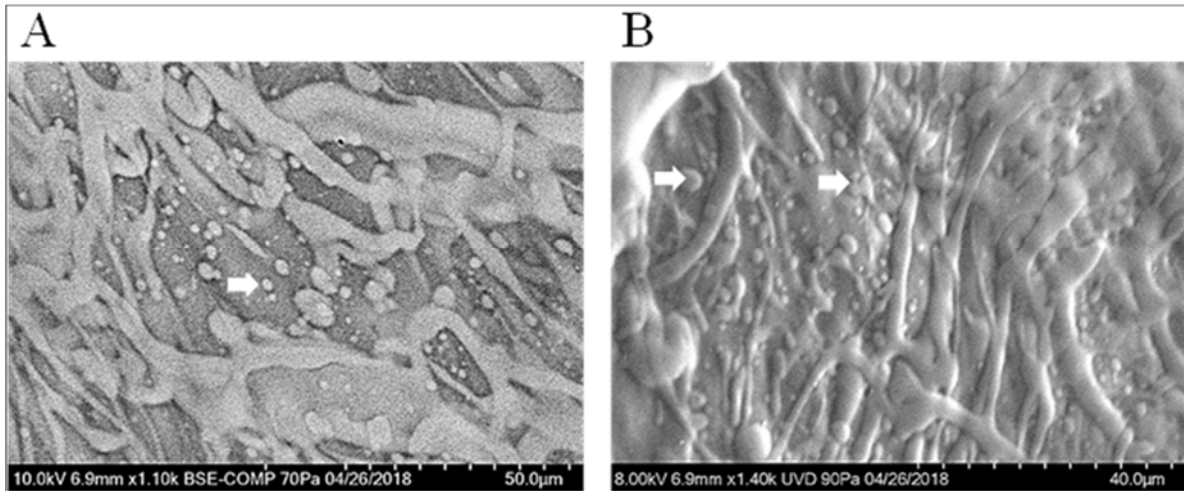


Figure 5.7: Shown in (A, B) are characteristic images of mouse MSC printed in lattice structures. Elongated cell morphologies and the extensive coverage area by the cells both confirm the biocompatibility of the lattice design and the bioink used. White arrows point to the extracellular matrix deposited by the cells cultured.

(Figure 5.7 (A, B)), as is also supported by previously published work [66]. These results indicated that the lattice is a favorable scaffold design permissive towards cell growth and proliferation, owing to its macroporosity.

#### 5.4.2.1 Flow cytometry

Flow cytometric analysis was performed to estimate the cell proliferation in both the lattice and rectangular printed structures. The results obtained indicated that the cells that were encapsulated within the lattice structure showed enhanced proliferation when compared to those seeded in the rectangular-sheet after 3 days of culture from 24- to 72- hr (Figure 5.8). This was because the Gated X-A mean value, which is a measure of the dye intensity, was significantly

reduced in its value from 24- to 72- hr (Figure 5.8 (A, B)) in cells cultured within the lattice (1.23 versus 0.44, respectively) indicating dilution of the dye due to increasing generations of cells within the same culture. The Gated X-A mean values for the cells seeded in the rectangular-sheet structure did not show differ significantly from 24- to 72- hr of culture (Figure 5.8 (C, D)) (0.60 versus 0.62, respectively). Additionally, the occurrence of multiple peaks confirmed the presence of consecutive proliferating generations of cells within the bioprinted structures. Additionally, the multiple peaks confirmed the presence of consecutive proliferating generations of cells within the bioprinted structures. CTV stained cells cultured on plastic for 24- to 72- hr served as positive controls and showed enhanced dye dilution and cell generations for the duration of culture as depicted by Gated Mean-X values (A.1.3).

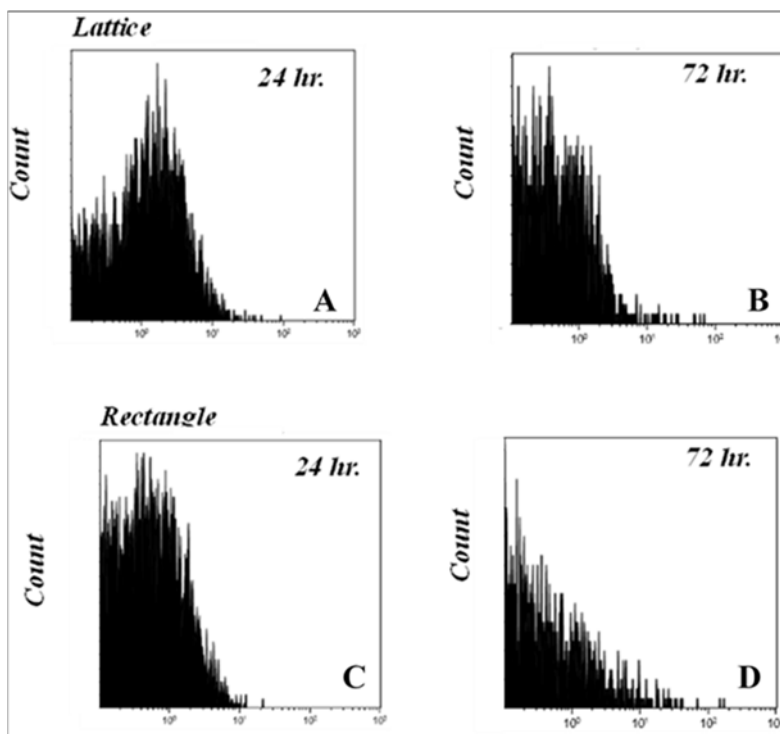


Figure 5.8: FACS analysis to show cell proliferation and biocompatibility of the printed and crosslinked lattice and rectangular-sheet structures, respectively. Cells pre-stained with CTV were cultured up to 24 and 72-hr within printed constructs, respectively.

In a nutshell, the lattice structures allowed cells to connect and communicate better, resulting in more enhanced cell growth indicated by the greater extent of dye dilution, compared to the rectangular-sheet structures. These results were cross verified from absolute cell counts, as described earlier. For the 3D printed constructs,  $2 \times 10^5$  cells/mL were used for cell encapsulation. Since the lattice had a larger volume (1.5 cm x 1.5 cm x 1 mm) than the rectangular sheet (1.5 cm x 1 cm x 1 mm), more cells could be encapsulated within the lattice compared to the rectangle when analyzed after 24 hr, at which time the lattice revealed a cell density of  $4.2 \times 10^5$  cells/mL, when compared to the rectangular sheet which had a value of  $2.4 \times 10^5$  cells/mL. After 72 hr, cells in both samples had proliferated about four times compared to the initial cell seeding density. In a previously published study [110], the CTV dye was used at a 1:1000 dilution and so the proportional decrease in the intensity of the dye with enhancing cell populations could not be well detected. So, in this study, a 1:5000 dilution was applied in order to detect the proportional decrease in the intensity of the dye, as expressed by generations of proliferating cells.

## **5.5 Conclusion**

In this study, lattice mesh geometries were printed in a comparative study to test against the properties of a traditional rectangular-sheet. After 3D printing and crosslinking, both structures were analysed for swelling and rheological properties, and their porosity was estimated using scanning electron microscopy. The results showed that the lattice structure was relatively more porous with enhanced rheological properties and exhibited a lower degradation rate compared to the rectangular-sheet. Additionally, the lattice allowed cells to proliferate to a greater extent with respect to the rectangular-sheet, which retained fewer cells. All of these results collectively affirmed that the lattice poses as a superior scaffold design for tissue engineering applications.

## **Chapter 6: Development of a fibrin-gelatin based bioink for the fabrication of “cardiac patches”**

### **6.1 Introduction**

In the previous studies, f-gelatin had been successfully employed to develop novel, visible light crosslinkable bioinks that could be 3D bioprinted into scaffolds that could ensure cell viability and proliferation [110]. Despite the success of the experiments with different cell-types such as STO fibroblasts, C2C12 myoblasts and mouse MSC, the elastic modulus of the crosslinked f-gelatin hydrogel generated by the rheological analysis was found to be 1.7 kPa [110] was staggeringly low as compared to the elastic modulus of the native myocardium tissue which has been reported to be ~9kPa according to existing literature [114]. This necessitated an immediate need to select a new biomaterial to be used in tandem with the f-gelatin based hydrogel mixture, targeted towards developing a scaffold with an elastic modulus closely mimicking the mechanical properties of the native heart tissue. The extensive and widespread usage of fibrin as a surgical sealant [115, 116] and its applications as a scaffold material in tissue engineering [117] made it the most obvious choice to be used as an additive to the existing f-gelatin hydrogel for the development of a cardiac construct. Numerous studies conducted by other research groups have established the efficacy of employing fibrin glue as an injectable scaffold that could preserve the infarct wall thickness and the cardiac function following myocardial infarction in rats making it useful as a biomaterial scaffold in myocardial cell transplantation [118]. There is also literary evidence validating the utility of fibrin-based scaffolds for delivering CM to the myocardium [119]. The present study incorporates fibrin into the previously mentioned based bioink to test its feasibility as a scaffold for the culture of CM as it is known to promote vascularization [120], envisioning a future in vivo application of this lab-engineered cardiac construct. HA was excluded

from the fibrin-gelatin based hydrogel mixture as it had only been used as a viscosity enhance in the previous studies and it was not chemically crosslinked within the bioprinted construct.

The fibrin-gelatin based hydrogel was formulated as described under the Biofabrication section and used to print as explained in earlier chapters. The printed constructs were subjected to a dual step cross-linking process, first by exposing them to visible light to facilitate the cross-linking of the f-gelatin, followed by the addition of a thrombin-CaCl<sub>2</sub> solution to the samples to induce the cross-linking of fibrinogen to form fibrin. The acellular scaffold was characterized using material analysis techniques as done previously [110]. This fibrin-gelatin based bioink was used to bioprint human induced pluripotent stem cells (iPSC)-derived CM or human CM cell lines to show their cytocompatibility.

## **6.2 Biofabrication**

The ALLEVI 2 (formerly known as BIOBOT 1, Allevi, Philadelphia, PA, USA), employed in previous studies, was used to bioprint the fibrin-gelatin based scaffolds. 1 mL of the fibrinogen-gelatin bioink was formulated by weighing out 155 mg of f-gelatin and adding it to 990  $\mu$ L of 60 mg/mL fibrinogen solution (made as described in Materials and Methods) at 25°C. The mixture was then heated at 37°C for about 1 hr with stirring to facilitate the formation of a homogenous and viscous mixture. RB (10  $\mu$ L) was subsequently added as a photo sensitizer and mixed homogeneously with the existing bioink mixture [110]. Optimization of the fibrinogen solution and f-gelatin concentrations for making the bioink, has been tabularised (Table 6.1).

Table 6.1: Optimization of the fibrin-gelatin based bioink

S.no.	Fibrinogen	Gel-fu	Rose Bengal (RB)	State of the bio ink	Observations post printing
1	1 mL of 60 mg/mL	150 mg	50 mg (5% w/v as per our previous study [110])	Highly viscous with clumps, in addition black lumps were noted	The printed structure was incomplete and discontinuous, but sample did not degrade for four days.
2	1 mL of 60 mg/mL	100 mg	50 mg	Less viscous than #1, but clumps were present	The printed structure was incomplete and discontinuous, but the sample did not degrade for four days.
3	990 $\mu$ L of 60 mg/mL (~59.4 mg/mL)	155 mg	10 $\mu$ L solution aliquot from a stock of 5 % (w/v)	The solution appeared to have sufficient viscosity to enable printing.	Printed a clear rectangular sheet easily and structural fidelity was maintained for four days.
4 <b>Control</b>	1 mL of 60 mg/mL	150 mg of porcine gelatin	None used	Looked ideal for printing. Not too thick or watery.	Printed a neat two-layered sheet however, the structure dissolved much earlier than the above samples.

The concentration of fibrinogen solution used in the present study, 60 mg/mL was based on a previous experiment [121]. Cui et al. demonstrated that the best polymerization result obtained via bioprinting was observed with 60 mg/mL fibrinogen, 50 units/mL thrombin, and 80 mM CaCl<sub>2</sub> [121]. Cells were added to this bioink mixture, as explained later. These results served as the basis



for our present study as lower concentrations of fibrinogen solution (50 mg/mL), did not yield bioinks that could be printed.

The bioink mixture was loaded into a 10 mL plastic syringe (BD, Franklin lakes, NJ, USA), fitted with a stainless steel blunt-tip dispensing needle (Huaha, Amazon, USA), as done before and extruded using a low extrusion pressure (18 - 25.5 kPa). Patterns printed using this bioink were designed using SolidWorks and saved as .stl files. The structures were square-shaped having dimensions of 1 cm x 1 cm and a thickness of 500  $\mu$ m and were printed on 100 mm x 15 mm petri-dishes (Thermo Fisher Scientific, Waltham, MA, USA). The .stl file used for printing was uploaded to the Repetier Host program available via the Allevi server and converted into a g-code. The g-code file was then uploaded and used to print structures which were subjected to a dual step cross-linking process, first by exposing them to visible light for an optimized duration of 2.5 min at 100% intensity (Intelli-Ray 600, Uvitron International, West Springfield, MA, USA), based on our previous study [110]. Next, the chemical crosslinking of fibrinogen into fibrin was induced by treating the printed constructs with a 1 mL solution comprised of 900  $\mu$ L of 80mM CaCl<sub>2</sub> and 100 $\mu$ L of thrombin in PBS at a concentration of 50 units/mL, for about 20 min.

### **6.3 Cell culture, characterization and viability in the bioprinted constructs**

#### ***6.3.1 Live/Dead Cytotoxicity assay***

Human induced pluripotent stem cell (iPSC)-derived cardiomyocytes (CM) were procured from Axol Bioscience (Cambridge, UK) and human CM AC16 cell lines (ATCC, Manassas, VA, USA) were cultured and stabilized before experiments. For the human iPSC-derived CM, cells were bioprinted and cultured for a day for testing the compatibility of the printing technique and

the fibrin-gelatin based bioinks for primary cell culture, viability and retention. About  $2 \times 10^5$  cells/mL were added and printed within casted 3D patterns, and incubated (37 °C, 5% CO<sub>2</sub>). Controls, seeded in 2D wells (24 wells) received  $5 \times 10^4$  cells/mL. This difference in cell seeding density was because cells in 3D structures occupied a larger volume compared to their 2D controls. After 24- and 72- hr respectively, the cultures were analyzed using a Live/Dead assay (Thermo Fisher Scientific, Waltham, MA, USA) with Calcein AM (green) and Ethidium homodimer (red) that stained the live and dead cells, respectively. After 24 hr of culture, the cell laden constructs were processed for immunohistochemistry and stained with antibodies against Troponin T (Anti-Cardiac Troponin T antibody [1C11], Abcam, MA, USA) to validate their functionality and cardiac specific characteristics in bioprinted constructs as described in later sections.

A similar procedure was carried out for the human CM AC16 cells that were seeded and then subjected to the Live/Dead assay. All Live/Dead stained cells were then imaged using a confocal fluorescence microscopy (Olympus IX81 inverted fluorescence motorized microscope, Shinjuku, Tokyo, Japan) to confirm the retention of viable cells within the bioprinted structures.

As a means to validate the cardiac smooth muscle specificity of the human CM AC16 lines, the cells were immunostained with Myocardin (Myocd: Novus Biologicals, 1:200) antibody to confirm their phenotype as well as their sarcomeric organization (A.1.9). Additionally, the integrity of the CM was confirmed by co-immunostaining with Troponin T (TrpT:Cell Signaling, 1:300), which is a characteristic cardiac biomarker [122].

### ***6.3.2 Cell viability and orientation within the printed constructs***

The biocompatibility of the fibrin-gelatin based bioink was tested by probing the human CM encapsulated within this mixture for their expression of Troponin I, a cardiac marker after

sustained in vitro culture. At the end of culture, the cells in bioprinted constructs were fixed with 4% paraformaldehyde (Sigma-Aldrich, St Louis, MO, USA) for 15 min (25 °C). Post fixation, these cell-laden constructs were permeabilized with 0.2% Triton X-100/PBS for about 1 hr. After blocking with 1% normal goat serum (NGS/PBS, Sigma-Aldrich, St Louis, MO, USA) overnight at 4 °C, the samples were incubated with a rabbit Polyclonal Antibody to Troponin I (at a dilution of 1:1000, 24 hr at 4 °C) followed by an anti-rabbit secondary antibody at a concentration of 1:4000 (2 hr at 25 °C) (Thermo Fisher Scientific, Waltham, MA, USA). The samples were then rinsed with 1X PBS thrice and mounted using Fluoromount-G with DAPI (Thermo Fisher Scientific, Waltham, MA, USA) and imaged using confocal fluorescence microscopy (Olympus IX81 inverted fluorescence motorized microscope, Shinjuku, Tokyo, Japan). Acquired images were processed using Image J to assess the preferential cell orientation along the printing direction in comparison with non-bioprinted samples (as detailed in the Appendix (A.1.4))

In order to confirm the viable cell encapsulation within the bioprinted constructs, the CM were labeled with PKH26 red fluorescent membrane staining dye (Sigma-Aldrich, St. Louis, MO, USA), prior to addition in the bioink mixture, as done before [110] and imaged after 24 hr of culture ,without fixing the cells in the gel-samples, using confocal fluorescence microscopy (Zeiss, Oberkochen, Germany). Cytotoxicity of the Rose Bengal in the bioink was assessed by determining the cell viability tracked over a period of five days, as explained in the Appendix (A.1.4)

## **6.4 Results**

### ***6.4.1 Material Characterization***

#### 6.4.1.1 Gross morphology and Scanning Electron Microscopy (SEM)

The square structure was constructed using CAD software and converted into a .stl file, which was adopted to print the fibrin-gelatin based cardiac constructs. The .stl file depicts the herringbone pattern, so named due to its resemblance to the cardiac muscle tissue [123]. The gross morphological en face SEM image of a 3D printed square pattern fabricated using the fibrin-gelatin bioink was captured as shown (Figure 6.2 (A)). The architecture of the design was maintained through a dual cross-linking procedure, as described earlier. An actual pattern deposited by the 3D bioprinting process is also shown (Figure 6.1 (B)).

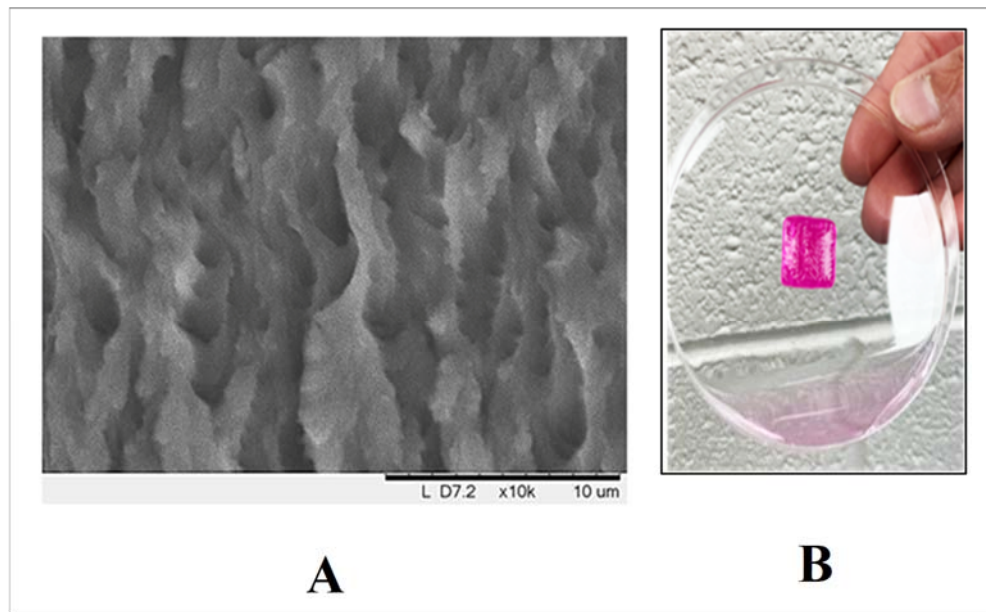


Figure 6.1: Gross Morphology of the structure printed using the fibrin-gelatin based bioink.

(A) Depicts a representative SEM en face image of a characteristic 3D printed pattern (B)

Depicts bioprinted herringbone construct.

Specifically, the bioprinted cell-laden construct was irradiated with visible light for 2.5 min at 100% intensity (Intelli-Ray 600, Uvitron International, West Springfield, MA, USA), based on parameters optimized during our previous study [110]. Next, the structure was treated with a 1mL

thrombin-calcium chloride ( $\text{CaCl}_2$ ) solution for 20 min, to chemically cross-link fibrinogen into fibrin. A representative cross-sectional image of a printed square pattern acquired by SEM as shown in (Figure 6.2 (A)) indicated a porous geometry with interconnected pores that appeared to be well distributed and equi-sized. A representative cross-sectional image of a f-gelatin based rectangular printed pattern generated by SEM is shown in Figure 6.2 (B), for comparison. The average pore diameter (end-to-end-length) was determined to be  $9.54 \pm 0.98 \mu\text{m}$  for the fibrin-gelatin based constructs, in comparison with  $15.62 \pm 3.05 \mu\text{m}$  for the f-gelatin patterns. These values were significantly different with a  $p=0.0032$ .

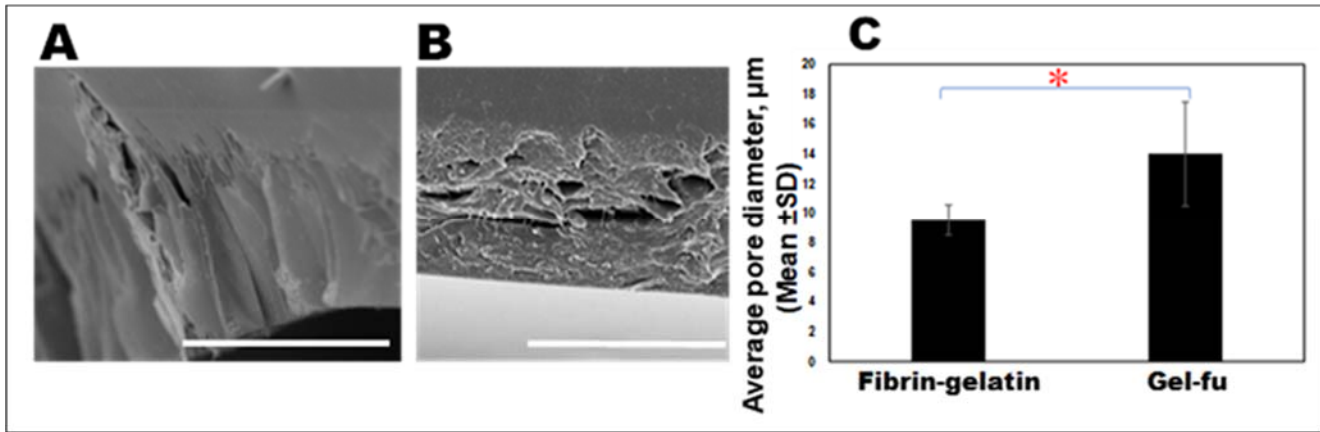


Figure 6.2: SEM analysis for pore size estimation. (A) A representative SEM image of the edge of a characteristic fibrin-gelatin film. At least 5 representative images were acquired per sample and used to determine the average pore size depicted in (C), in comparison with the f-gelatin structures as depicted in (B). (C) Depicts a plot comparing the average pore diameters for the fibrin-gelatin (current study) and f-gelatin (gel-fu) based constructs [110]. In (A) scale bar corresponds to  $50 \mu\text{m}$  and in (B) corresponds to  $20 \mu\text{m}$ .

The results implied that enhancing the cross-linking density of gelatin using fibrin would decrease its porosity compared to gelatin [92]. However, the average pore size of these scaffolds is in the permissible range for cardiovascular tissue engineering and angiogenesis as per earlier

publications [107, 124]. A comparative analysis of the average pore sizes of the fibrin-gelatin based square pattern and the gelatin-based rectangular sheet that was fabricated in our previous study [110] was performed (Figure 6.2 (C)). These observations implied that the pore size of the fibrin-gelatin based structure was slightly reduced in comparison to the previous study [110], which may have been a result of the herringbone pattern, the addition of fibrin and the dual cross-linking chemistry adopted in this study.

#### 6.4.1.2 Rheology

Rheology analysis performed on the discs acquired from the fibrin-gelatin printed structures generated results as depicted (Figure 6.3). Amplitude and frequency sweeps were performed to ensure that the strain and frequency range were within the linear viscoelastic range of the gels. As shown (Figure 6.3 (A)), the elastic modulus was found to be 9.76 kPa which closely resembles the modulus of the native myocardium [114]. The complex viscosity calculated at an angular

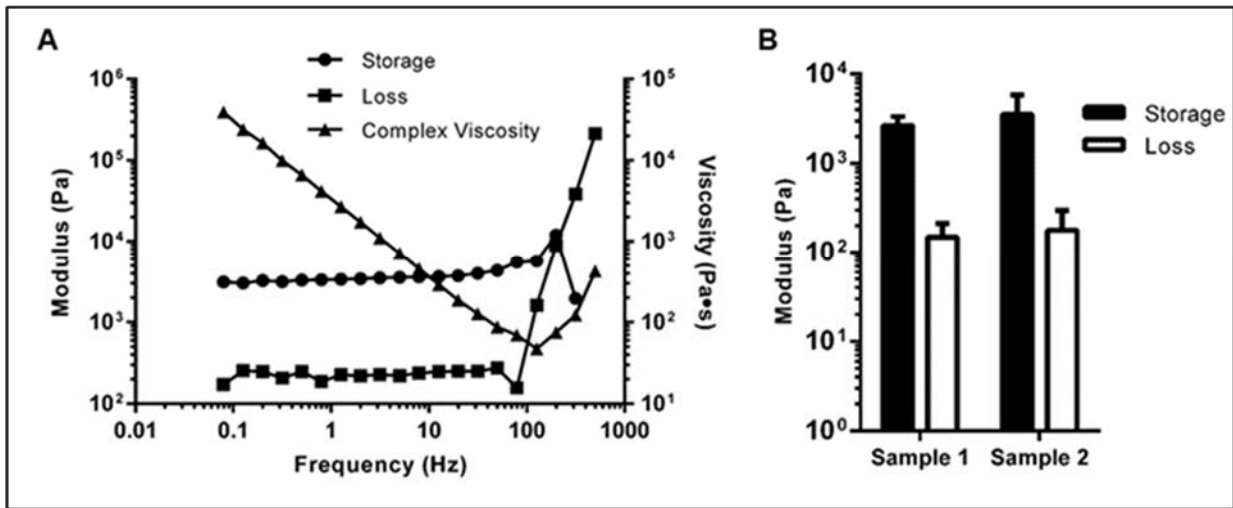


Figure 6.3: Rheology analysis of fibrin-gelatin based square structures. (A) Representative storage- and loss-moduli and complex viscosity from one characteristic gel-sample. Therefore, it does not have error bars. Shown in inset (B) is the average storage and loss moduli for similar sample patterns (#1 and #2, n=2) analyzed during rheological characterization.

frequency of 1.99 Hz was found to be 1.63 Pa-s. The average storage and loss moduli for the tested samples (Samples #1 and #2) were determined as represented in Figure 6.3 (B). The higher storage modulus in both cases indicates that the elastic behavior of the gel is more predominant as compared to its viscous properties, which is characteristic of a stably cross-linked hydrogel [125].

#### 6.4.1.3 Fourier Transform Infrared Spectroscopy (FTIR)

FTIR was performed on the fibrin-gelatin based hydrogels to validate the formation of a crosslinked composite and the spectra obtained has been depicted (Figure 6.4). The peaks observed at around  $1636\text{ cm}^{-1}$ ,  $1533\text{ cm}^{-1}$  and  $1238\text{ cm}^{-1}$  correspond to the amide I-, amide II- and amide III- vibrations respectively and are characteristic of the fibrin [126-128]. Additionally, the  $\text{CH}_2$  deformation in the protein's structure was observed at around  $1451\text{ cm}^{-1}$  with amino acid chain vibrations appearing around  $1400\text{ cm}^{-1}$  in accordance with published literature [128]. The vibrational mode corresponding to the C=O stretching in f-gelatin was found near  $1636\text{ cm}^{-1}$  and the N-H and C-N stretching modes were found at  $1530\text{ cm}^{-1}$ . The deformation of the =C-H bond in the furan ring is observed at around  $920\text{ cm}^{-1}$  as reported in earlier studies [129]. A broad band that corresponded with the N-H vibrational mode was observed at  $3282\text{ cm}^{-1}$ . The FTIR spectra for control samples have been included in the Appendix (A.1.5). Although no major differences were observed between the raw composite mixture with the photo-polymerized mixture, the cross-linking of fibrinogen into fibrin was validated by the appearance of the vibrational mode of C-N stretching at around  $1150 - 1000\text{ cm}^{-1}$ , as has been reported in existing literature [130].

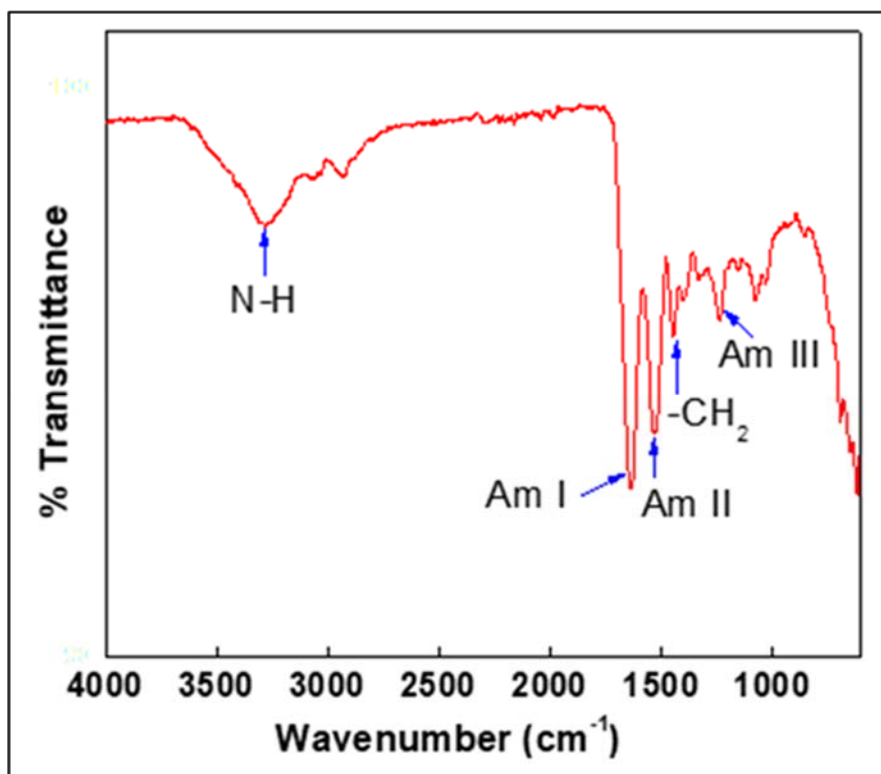


Figure 6.4: FTIR spectra for the fibrin-gelatin based sample.

#### 6.4.1.4 Swelling and degradation

The swelling behaviour of the fibrin-gelatin based hydrogels when preswollen in cell culture has been depicted (Figure 6.5). It was observed that the maximum swelling of the tested samples occurred after 96 hr (four days) following which the samples reached an equilibrium swelling degree. This time point was achieved much earlier in the previous study involving f-gelatin based scaffolds where the tested samples reached their equilibrium swelling ratios after only 24 hr (one day) in culture ( $p=0.02$ ) [110]. This is proof that the dual-crosslinking mechanism that was applied to the fibrin-gelatin based constructs resulted in them having more enhanced structural fidelity as compared to the f-gelatin based constructs that were developed in the previous study [110].



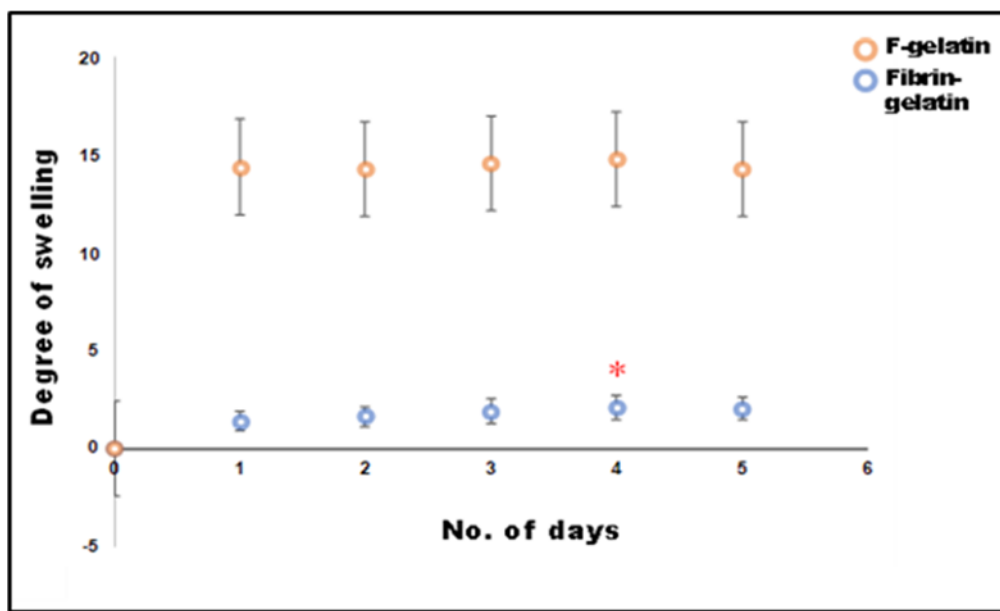


Figure 6.5: Swelling behavior of the fibrin-gelatin based hydrogel samples with respect to the f-gelatin samples used in a previous study [110].

## 6.4.2 Biocompatibility

### 6.4.2.1 Live/Dead Toxicity assay

Images acquired after performing the Live/Dead assay on the both human iPSC-derived CM and human CM, incorporated separately into the fibrin-gelatin hydrogels and bioprinted confirmed that both cell types were able to withstand the extrusion printing and the crosslinking processes as shown (Figure 6.6 (A, B)). Since the iPSC-derived CM had a short shelf life, it was imperative to employ the human cell lines to further validate the results that were exhibited by the primary cell cultures used. These human CM cell lines presented a sarcomeric structure when probed using appropriate biomarkers, which confirmed their functional and morphological resemblance to human cardiomyocytes.

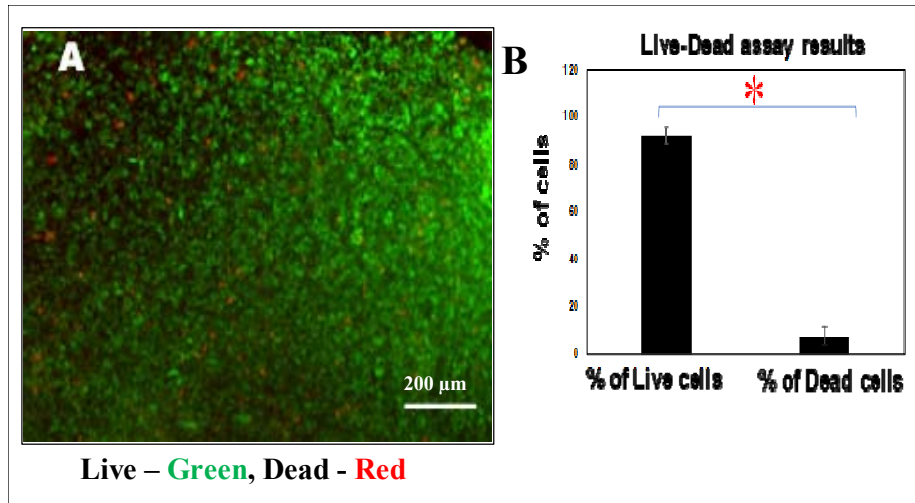


Figure 6.6: Cell retention, viability and proliferation. (A) Shows characteristic images of human CM cell lines, that were bioprinted within fibrin-gelatin patterns and imaged using Live (Green)/Dead (Red) assay, and (B) Quantification of cell viability estimated by Live-Dead assay after 5 days of culture. Statistically significant differences are denoted by  $*(p<0.05)$

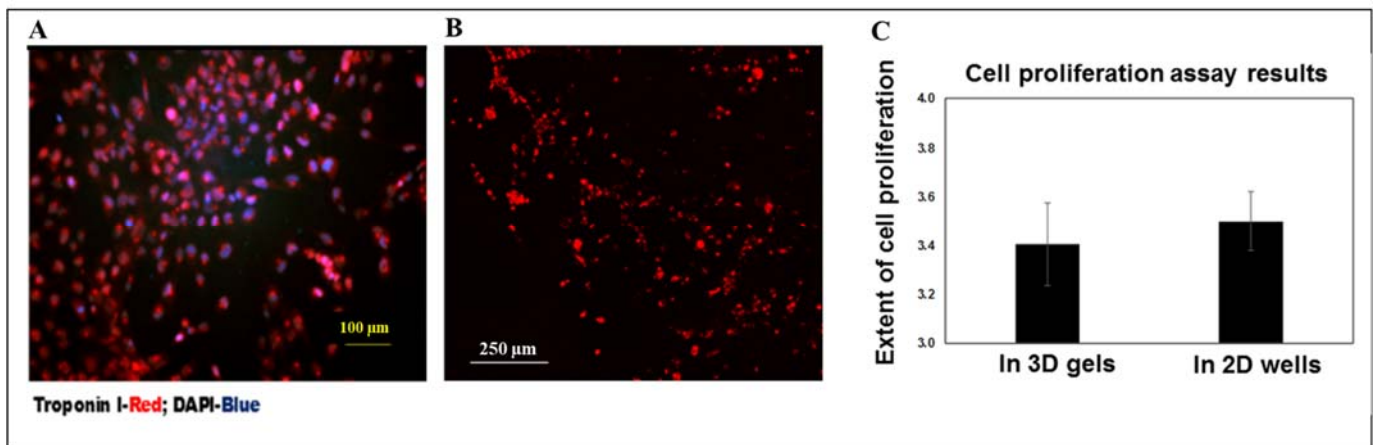


Figure 6.7: (A) Characteristic image of human CM cell lines stained with Troponin I antibody (red) and DAPI (blue) after 5 days of culture. (B) PKH26 (red) prestained cells bioprinted using a herringbone design were seen to align along this pattern after 24 hr of culture, in a maximum intensity projection of a Z-stack of confocal microscope images.(C) Extent of cell proliferation in both 3D gels and 2D controls after 5 days of culture is depicted.

The Live/Dead assay carried out on the human CM cell lines printed within the fibrin-gelatin based constructs and imaged after a duration of five days of culture, has been shown (Figure 6.6 (A)) along with 2D culture controls. The characteristic images of human iPSC derived-CM, which were bioprinted within the fibrin-gelatin based structures and imaged after the Live/Dead assay have also been included (A.1.6 (A, B)). Troponin T staining (red) validated the presence of cardiac myocytes within the bioprinted constructs (A.1.6 (C)). Further, the human CM cell-lines that were bioprinted within the fibrin-gelatin based constructs and stained with Troponin I [131] and DAPI were imaged after five days (Figure 6.7 (A)). Troponin I is a marker that is employed to positively stain and characterize CM expression in cultures [131]. It was observed that there was an increased number of cells confirming biocompatibility of the fibrin-gelatin based gel with the human CM encapsulated within printed constructs (Figure 6.6 (B)).

The characteristic 2D controls for Troponin I-stained images of human CM cell lines were cultured in tissue culture wells and imaged after 24 hr (A.1.7 (B)). Viable human CM were imaged within fibrin-gelatin based constructs after 24 hr of culture (Figure 6.7 (B)). Cells were observed to align along the herringbone pattern and form networks as shown in the representative image (Figure 6.7 (B)). On the contrary, non-printed controls for cells in gels (A.1.7 (C)), did not exhibit any pattern in cell alignment. Moreover, the thickness of the gel cannot be controlled when casted manually, which obstructs the visual detection of the encapsulated cells. Thus, the herringbone pattern was specifically advantageous as it guided the cells to form networks which could potentially induce cardiomyogenesis.

Based on all the confocal microscopy images that were acquired post the Live/Dead assay (Figure 6.6 (A)), the percentage of dead cells was estimated to be about  $8 \pm 4\%$ , a value that negligible with respect to the percentage of viable cells that was found to be  $92 \pm 3\%$  (Figure 6.6 (B)). The values were considered significantly different with  $p=0.0012$ . These trends continued

even after 72 hr of culture with the numbers of dead and live cells calculated to be  $10 \pm 5\%$  and  $98 \pm 4\%$ , respectively. The increase in the characteristic cell count of the human CM cell lines from  $2.82 \times 10^5$  cells/mL at 24 hr to  $9.6 \times 10^5$  cells/mL at 72 hr, within the 3D printed constructs with respect to the 2D culture systems (controls) where the cell density increased from  $1.24 \times 10^5$  cells/mL to  $4.34 \times 10^5$  cells/mL for the same duration (Figure 6.7 (C)) provided evidence for cell proliferation. The cells seeded in the fibrin-gelatin based scaffolds were found to proliferate at the same rate as the cells cultured in the 2D culture systems implying that the fibrin-gelatin scaffolds were favorable for the cells and directed cellular growth and proliferation (Figure 6.7 (C)). This provided further proof that both the iPSC-derived CM and the human CM cell lines could not only survive the 3D bioprinting process and the dual crosslinking mechanism of the printed constructs but were able to proliferate as well. The minimal cell death that was observed implied that neither the bioink material nor the printing parameters posed any harm to the encapsulated cells but helped the cells retain their viability without disrupting the printed constructs, on the basis of past work [132-134].

Finally, the effects of RB on cell-encapsulated hydrogels in this study have also been reported (A.1.4). Although RB was gradually released from the f-gelatin-based hydrogels, the cells exhibited a growth behavior that was similar to controls, and no significant toxicity was observed. Almost all the cells exhibited green fluorescence derived from calcein AM, when stained after 24 hr of culture confirming cell viability in the presence of RB. These observations indicated that the RB released from the f-gelatin hydrogels posed no significant harm to cell viability.

## **Chapter 7 : Comparison study between f-gelatin- and PEGDA-alginate based bioink systems**

### **7.1 Introduction**

The successful fabrication of the f-gelatin based bioink into constructs that allowed cells seeded in them to retain their viability and functionality encouraged us to investigate other visible light crosslinkable bioink systems so as to validate the superiority of the f-gelatin-based scaffolds through a comparison study between the two bioink based scaffolds [110]. The popularity of PEGDA as a synthetically derived, photo-crosslinkable and biocompatible polymer extensively used as a scaffold in tissue engineering applications made it an appealing choice [135]. Pediatric bronchi models were printed using the previously existing f-gelatin bioink and a PEGDA based bioink based on a previously published work.

### **7.2 Biofabrication**

1 mL of the PEGDA bioink was made by dissolving 100mg of PEGDA (Alfa Aesar, Thermo Fisher Scientific, Haverhill, MA, USA) in 932  $\mu$ L of DI water. This was followed by the addition of 44  $\mu$ L of Triethanolamine (TEA) (Thermo Fisher Scientific, Waltham, MA, USA) and 4  $\mu$ L of N-vinyl-2-pyrrolidone (NVP) (Acros Organics, Thermo Fisher Scientific, Waltham, MA, USA) respectively to the PEGDA solution. 20  $\mu$ L of 10Mm Eosin Y (Thermo Fisher Scientific, Waltham, MA, USA) solution was added to the mixture under dark conditions and the resulting material, following which it was irradiated with visible light for 120 s (100% intensity, Intelli-Ray 600, Uvitron International, West Springfield, MA, USA) to induce the crosslinking of the PEGDA monomer by the Eosin Y-TEA photoinitiator system.

## 7.3 Results

### 7.3.1 Material characterization

#### 7.3.1.1 Gross morphology and Scanning Electron Microscopy (SEM)

The en-face images of the lyophilized and sputter coated PEGDA based samples exhibited a highly networked and homogenously distributed porous structure. The average pore size was estimated to be  $1.3334 \pm 0.57176 \mu\text{m}$  and the apparent porosity was calculated to be 14.5%. The thickness of the printed sample was measured to be  $1.009 \pm 0.199 \text{ cm}$ .

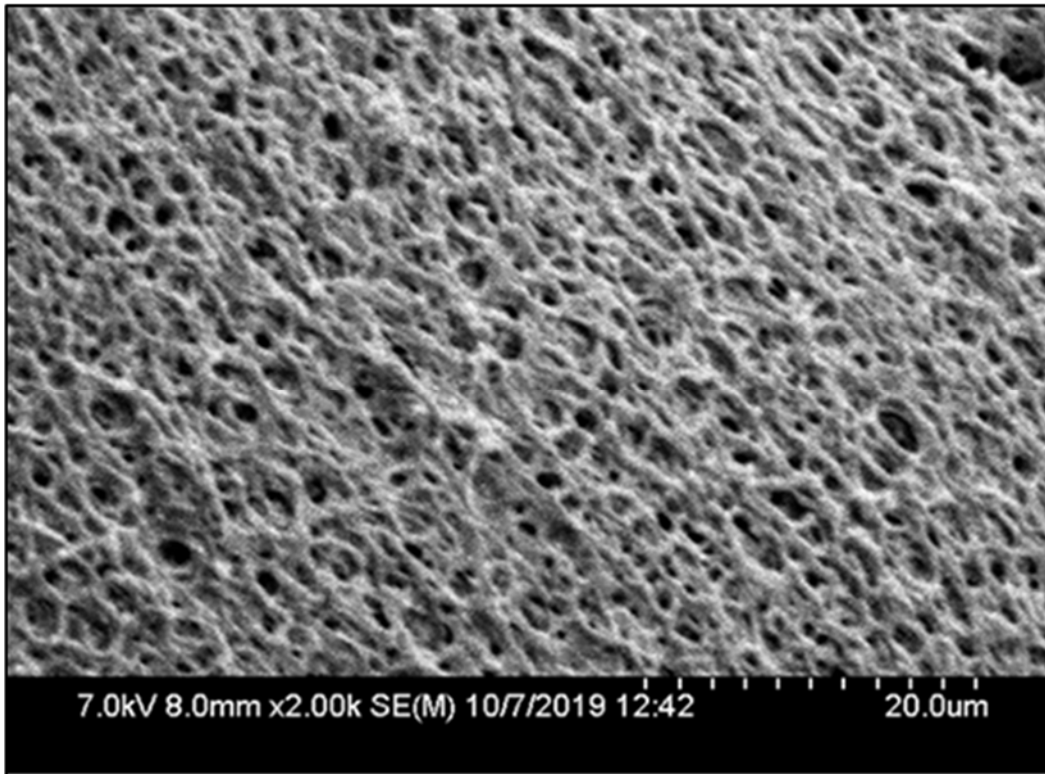


Figure 7.1: En face image of a crosslinked PEGDA-alginate based bioink

### 7.3.1.2 Rheology

The rheology analysis performed on the crosslinked PEGDA-alginate 3D printed samples generated an elastic modulus of  $7.093 \pm 0.708$  kPa and the complex viscosity was measured to be 5180 Pa.s (images not included).

### 7.3.2 Biocompatibility

Human CM AC16 cell lines used in the previous study, were seeded in casted PEGDA hydrogels and subjected to a Live/Dead assay after 24 hr of culture, following which confocal microscopy images of the cell samples were taken.

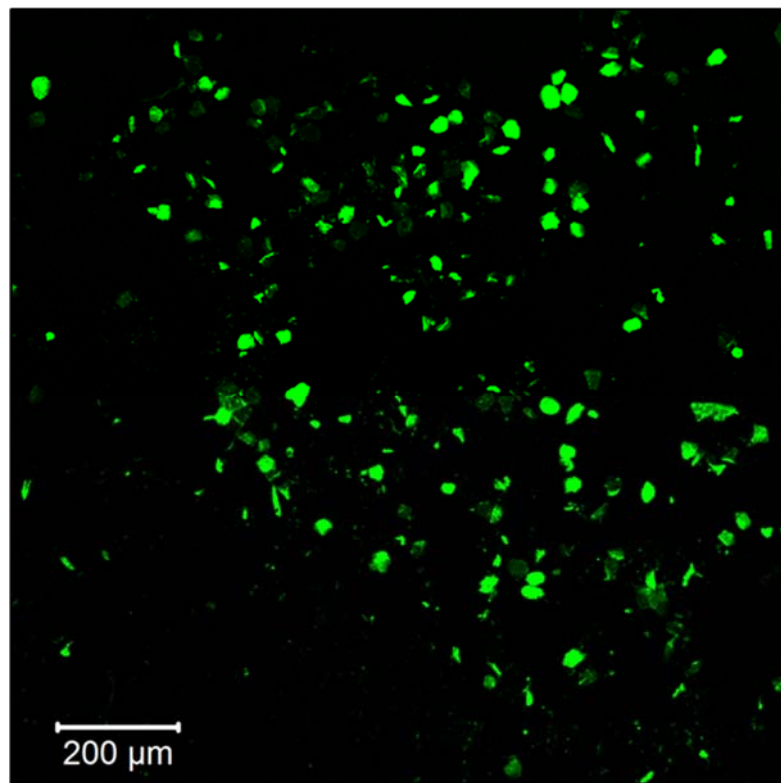


Figure 7.3: A representative confocal microscopy image obtained after Live/Dead assay performed on human CM cell lines encapsulated within casted PEGDA based gels 24 hr post culture

## Chapter 8: Summary and conclusions

### 8.1 Cardiac failure

Cardiac failure has become a major global health concern, affecting millions of patients all over the world [136]. The elderly population, along with the obesity pandemic, and sedentary lifestyle are all factors that will contribute to keeping cardiac failure as a leading cause of morbidity and mortality worldwide.

Despite the numerous breakthroughs and advances in medical and interventional therapies, the underlying pathology governing myocardial damage or death continues to be irreversible. Patients who survive myocardial infarction are likely to be condemned to a lifetime of medication and the inevitable progression of cardiac failure. Newer strategies to repair or regenerate injured myocardium would have the potential of transforming the global healthcare.

Noteworthy discoveries that have been made in the field of stem cell technology may bear the solution to answering this clinical problem. The abilities of stem cells for indefinite self-renewal and differentiation into a range of cell types should make them the ideal candidates for the repair of damaged cardiac tissue. Work in this field has caught the attention of clinicians and the public. For instance, early pre-clinical work has demonstrated the formation of human myocardium within infarcted rat hearts using embryonic stem cell-derived cardiomyocytes (ESC-CM) [27, 28], and studies have also shown improved cardiac functions following stem cell therapy [137].

Adult stem cell populations have also been able to address the ethical concerns that accompany the use of embryonic tissue, as well as immunological issues and safety concerns concerning teratoma formation while also producing significant improvements in cardiac function in animal models from a range of different cells. These results paved the way for numerous clinical



trials, the majority of which, have used autologous stem cells of bone marrow origin (BMC), with small sample sizes.

Although the outcomes of these trials were modest, these studies demonstrated safety with no increased risk of events including arrhythmia, restenosis/thrombosis, worsening heart failure, recurrent MI, death, and re-hospitalisation. Further work in this area is clearly required to optimize cell therapy strategies.

The field of biomaterials has also made countless advances in the past decade, with the focus now extending beyond bulk mechanical properties, and allowing design on the cellular, molecular and chemical level for improving the interaction and integration between synthetic and biological systems radically. This led to the emergence of tissue engineering with the intention of developing biological substitutes that can restore, maintain or improve tissue and organ function. Cardiac failure seems to be an ideal clinical candidate for these strategies.

The primary objective of this dissertation to fabricate a “cardiac” patch by utilizing a combination of various biocompatible materials in optimised quantities, followed by the addition of cardiomyocytes, resulting in a solution (bioink) that could be extruded in specific design patterns via 3D bioprinting.

## **8.2 Development of f-gelatin based bioink**

Chapter 4 outlines the optimization and development of a novel visible light crosslinkable f-gelatin based bioink . The bioink also comprised of HA which served as a viscosity enhancer to make the material extrudable during the 3D bioprinting process and RB, a photosensitizer that could facilitate the crosslinking of the f-gelatin macromolecules upon irradiation with visible light.

The numerous techniques that were employed to characterize the f-gelatin based printed structures indicated that they possessed a well-networked porous geometry and had good structural fidelity, with an elastic modulus of 1.7 kPa. The bioink was tested for its compatibility with cells by printing mono- and bi-layered rectangular sheets seeded with mouse MSC which demonstrated good cell viability and functionality. Further, the bioink was also used to print bi-layered sheets with two different cell-types such as STO fibroblasts (bottom) and C2C12 myoblasts (top) and the cellular crosstalk between the two cell types even though they were confined to separate layers of the printed structure confirmed that the bioink was not cytocompatible but could be used to print complex structures that were comprised of multiple cell types.

### **8.3 Significance of scaffold design in tissue engineering**

Chapter 5 discusses the study conducted with the aim to compare the performance of scaffolds with two different geometries, namely lattice and rectangular-sheet structures, but printed using the same f-gelatin based bioink. The material characterization studies performed on both structures revealed that the lattice structure was relatively more porous with enhanced rheological properties and exhibited a lower degradation rate compared to the rectangular-sheet. Further, it was also observed that the lattice allowed cells to proliferate to a greater extent compared to the rectangular-sheet, which initially retained a lower number of cells. All of these results collectively affirmed that the lattice poses as a superior scaffold design for tissue engineering applications.

### **8.4 Incorporation of fibrin into f-gelatin based bioinks to fabricate “cardiac” patches**

Chapter 6 describes the incorporation of fibrin into the existing f-gelatin based bioink developed in Chapter 4 to develop a novel dual crosslinkable bioink with superior mechanical properties. Although the f-gelatin based constructs proved to be good scaffolds for tissue engineering applications, their mechanical properties were significantly lower than those of the native myocardium tissue, necessitating the need to use an additive which would significantly enhance the mechanical properties. The extensive usage of platelet-rich fibrin, its capacity to offer patient specificity and the similarity in composition to surgical glue made it an obvious and natural choice for the additive. This new fibrin-gelatin based bioink was 3D printed into cardiac cell-laden constructs seeded with human induced pluripotent stem cell-derived cardiomyocytes (iPS-CM) or CM cell lines.

The cell-laden bioprinted constructs were cross-linked to retain a herringbone pattern via a two-step procedure including the visible-light cross-linking of furfuryl-gelatin followed by the chemical cross-linking of fibrinogen by treatment with a thrombin-CaCl<sub>2</sub> solution. The printed constructs revealed an extremely porous, networked structure that afforded long-term in vitro stability. Cardiomyocytes that were printed within the sheet structure showed excellent viability, proliferation, and expression of the Troponin I cardiac marker.

## **8.5 Conclusions**

The numerous studies conducted throughout this dissertation were designed with the objective of fabricating an ideal scaffold specifically meant for applications in cardiac tissue engineering in order to treat myocardial infarction. Each of the studies performed combined all the aspects of tissue engineering, namely, biomaterial scaffolds, cells and growth factors. The novelty of our work lies in developing a visible light crosslinkable bioink that is composed of furfuryl-gelatin, a derivative of porcine gelatin and fibrin, a combination that has never been investigated

before despite each of the components being successfully employed for tissue engineering by themselves or in tandem with other biomaterials. The results of our studies have far reaching implications and can potentially pave the way for future investigations to have a better understanding about fibrin-gelatin based bioinks as scaffolds specifically for cardiac tissue engineering and their eventual adoption into clinical trials.

## Bibliography

1. Whitesides, George M., and Amy P. Wong. "The intersection of biology and materials science." *MRS bulletin* 31, no. 1 (2006): 19-27.
2. Ashammakhi, Nureddin, Mohammad Ali Darabi, Nermin Seda Kehr, Ahmet Erdem, Shukai Hu, Mehmet R. Dokmeci, Ali S. Nasr, and Ali Khademhosseini. "Advances in Controlled Oxygen Generating Biomaterials for Tissue Engineering and Regenerative Therapy." *Biomacromolecules* (2019).
3. Patel, Nitesh R., and Piyush P. Gohil. "A review on biomaterials: scope, applications & human anatomy significance." *International Journal of Emerging Technology and Advanced Engineering* 2, no. 4 (2012): 91-101.4. Ratner, B.D., et al., *Biomaterials science: a multidisciplinary endeavor*. 2004: p. 1-9.
5. Go, Alan S., Dariush Mozaffarian, Véronique L. Roger, Emelia J. Benjamin, Jarett D. Berry, Michael J. Blaha, Shifan Dai et al. "Executive summary: heart disease and stroke statistics—2014 update: a report from the American Heart Association." *Circulation* 129, no. 3 (2014): 399-410.
6. National, Clinical Guideline Centre UK. "Myocardial Infarction with ST-Segment Elevation: The Acute Management of Myocardial Infarction with ST-Segment Elevation." (2013).
7. Burchfield, Jana S., Min Xie, and Joseph A. Hill. "Pathological ventricular remodeling: mechanisms: part 1 of 2." *Circulation* 128, no. 4 (2013): 388-400.
8. Noppe, Gauthier, Cécile Dufeys, Patricia Buchlin, Nicolas Marquet, Diego Castanares-Zapatero, Magali Balteau, Nerea Hermida et al. "Reduced scar maturation and contractility

- lead to exaggerated left ventricular dilation after myocardial infarction in mice lacking AMPK $\alpha$ 1." *Journal of molecular and cellular cardiology* 74 (2014): 32-43.
9. Yacoub, Magdi H., and John Terrovitis. "CADUCEUS, SCIPIO, ALCADIA: cell therapy trials using cardiac-derived cells for patients with post myocardial infarction LV dysfunction, still evolving." *Global Cardiology Science and Practice* 2013, no. 1 (2013): 3.
  10. Segers, Vincent FM, and Richard T. Lee. "Stem-cell therapy for cardiac disease." *Nature* 451, no. 7181 (2008): 937.
  11. Hong, Liu, Ioana Peptan, Paul Clark, and Jeremy J. Mao. "Ex vivo adipose tissue engineering by human marrow stromal cell seeded gelatin sponge." *Annals of biomedical engineering* 33, no. 4 (2005): 511-517.
  12. Rose, James B., Settimio Pacelli, Alicia J. El Haj, Harminder S. Dua, Andrew Hopkinson, Lisa J. White, and Felicity RAJ Rose. "Gelatin-based materials in ocular tissue engineering." *Materials* 7, no. 4 (2014): 3106-3135.
  13. Javadian, Neda, Habibollah Mirzai, and NAFCHI ABDORREZA MOHAMMADI. "The effects of ribose on mechanical and physicochemical properties of cold water fish gelatin films." (2014): 39-45.
  14. Nahar, Manoj, Dinesh Mishra, Vaibhav Dubey, and Narendra Kumar Jain. "Development, characterization, and toxicity evaluation of amphotericin B-loaded gelatin nanoparticles." *Nanomedicine: Nanotechnology, Biology and Medicine* 4, no. 3 (2008): 252-261.
  15. Savarese, G. and L.H.J.C.f.r. Lund, *Global public health burden of heart failure*. 2017. **3**(1): p. 7. Savarese, Gianluigi, and Lars H. Lund. "Global public health burden of heart failure." *Cardiac failure review* 3, no. 1 (2017): 7.

16. Benjamin, Emelia J., Paul Muntner, and Márcio Sommer Bittencourt. "Heart disease and stroke statistics-2019 update: a report from the American Heart Association." *Circulation* 139, no. 10 (2019): e56-e528.
17. Roger, Véronique L., Alan S. Go, Donald M. Lloyd-Jones, Emelia J. Benjamin, Jarett D. Berry, William B. Borden, Dawn M. Bravata et al. "Heart disease and stroke statistics--2012 update: a report from the American Heart Association." *Circulation* 125, no. 1 (2012): e2-e220.
18. Levy, Daniel, Satish Kenchaiah, Martin G. Larson, Emelia J. Benjamin, Michelle J. Kupka, Kalon KL Ho, Joanne M. Murabito, and Ramachandran S. Vasan. "Long-term trends in the incidence of and survival with heart failure." *New England Journal of Medicine* 347, no. 18 (2002): 1397-1402.
19. Roger, Veronique L., Susan A. Weston, Margaret M. Redfield, Jens P. Hellermann-Homan, Jill Killian, Barbara P. Yawn, and Steven J. Jacobsen. "Trends in heart failure incidence and survival in a community-based population." *Jama* 292, no. 3 (2004): 344-350.
20. Cowie, M. R., D. A. Wood, A. J. S. Coats, S. G. Thompson, V. Suresh, P. A. Poole-Wilson, and G. C. Sutton. "Survival of patients with a new diagnosis of heart failure: a population based study." *Heart* 83, no. 5 (2000): 505-510.
21. McMurray, J.J. and Marc A. Pfeffer, *Heart failure*. 2005. **365**(9474): p. 1877-1889.
22. Kannel, W.B. and A.J.J.A.h.j. Belanger, *Epidemiology of heart failure*. 1991. **121**(3): p. 951-957.
23. Hunt, Sharon Ann. "American College of Cardiology; American Heart Association Task Force on Practice Guidelines; American College of Chest Physicians; International Society for Heart and Lung Transplantation; Heart Rhythm Society. ACC/AHA 2005 guideline

- update for the diagnosis and management of chronic heart failure in the adult: A report of the American College of Cardiology/American Heart Association Task Force on Practice Guidelines (writing committee to update the 2001 guidelines for the evaluation and management of ...." *Circulation* 112 (2005): e154-e235.
24. Guerci, Alan D., Gary Gerstenblith, Jeffrey A. Brinker, Nisha C. Chandra, Sidney O. Gottlieb, Raymond D. Bahr, James L. Weiss et al. "A randomized trial of intravenous tissue plasminogen activator for acute myocardial infarction with subsequent randomization to elective coronary angioplasty." *New England Journal of Medicine* 317, no. 26 (1987): 1613-1618.
  25. Rose, Eric A., Annetine C. Gelijns, Alan J. Moskowitz, Daniel F. Heitjan, Lynne W. Stevenson, Walter Dembitsky, James W. Long et al. "Long-term use of a left ventricular assist device for end-stage heart failure." *New England Journal of Medicine* 345, no. 20 (2001): 1435-1443.
  26. Buttery, Lee, and Kevin M. Shakesheff. "A brief introduction to different cell types." In *Advances in tissue engineering*, pp. 15-41. 2008.
  27. Laflamme, Michael A., Joseph Gold, Chunhui Xu, Mohammad Hassanipour, Elen Rosler, Shailaja Police, Veronica Muskheli, and Charles E. Murry. "Formation of human myocardium in the rat heart from human embryonic stem cells." *The American journal of pathology* 167, no. 3 (2005): 663-671.
  28. Laflamme, Michael A., Kent Y. Chen, Anna V. Naumova, Veronica Muskheli, James A. Fugate, Sarah K. Dupras, Hans Reinecke et al. "Cardiomyocytes derived from human embryonic stem cells in pro-survival factors enhance function of infarcted rat hearts." *Nature biotechnology* 25, no. 9 (2007): 1015.



29. Oh, Hidemasa, Steven B. Bradfute, Teresa D. Gallardo, Teruya Nakamura, Vinciane Gaussin, Yuji Mishina, Jennifer Pocius et al. "Cardiac progenitor cells from adult myocardium: homing, differentiation, and fusion after infarction." *Proceedings of the National Academy of Sciences* 100, no. 21 (2003): 12313-12318.
30. Wang, Xiaohong, Qingsong Hu, Yasuhiro Nakamura, Joseph Lee, Ge Zhang, Arthur HL From, and Jianyi Zhang. "The role of the sca-1+/CD31- cardiac progenitor cell population in postinfarction left ventricular remodeling." *Stem cells* 24, no. 7 (2006): 1779-1788.
31. Carr, Carolyn A., Daniel J. Stuckey, Jun Jie Tan, Suat Cheng Tan, Renata SM Gomes, Patrizia Camelliti, Elisa Messina, Alessandro Giacomello, Georgina M. Ellison, and Kieran Clarke. "Cardiosphere-derived cells improve function in the infarcted rat heart for at least 16 weeks—an MRI study." *PloS one* 6, no. 10 (2011): e25669.
32. Lee, Shuo-Tsan, Anthony J. White, Satoshi Matsushita, Konstantinos Malliaras, Charles Steenbergen, Yiqiang Zhang, Tao-Sheng Li et al. "Intramyocardial injection of autologous cardiospheres or cardiosphere-derived cells preserves function and minimizes adverse ventricular remodeling in pigs with heart failure post-myocardial infarction." *Journal of the American College of Cardiology* 57, no. 4 (2011): 455-465.
33. Menasché, Philippe, Ottavio Alfieri, Stefan Janssens, William McKenna, Hermann Reichenspurner, Ludovic Trinquart, Jean-Thomas Vilquin et al. "CLINICAL PERSPECTIVE." *Circulation* 117, no. 9 (2008): 1189-1200.
34. Cai, L. "Human adipose tissue-derived stem cells induce angiogenesis and nerve sprouting following myocardial infarction, in conjunction with potent preservation of cardiac function." *Stem Cells* 4 (2008).
35. Schenke-Layland, Katja, Brian M. Strem, Maria C. Jordan, Michael T. DeEmedio, Marc H. Hedrick, Kenneth P. Roos, John K. Fraser, and W. Robb MacLellan. "Adipose tissue-

- derived cells improve cardiac function following myocardial infarction." *Journal of Surgical Research* 153, no. 2 (2009): 217-223.
36. Nelson, Timothy J., Almudena Martinez-Fernandez, Satsuki Yamada, Carmen Perez-Terzic, Yasuhiro Ikeda, and Andre Terzic. "Repair of acute myocardial infarction with iPS induced by human stemness factors." *Circulation* 120, no. 5 (2009): 408.
37. Silva, Guilherme V., Silvio Litovsky, Joao AR Assad, Andre LS Sousa, Bradley J. Martin, Deborah Vela, Stephanie C. Coulter et al. "Mesenchymal stem cells differentiate into an endothelial phenotype, enhance vascular density, and improve heart function in a canine chronic ischemia model." *Circulation* 111, no. 2 (2005): 150-156.
38. Ramesh, Balasundari, Dillip Kumar Bishi, Suneel Rallapalli, Sarasabarathi Arumugam, Kotturathu Mammen Cherian, and Soma Guhathakurta. "Ischemic cardiac tissue conditioned media induced differentiation of human mesenchymal stem cells into early stage cardiomyocytes." *Cytotechnology* 64, no. 5 (2012): 563-575.
39. Wollert, Kai C., and Helmut Drexler. "Cell therapy for the treatment of coronary heart disease: a critical appraisal." *Nature Reviews Cardiology* 7, no. 4 (2010): 204.
40. Janssens, Stefan, Christophe Dubois, Jan Bogaert, Koen Theunissen, Christophe Deroose, Walter Desmet, Maria Kalantzi et al. "Autologous bone marrow-derived stem-cell transfer in patients with ST-segment elevation myocardial infarction: double-blind, randomised controlled trial." *The Lancet* 367, no. 9505 (2006): 113-121.
41. Huikuri, Heikki V., Kari Kervinen, Matti Niemelä, Kari Ylitalo, Marjaana Säily, Pirjo Koistinen, Eeva-Riitta Savolainen et al. "Effects of intracoronary injection of mononuclear bone marrow cells on left ventricular function, arrhythmia risk profile, and restenosis after thrombolytic therapy of acute myocardial infarction." *European heart journal* 29, no. 22 (2008): 2723-2732.

42. Assmus, Birgit, Jörg Honold, Volker Schächinger, Martina B. Britten, Ulrich Fischer-Rasokat, Ralf Lehmann, Claudius Teupe et al. "Transcoronary transplantation of progenitor cells after myocardial infarction." *New England Journal of Medicine* 355, no. 12 (2006): 1222-1232.
43. Menasche, Philippe. "Cardiac cell therapy: lessons from clinical trials." *Journal of molecular and cellular cardiology* 50, no. 2 (2011): 258-265.
44. Takahashi, Kazutoshi, and Shinya Yamanaka. "Induction of pluripotent stem cells from mouse embryonic and adult fibroblast cultures by defined factors." *cell* 126, no. 4 (2006): 663-676.
45. Hofmann, Michael, Kai C. Wollert, Gerd P. Meyer, Alix Menke, Lubomir Arseniev, Bernd Hertenstein, Arnold Ganser, Wolfram H. Knapp, and Helmut Drexler. "Monitoring of bone marrow cell homing into the infarcted human myocardium." *Circulation* 111, no. 17 (2005): 2198-2202.
46. Teng, Carolyn J., Jun Luo, Ray CJ Chiu, and Dominique Shum-Tim. "Massive mechanical loss of microspheres with direct intramyocardial injection in the beating heart: implications for cellular cardiomyoplasty." *The Journal of thoracic and cardiovascular surgery* 132, no. 3 (2006): 628-632.
47. Zhang, Ming, Danielle Methot, Veronica Poppa, Yasushi Fujio, Kenneth Walsh, and Charles E. Murry. "Cardiomyocyte grafting for cardiac repair: graft cell death and anti-death strategies." *Journal of molecular and cellular cardiology* 33, no. 5 (2001): 907-921.
48. Lavik, Erin, and Robert Langer. "Tissue engineering: current state and perspectives." *Applied microbiology and biotechnology* 65, no. 1 (2004): 1-8.
49. Williams, David F. "On the nature of biomaterials." *Biomaterials* 30, no. 30 (2009): 5897-5909.

50. Place, Elsie S., Nicholas D. Evans, and Molly M. Stevens. "Complexity in biomaterials for tissue engineering." *Nature materials* 8, no. 6 (2009): 457.
51. Christman, Karen L., and Randall J. Lee. "Biomaterials for the treatment of myocardial infarction." *Journal of the American College of Cardiology* 48, no. 5 (2006): 907-913.
52. Venugopal, Jayarama Reddy, Molamma P. Prabhakaran, Shayanti Mukherjee, Rajeswari Ravichandran, Kai Dan, and Seeram Ramakrishna. "Biomaterial strategies for alleviation of myocardial infarction." *Journal of the Royal Society Interface* 9, no. 66 (2011): 1-19.
53. Seif-Naraghi, Sonya B., Jennifer M. Singelyn, Michael A. Salvatore, Kent G. Osborn, Jean J. Wang, Unatti Sampat, Oi Ling Kwan et al. "Safety and efficacy of an injectable extracellular matrix hydrogel for treating myocardial infarction." *Science translational medicine* 5, no. 173 (2013): 173ra25-173ra25.
54. Stuckey, Daniel J., Hikaru Ishii, Qi-Zhi Chen, Aldo R. Boccaccini, Ulrich Hansen, Carolyn A. Carr, Judith A. Roether et al. "Magnetic resonance imaging evaluation of remodeling by cardiac elastomeric tissue scaffold biomaterials in a rat model of myocardial infarction." *Tissue Engineering Part A* 16, no. 11 (2010): 3395-3402.
55. Wang, Feng, and Jianjun Guan. "Cellular cardiomyoplasty and cardiac tissue engineering for myocardial therapy." *Advanced drug delivery reviews* 62, no. 7-8 (2010): 784-797.
56. Chen, Qi-Zhi, Alexander Bismarck, Ulrich Hansen, Sarah Junaid, Michael Q. Tran, Siân E. Harding, Nadire N. Ali, and Aldo R. Boccaccini. "Characterisation of a soft elastomer poly (glycerol sebacate) designed to match the mechanical properties of myocardial tissue." *Biomaterials* 29, no. 1 (2008): 47-57.
57. Piao, Hainan, Jin-Sook Kwon, Shuguang Piao, Ju-Hee Sohn, Yeong-Shin Lee, Jang-Whan Bae, Kyung-Kuk Hwang et al. "Effects of cardiac patches engineered with bone marrow-

- derived mononuclear cells and PGCL scaffolds in a rat myocardial infarction model." *Biomaterials* 28, no. 4 (2007): 641-649.
58. Chi, Nai-Hsin, Ming-Chia Yang, Tze-Wen Chung, Nai-Kuan Chou, and Shoei-Shen Wang. "Cardiac repair using chitosan-hyaluronan/silk fibroin patches in a rat heart model with myocardial infarction." *Carbohydrate polymers* 92, no. 1 (2013): 591-597.
59. Kolehmainen, Kathleen, and Stephanie M. Willerth. "Preparation of 3D fibrin scaffolds for stem cell culture applications." *JoVE (Journal of Visualized Experiments)* 61 (2012): e3641.
60. Kačarević, Željka P., Patrick M. Rider, Said Alkildani, Sujith Retnasingh, Ralf Smeets, Ole Jung, Zrinka Ivanišević, and Mike Barbeck. "An introduction to 3D bioprinting: possibilities, challenges and future aspects." *Materials* 11, no. 11 (2018): 2199.
61. Rider, Patrick, Željka Perić Kačarević, Said Alkildani, Sujith Retnasingh, and Mike Barbeck. "Bioprinting of tissue engineering scaffolds." *Journal of tissue engineering* 9 (2018): 2041731418802090.
62. Ballyns, Jeffrey J., Jason P. Gleghorn, Vicki Niebrzydowski, Jeremy J. Rawlinson, Hollis G. Potter, Suzanne A. Maher, Timothy M. Wright, and Lawrence J. Bonassar. "Image-guided tissue engineering of anatomically shaped implants via MRI and micro-CT using injection molding." *Tissue Engineering Part A* 14, no. 7 (2008): 1195-1202.
63. Bishop, Elliot S., Sami Mostafa, Mikhail Pakvasa, Hue H. Luu, Michael J. Lee, Jennifer Moriatis Wolf, Guillermo A. Ameer, Tong-Chuan He, and Russell R. Reid. "3-D bioprinting technologies in tissue engineering and regenerative medicine: Current and future trends." *Genes & diseases* 4, no. 4 (2017): 185-195.
64. Cascone, Maria Grazia, Luigi Lazzeri, Enzo Sparvoli, Manuele Scatena, Lorenzo Pio Serino, and Serena Danti. "Morphological evaluation of bioartificial hydrogels as potential

- tissue engineering scaffolds." *Journal of Materials Science: Materials in Medicine* 15, no. 12 (2004): 1309-1313.
65. Allen, Shane C., Nancy D. Ebel, Ryan S. Stowers, Carla Van Den Berg, and Laura J. Suggs. "Dynamic increase in matrix stiffness promotes invasive tumor phenotype in vivo."
  66. Joddar, Binata, Eduardo Garcia, Atzimba Casas, and Calvin M. Stewart. "Development of functionalized multi-walled carbon-nanotube-based alginate hydrogels for enabling biomimetic technologies." *Scientific reports* 6 (2016): 32456.
  67. Murphy, Sean V., and Anthony Atala. "3D bioprinting of tissues and organs." *Nature biotechnology* 32, no. 8 (2014): 773.
  68. Yan, Yongnian, Xiaohong Wang, Yuqiong Pan, Haixia Liu, Jie Cheng, Zhuo Xiong, Feng Lin, Rendong Wu, Renji Zhang, and Qingping Lu. "Fabrication of viable tissue-engineered constructs with 3D cell-assembly technique." *Biomaterials* 26, no. 29 (2005): 5864-5871.
  69. Ferris, Cameron J., Kerry J. Gilmore, Stephen Beirne, Donald McCallum, and Gordon G. Wallace. "Bio-ink for on-demand printing of living cells." *Biomaterials Science* 1, no. 2 (2013): 224-230.
  70. Drury, Jeanie L., and David J. Mooney. "Hydrogels for tissue engineering: scaffold design variables and applications." *Biomaterials* 24, no. 24 (2003): 4337-4351.
  71. Kang, Hye-Won, Yasuhiko Tabata, and Yoshito Ikada. "Fabrication of porous gelatin scaffolds for tissue engineering." *Biomaterials* 20, no. 14 (1999): 1339-1344.
  72. Lee, Kuen Yong, and David J. Mooney. "Hydrogels for tissue engineering." *Chemical reviews* 101, no. 7 (2001): 1869-1880.
  73. Boskey, A. L., M. Maresca, W. Ullrich, S. B. Doty, W. T. Butler, and C. W. Prince. "Osteopontin-hydroxyapatite interactions in vitro: inhibition of hydroxyapatite formation and growth in a gelatin-gel." *Bone and mineral* 22, no. 2 (1993): 147-159.

74. Gorgieva, Selestina, and Vanja Kokol. "Collagen-vs. gelatine-based biomaterials and their biocompatibility: review and perspectives." *Biomaterials applications for nanomedicine 2* (2011): 17-52.
75. Angele, P., R. Kujat, M. Nerlich, Jung Yoo, V. Goldberg, and Brian Johnstone. "Engineering of osteochondral tissue with bone marrow mesenchymal progenitor cells in a derivatized hyaluronan-gelatin composite sponge." *Tissue Engineering 5*, no. 6 (1999): 545-553.
76. Ifkovits, Jamie L., and Jason A. Burdick. "Photopolymerizable and degradable biomaterials for tissue engineering applications." *Tissue engineering 13*, no. 10 (2007): 2369-2385.
77. Ovsianikov, Aleksandr, Andrea Deiwick, Sandra Van Vlierberghe, Peter Dubrue, Lena Möller, Gerald Dräger, and Boris Chichkov. "Laser fabrication of three-dimensional CAD scaffolds from photosensitive gelatin for applications in tissue engineering." *Biomacromolecules 12*, no. 4 (2011): 851-858.
78. Sakai, Shinji, Keisuke Hirose, Kenichi Taguchi, Yuko Ogushi, and Koei Kawakami. "An injectable, in situ enzymatically gellable, gelatin derivative for drug delivery and tissue engineering." *Biomaterials 30*, no. 20 (2009): 3371-3377.
79. Van Den Bulcke, An I., Bogdan Bogdanov, Nadine De Rooze, Etienne H. Schacht, Maria Cornelissen, and Hugo Berghmans. "Structural and rheological properties of methacrylamide modified gelatin hydrogels." *Biomacromolecules 1*, no. 1 (2000): 31-38.
80. Shu, Xiao Zheng, Yanchun Liu, Fabio Palumbo, and Glenn D. Prestwich. "Disulfide-crosslinked hyaluronan-gelatin hydrogel films: a covalent mimic of the extracellular matrix for in vitro cell growth." *Biomaterials 24*, no. 21 (2003): 3825-3834.

81. Mazaki, Tetsuro, Yasuyuki Shiozaki, Kentaro Yamane, Aki Yoshida, Mariko Nakamura, Yasuhiro Yoshida, Di Zhou et al. "A novel, visible light-induced, rapidly cross-linkable gelatin scaffold for osteochondral tissue engineering." *Scientific reports* 4 (2014): 4457.
82. Zhao, Xin, Qi Lang, Lara Yildirimer, Zhi Yuan Lin, Wenguo Cui, Nasim Annabi, Kee Woei Ng, Mehmet R. Dokmeci, Amir M. Ghaemmaghami, and Ali Khademhosseini. "Photocrosslinkable gelatin hydrogel for epidermal tissue engineering." *Advanced healthcare materials* 5, no. 1 (2016): 108-118.
83. Lemes, Gislaine Franco, Nicolli Grecco Marchiore, Thaysa Fernandes Moya Moreira, Tamires Barlati Vieira Da Silva, Claudia Sayer, Marianne Ayumi Shirai, Odinei Hess Gonçalves, Angela Maria Gozzo, and Fernanda Vitória Leimann. "Enzymatically crosslinked gelatin coating added of bioactive nanoparticles and antifungal agent: Effect on the quality of Benitaka grapes." *LWT* 84 (2017): 175-182.
84. Yang, Gang, Zhenghua Xiao, Xiaomei Ren, Haiyan Long, Hong Qian, Kunlong Ma, and Yingqiang Guo. "Enzymatically crosslinked gelatin hydrogel promotes the proliferation of adipose tissue-derived stromal cells." *PeerJ* 4 (2016): e2497.
85. Daly, Andrew C., Susan E. Critchley, Emily M. Rencsok, and Daniel J. Kelly. "A comparison of different bioinks for 3D bioprinting of fibrocartilage and hyaline cartilage." *Biofabrication* 8, no. 4 (2016): 045002.86. Kuo, W.-T., et al., *Surface modification of gelatin nanoparticles with polyethylenimine as gene vector*. 2011. **2011**: p. 28.
87. Lai, Jui-Yang. "Biocompatibility of chemically cross-linked gelatin hydrogels for ophthalmic use." *Journal of Materials Science: Materials in Medicine* 21, no. 6 (2010): 1899-1911.



88. Son, Tae Il, Makoto Sakuragi, Sawa Takahashi, Sei Obuse, Jeonghwa Kang, Masako Fujishiro, Haruhiko Matsushita et al. "Visible light-induced crosslinkable gelatin." *Acta biomaterialia* 6, no. 10 (2010): 4005-4010.
89. Park, Shin-Hye, Si-Yoong Seo, Jeong-Hwa Kang, Yoshihiro Ito, and Tae-II Son. "Preparation of photocured azidophenyl-fish gelatin and its capturing of human epidermal growth factor on titanium plate." *Journal of Applied Polymer Science* 127, no. 1 (2013): 154-160.
90. Pati, Falguni, Jinah Jang, Dong-Heon Ha, Sung Won Kim, Jong-Won Rhie, Jin-Hyung Shim, Deok-Ho Kim, and Dong-Woo Cho. "Printing three-dimensional tissue analogues with decellularized extracellular matrix bioink." *Nature communications* 5 (2014): 3935.
91. Jakab, Karoly, Cyrille Norotte, Francoise Marga, Keith Murphy, Gordana Vunjak-Novakovic, and Gabor Forgacs. "Tissue engineering by self-assembly and bio-printing of living cells." *Biofabrication* 2, no. 2 (2010): 022001.
92. Chimene, David, Kimberly K. Lennox, Roland R. Kaunas, and Akhilesh K. Gaharwar. "Advanced bioinks for 3D printing: a materials science perspective." *Annals of biomedical engineering* 44, no. 6 (2016): 2090-2102.
93. Monheit, Gary D., and Kyle M. Coleman. "Hyaluronic acid fillers." *Dermatologic therapy* 19, no. 3 (2006): 141-150.
94. Shrestha, Annie, Michael R. Hamblin, and Anil Kishen. "Photoactivated rose bengal functionalized chitosan nanoparticles produce antibacterial/biofilm activity and stabilize dentin-collagen." *Nanomedicine: Nanotechnology, Biology and Medicine* 10, no. 3 (2014): 491-501.

95. Wollensak, Gregor, Henning Aurich, Duy-Thoai Pham, and Christopher Wirbelauer. "Hydration behavior of porcine cornea crosslinked with riboflavin and ultraviolet A." *Journal of cataract & refractive surgery* 33, no. 3 (2007): 516-521.
96. Nagyova, Miriam, Lucia Slovinska, Juraj Blasko, Ivana Grulova, Maria Kuricova, Viera Cigankova, Denisa Harvanova, and Dasa Cizkova. "A comparative study of PKH67, DiI, and BrdU labeling techniques for tracing rat mesenchymal stem cells." *In Vitro Cellular & Developmental Biology-Animal* 50, no. 7 (2014): 656-663.
97. Montiel-Herrera, Marcelino, Alessandro Gandini, Francisco M. Goycoolea, Neil E. Jacobsen, Jaime Lizardi-Mendoza, Maricarmen Recillas-Mota, and Waldo M. Argüelles-Monal. "N-(furfural) chitosan hydrogels based on Diels–Alder cycloadditions and application as microspheres for controlled drug release." *Carbohydrate polymers* 128 (2015): 220-227.
98. Sheu, Shiow-Yunn, Wen-Shan Chen, Jui-Sheng Sun, Feng-Huei Lin, and Tuoh Wu. "Biological characterization of oxidized hyaluronic acid/resveratrol hydrogel for cartilage tissue engineering." *Journal of Biomedical Materials Research Part A: An Official Journal of The Society for Biomaterials, The Japanese Society for Biomaterials, and The Australian Society for Biomaterials and the Korean Society for Biomaterials* 101, no. 12 (2013): 3457-3466.
99. Contreras-Shannon, Verónica, Dylan L. Heart, R. Madelaine Paredes, Erica Navaira, Gabriel Catano, Shivani Kaushal Maffi, and Consuelo Walss-Bass. "Clozapine-induced mitochondria alterations and inflammation in brain and insulin-responsive cells." *PloS one* 8, no. 3 (2013): e59012.

100. Park, Yun-Gwi, Seung-Eun Lee, Eun-Young Kim, Hyuk Hyun, Min-Young Shin, Yeo-Jin Son, Su-Young Kim, and Se-Pill Park. "Effects of feeder cell types on culture of mouse embryonic stem cell in vitro." *Development & reproduction* 19, no. 3 (2015): 119.
101. Malafaya, Patrícia B., Gabriela A. Silva, and Rui L. Reis. "Natural–origin polymers as carriers and scaffolds for biomolecules and cell delivery in tissue engineering applications." *Advanced drug delivery reviews* 59, no. 4-5 (2007): 207-233.
102. Wessels, Andy, and David Sedmera. "Developmental anatomy of the heart: a tale of mice and man." *Physiological genomics* 15, no. 3 (2003): 165-176.
103. Hansen, Arne, Alexandra Eder, Marlene Bönstrup, Marianne Flato, Marco Mewe, Sebastian Schaaf, Bülent Aksehirlioglu, Alexander Schwörer, June Uebeler, and Thomas Eschenhagen. "Development of a drug screening platform based on engineered heart tissue." *Circulation research* 107, no. 1 (2010): 35.
104. Hirt, Marc N., Arne Hansen, and Thomas Eschenhagen. "Cardiac tissue engineering: state of the art." *Circulation research* 114, no. 2 (2014): 354-367.
105. O'brien, Fergal J. "Biomaterials & scaffolds for tissue engineering." *Materials today* 14, no. 3 (2011): 88-95.
106. Chan, B. P., and K. W. Leong. "Scaffolding in tissue engineering: general approaches and tissue-specific considerations." *European spine journal* 17, no. 4 (2008): 467-479.
107. Loh, Qiu Li, and Cleo Choong. "Three-dimensional scaffolds for tissue engineering applications: role of porosity and pore size." *Tissue Engineering Part B: Reviews* 19, no. 6 (2013): 485-502.
108. Patel, Hetal, Minal Bonde, and Ganga Srinivasan. "Biodegradable polymer scaffold for tissue engineering." *Trends Biomater Artif Organs* 25, no. 1 (2011): 20-9.
109. Shenoy, Manjula. *Animal Biotechnology*. Firewall Media, 2007.

110. Anil Kumar, Shweta, Shane C. Allen, Nishat Tasnim, Tahmina Akter, Shinhye Park, Alok Kumar, Munmun Chattopadhyay, Yoshihiro Ito, Laura J. Suggs, and Binata Joddar. "The applicability of furfuryl-gelatin as a novel bioink for tissue engineering applications." *Journal of Biomedical Materials Research Part B: Applied Biomaterials* 107, no. 2 (2019): 314-323.
111. Gaetani, Roberto, Dries AM Feyen, Vera Verhage, Rolf Slaats, Elisa Messina, Karen L. Christman, Alessandro Giacomello, Pieter AFM Doevendans, and Joost PG Sluijter. "Epicardial application of cardiac progenitor cells in a 3D-printed gelatin/hyaluronic acid patch preserves cardiac function after myocardial infarction." *Biomaterials* 61 (2015): 339-348.
112. Ornelas, Alfredo, Kaitlyn N. Williams, Kevin A. Hatch, Aurelio Paez, Angela C. Aguilar, Cameron C. Ellis, Nishat Tasnim et al. "Synthesis and characterization of a photocleavable collagen-like peptide." *Organic & biomolecular chemistry* 16, no. 6 (2018): 1000-1013.
113. Nair, Kalyani, Milind Gandhi, Saif Khalil, Karen Chang Yan, Michele Marcolongo, Kenneth Barbee, and Wei Sun. "Characterization of cell viability during bioprinting processes." *Biotechnology Journal: Healthcare Nutrition Technology* 4, no. 8 (2009): 1168-1177.
114. Boothe, Sean D., Jackson D. Myers, Seokwon Pok, Junping Sun, Yutao Xi, Raymond M. Nieto, Jie Cheng, and Jeffrey G. Jacot. "The effect of substrate stiffness on cardiomyocyte action potentials." *Cell biochemistry and biophysics* 74, no. 4 (2016): 527-535.
115. Jackson, Mark R. "Fibrin sealants in surgical practice: an overview." *The American journal of surgery* 182, no. 2 (2001): S1-S7.
116. Schlag, G. Ü. N. T. H. E. R., and Heinz Redl. "Fibrin sealant in orthopedic surgery." *Clinical orthopaedics and related research* 227 (1988): 269-285.

117. Ahmed, Tamer AE, Emma V. Dare, and Max Hincke. "Fibrin: a versatile scaffold for tissue engineering applications." *Tissue Engineering Part B: Reviews* 14, no. 2 (2008): 199-215.
118. Christman, Karen L., Andrew J. Vardanian, Qizhi Fang, Richard E. Sievers, Hubert H. Fok, and Randall J. Lee. "Injectable fibrin scaffold improves cell transplant survival, reduces infarct expansion, and induces neovasculature formation in ischemic myocardium." *Journal of the American College of Cardiology* 44, no. 3 (2004): 654-660.
119. Zhang, Jianyi, Wuqiang Zhu, Milica Radisic, and Gordana Vunjak-Novakovic. "Can we engineer a human cardiac patch for therapy?." *Circulation research* 123, no. 2 (2018): 244-265.
120. West, Jennifer L., and James J. Moon. "Vascularization of engineered tissues: approaches to promote angiogenesis in biomaterials." *Current topics in medicinal chemistry* 8, no. 4 (2008): 300-310.
121. Cui, Xiaofeng, and Thomas Boland. "Human microvasculature fabrication using thermal inkjet printing technology." *Biomaterials* 30, no. 31 (2009): 6221-6227.
122. Wu, Alan HB, ed. *Cardiac markers*. Springer Science & Business Media, 2003.
123. Hughes, S. E. "The pathology of hypertrophic cardiomyopathy." *Histopathology* 44, no. 5 (2004): 412-427.
124. Lu, Qijin, Kavitha Ganesan, Dan T. Simionescu, and Narendra R. Vyavahare. "Novel porous aortic elastin and collagen scaffolds for tissue engineering." *Biomaterials* 25, no. 22 (2004): 5227-5237.
125. Stowers, Ryan S., Shane C. Allen, and Laura J. Suggs. "Dynamic phototuning of 3D hydrogel stiffness." *Proceedings of the National Academy of Sciences* 112, no. 7 (2015): 1953-1958.

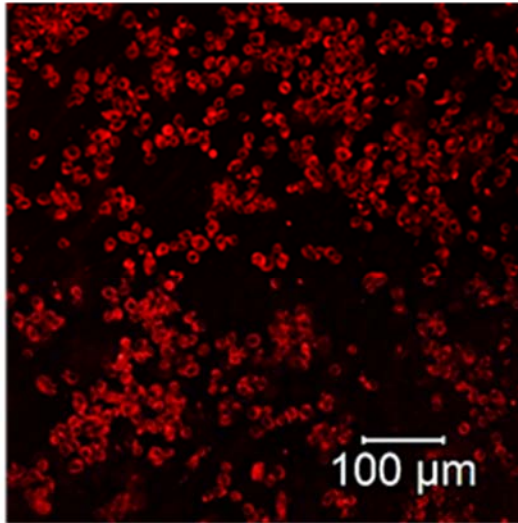
126. Deepthi, S., and R. Jayakumar. "Alginate nanobeads interspersed fibrin network as in situ forming hydrogel for soft tissue engineering." *Bioactive materials* 3, no. 2 (2018): 194-200.
127. Perumcherry, Sreerekha Raman, Krishna Prasad Chennazhi, Shantikumar V. Nair, Deepthy Menon, and Rajan Afeesh. "A novel method for the fabrication of fibrin-based electrospun nanofibrous scaffold for tissue-engineering applications." *Tissue Engineering Part C: Methods* 17, no. 11 (2011): 1121-1130.
128. Tunc, Sibel, Manfred F. Maitz, Gerald Steiner, Luis Vázquez, Minh T. Pham, and Reiner Salzer. "In situ conformational analysis of fibrinogen adsorbed on Si surfaces." *Colloids and Surfaces B: Biointerfaces* 42, no. 3-4 (2005): 219-225.
129. García-Astrain, C., A. Gandini, C. Peña, I. Algar, A. Eceiza, M. Corcuera, and N. Gabilondo. "Diels–Alder “click” chemistry for the cross-linking of furfuryl-gelatin-polyetheramine hydrogels." *RSC Advances* 4, no. 67 (2014): 35578-35587.
130. Stamatina, L., R. Cristescu, G. Socol, A. Moldovan, D. Mihaiescu, I. Stamatina, I. N. Mihaiescu, and D. B. Chrisey. "Laser deposition of fibrinogen blood proteins thin films by matrix assisted pulsed laser evaporation." *Applied surface science* 248, no. 1-4 (2005): 422-427.
131. Bersell, Kevin, Jainy Savla, Maria Mollova, Stuart Walsh, Tanmoy DasLala, Shin-Young Park, Leslie Silberstein et al. "Cardiomyocyte Proliferation Contributes to Post-Natal Heart Growth in Humans." (2011): A15232-A15232.
132. Wu, Zhengjie, Xin Su, Yuanyuan Xu, Bin Kong, Wei Sun, and Shengli Mi. "Bioprinting three-dimensional cell-laden tissue constructs with controllable degradation." *Scientific reports* 6 (2016): 24474.

133. Faulkner-Jones, Alan, Catherine Fyfe, Dirk-Jan Cornelissen, John Gardner, Jason King, Aidan Courtney, and Wenmiao Shu. "Bioprinting of human pluripotent stem cells and their directed differentiation into hepatocyte-like cells for the generation of mini-livers in 3D." *Biofabrication* 7, no. 4 (2015): 044102.
134. Rosenzweig, Derek, Eric Carelli, Thomas Steffen, Peter Jarzem, and Lisbet Haglund. "3D-printed ABS and PLA scaffolds for cartilage and nucleus pulposus tissue regeneration." *International journal of molecular sciences* 16, no. 7 (2015): 15118-15135.
135. Bahney, C. S., T. J. Lujan, C. W. Hsu, M. Bottlang, J. L. West, and Brian Johnstone. "Visible light photoinitiation of mesenchymal stem cell-laden bioresponsive hydrogels." *European cells & materials* 22 (2011): 43.
136. Ziaeeian, Boback, and Gregg C. Fonarow. "Epidemiology and aetiology of heart failure." *Nature Reviews Cardiology* 13, no. 6 (2016): 368-378.
137. Wernly, Bernhard, Moritz Mirna, Richard Rezar, Christine Proding, Christian Jung, Bruno K. Podesser, Attila Kiss, Uta C. Hoppe, and Michael Lichtenauer. "Regenerative cardiovascular therapies: stem cells and beyond." *International journal of molecular sciences* 20, no. 6 (2019): 1420.

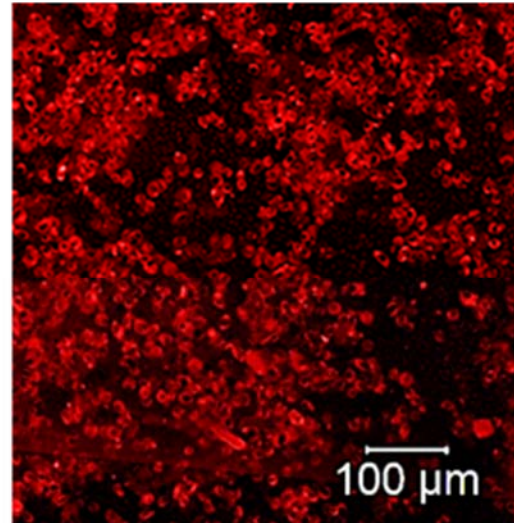
## Appendix

### A.1 Supplementary information

#### A.1.1 Retention of cells in mono- and bi-layered f-gelatin printed constructs

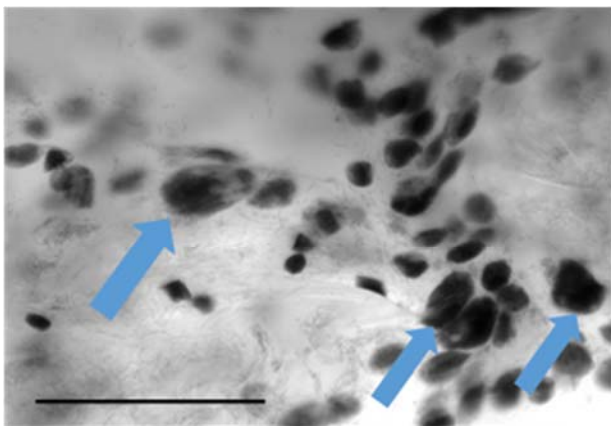


(A) Mouse MSC, pre-stained with PKH26 (red) showing viability when printed within monolayer sheets, after 5 days of culture.

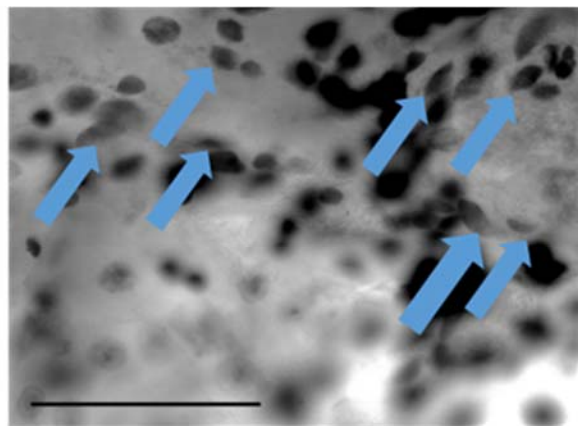


(B) Mouse MSC, pre-stained with PKH26 showing viability when printed within bilayer sheets (bottom layer), after 5 days of culture

#### A.1.2 Confocal microscopy to observe the cellular crosstalk between STO (bottom layer) and C2C12 (top layer) cells in the f-gelatin based bi-layered sheets



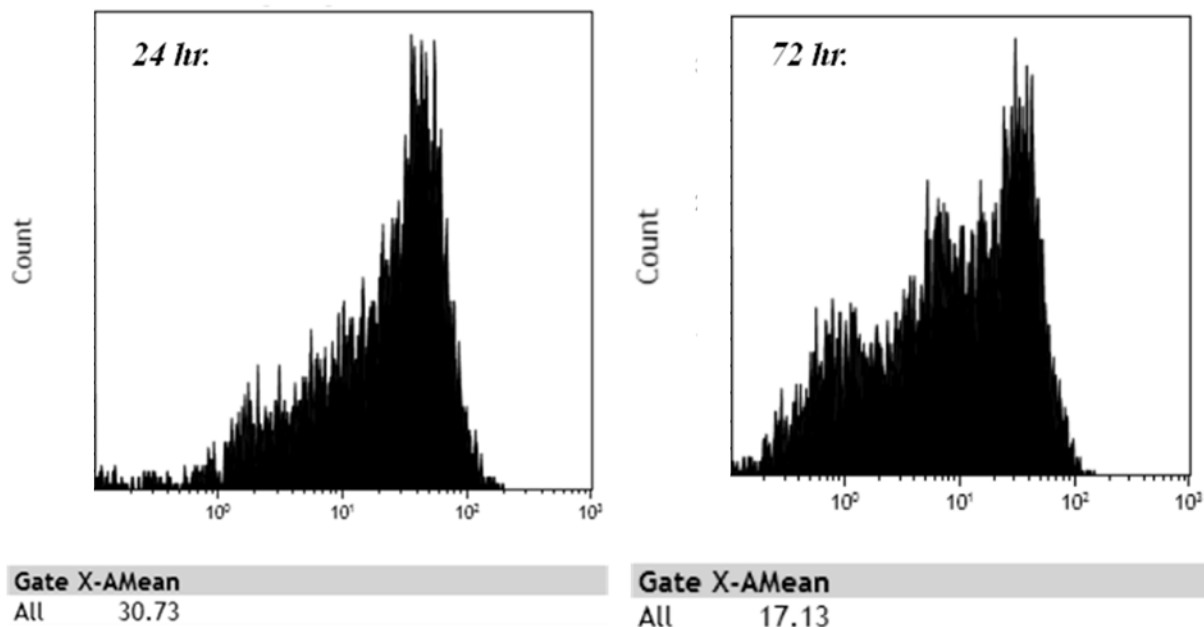
(A) C2C12 focused in this image plane



(B) STO focused in this image plane



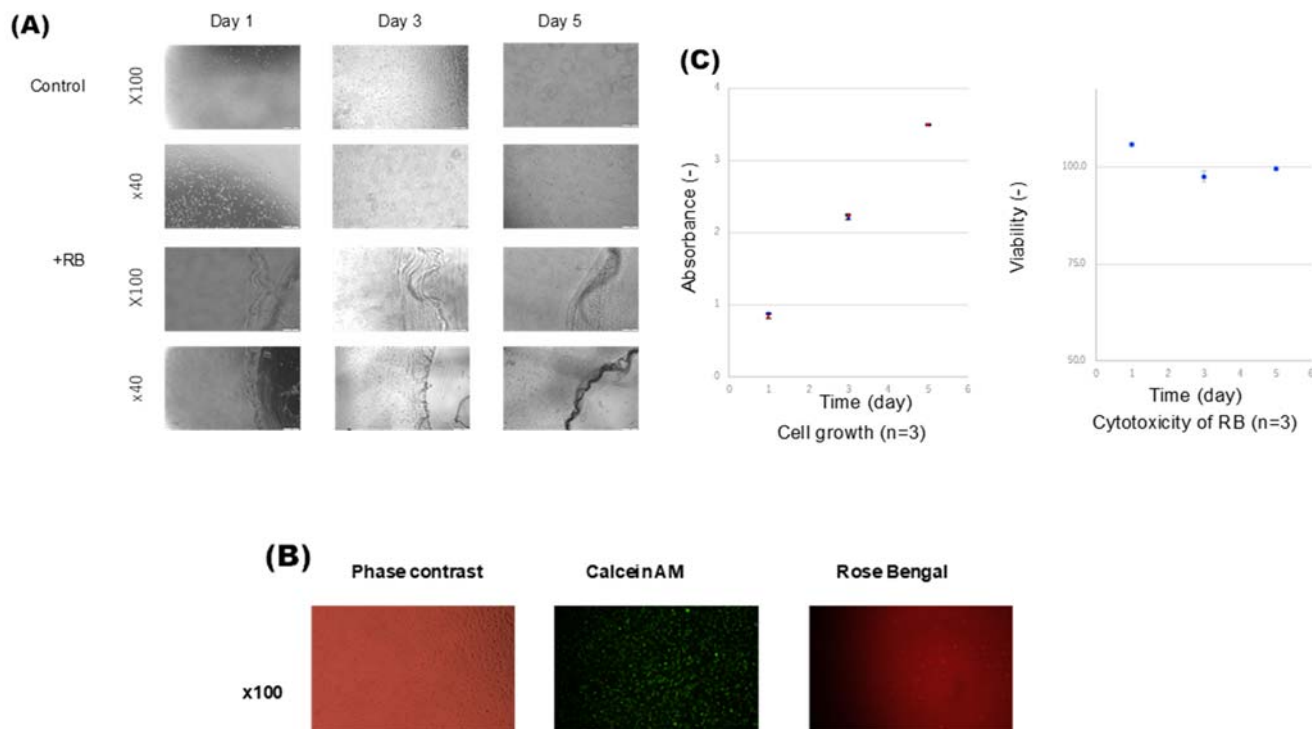
### A.1.3 FACS analysis on CTV stained cells culture on plastic for 24- and 72- hr



### A.1.4 Cytotoxicity Assessment of Rose Bengal

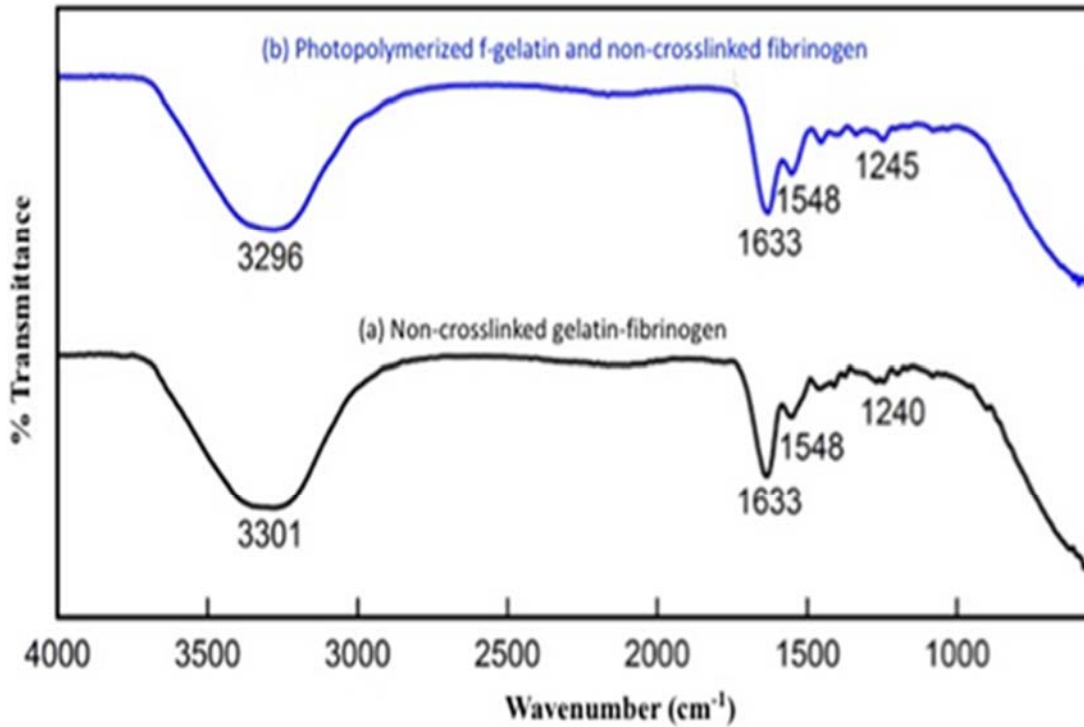
f-gelatin (10 wt %) and RB (0.5 wt %) was mixed together and a 50  $\mu$ l aliquot was drop-pipetted onto a 12-well cell culture plate (Iwaki, Tokyo, Japan). The droplets were exposed to visible light with a white light-emitting diode source (Luminar ace LA-HDF158A, Hayashi Watch Works, Tokyo, Japan) at a distance of 1 cm for 5 min. Crosslinked hydrogels were incubated in Dulbecco's modified phosphate buffered saline for 24 h at 37 °C, and then sterilized with UV light exposure. NIH/3T3 cells (mouse fibroblast) were cultured for this experiment and passaged using Dulbecco's modified Eagle's medium (DMEM) containing 5% fetal bovine serum (FBS) at 37 °C in a 5% CO<sub>2</sub> incubator. These cells ( $5.0 \times 10^4$  cells/well) were seeded in 12-well plate with or without the hydrogels. All samples were cultured for 5 days and their culture medium was replaced every other day. After 5 days, the cells were trypsinized using 0.25% Trypsin-EDTA cell number and their numbers determined by Cell Counting Kit-8 (Dojindo, Kumamoto, Japan) and reported

as percent viability. Absorbance assay of spent culture medium which correlated directly with cell growth was measured at 450 nm. Furthermore, bright field images of cells cultured with or without the hydrogels were tracked at varying time points. In addition, after 24 hr of culture, Calcein AM (Thermo Fisher Scientific, Waltham, MA, USA) was added to the cultured to visually confirm the presence of viable cells in hydrogels and in other samples. Images were acquired using a fluorescent microscope (Olympus, Tokyo, Japan).



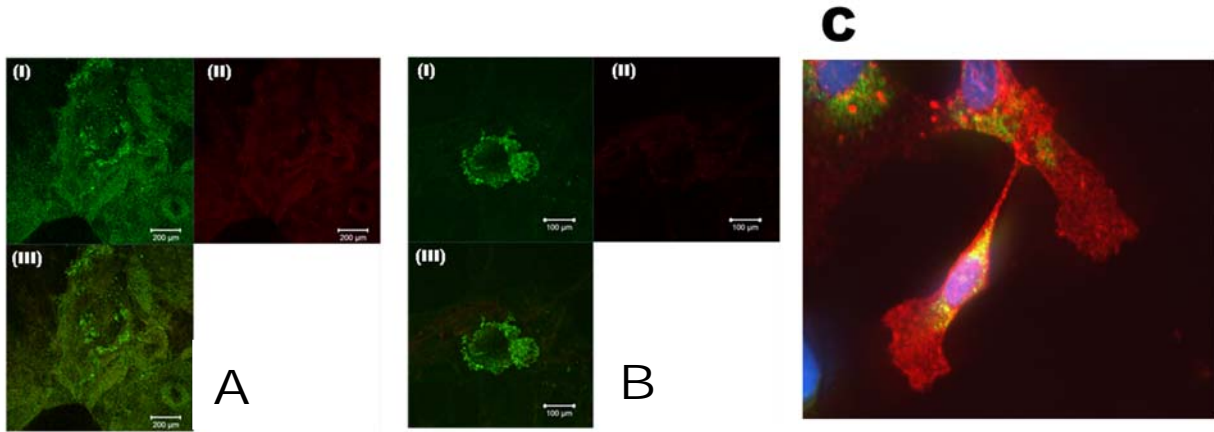
(A) Bright-field images of cells cultured in TCPS (Control) or in the presence of Rose Bengal (+RB) at days 1, 3 and 5. (B) Confirmation of cell viability after addition of Rose Bengal using (continued from the previous page) Calcein AM, which only stains for viable cells after 24 h of in vitro culture. (C) Absorbance assay conducted at days 1, 3 and 5 depict an increase in cell growth while viability was also maintained across samples at different time points..

### A.1.5 FTIR spectra for controls



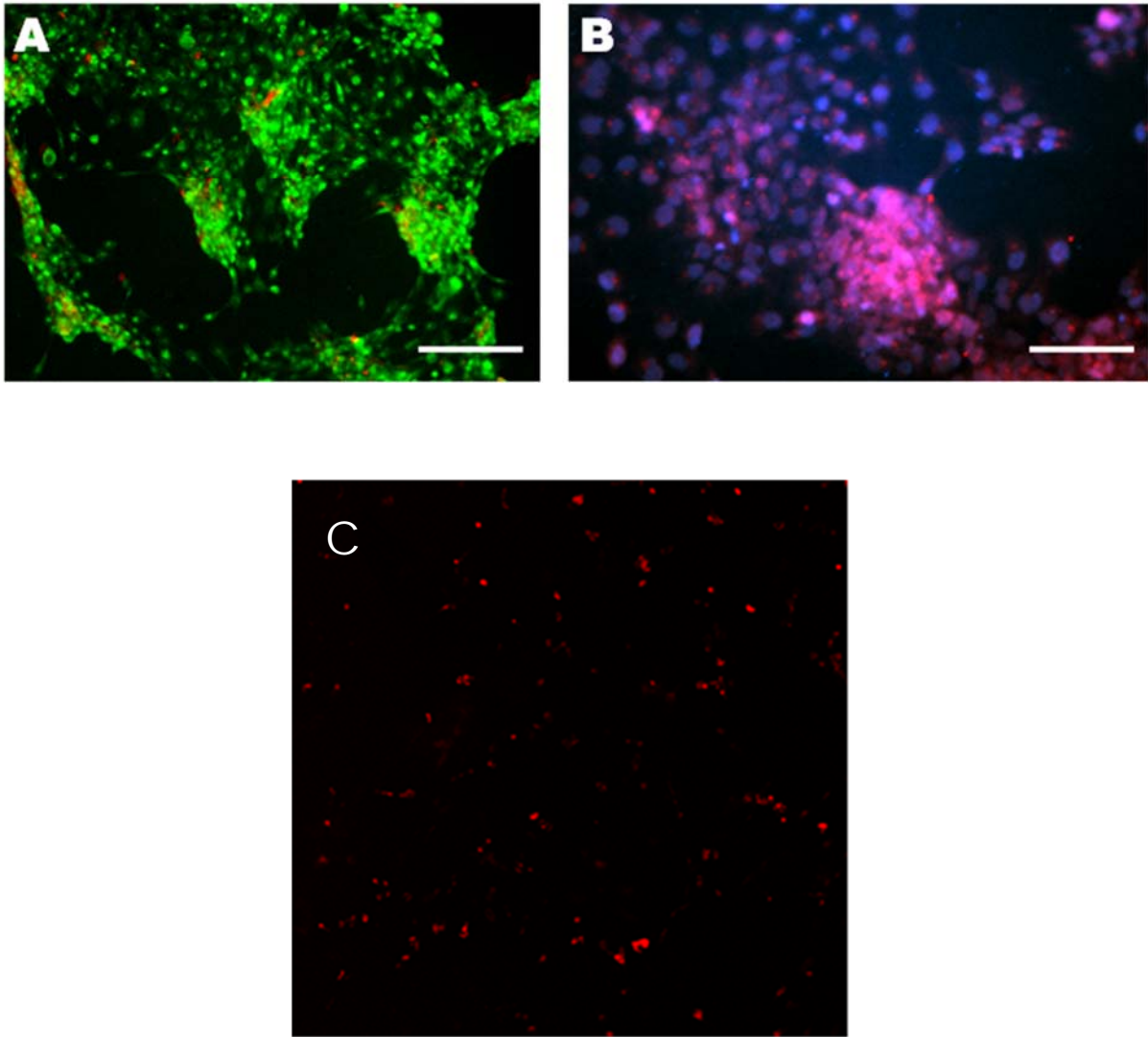
The spectra obtained from two controls, namely spectra (a) showing signatures for the non-cross-linked gelatin-fibrinogen composite and spectrum (b) showing only photopolymerization of the f-gelatin component have also been illustrated.

*A.1.6 Live/Dead and Troponin-T/DAPI staining of human iPS-CM bioprinted within fibrin-gelatin patterns*



(A) and (B) shows characteristic images of human iPS-CM that were bioprinted within fibrin-gelatin patterns and imaged after 24 h using Live/Dead assay. Calcein AM (live cell stain: green) and Ethidium homodimer (dead cell stain: red) was used to depict live cells retained within the bioprinted and crosslinked construct as shown in A and B- panels (I), and dead cells depicted in panels (II), respectively. Panels (III) in both A and B depict overlaid images for both live and dead cell stained samples. (C) Shown is a characteristic image of Troponin-T staining (red) which confirms the presence of cardiac myocytes responsible for sarcomere contraction. CX43 (green) and DAPI counterstain is depicted in blue. Scale bar is 100 μm.


*A.1.7 Live/Dead and Troponin I staining of human CM cell lines cultured in tissue culture wells and imaged as controls*



(A) and (B) shows characteristic Live/Dead and Troponin-I stained images of human CM cell lines, which were cultured in tissue culture wells and imaged after 5-days, as controls. Scale bar depicts 200  $\mu\text{m}$  in (A) and 100  $\mu\text{m}$  in (B). (C) Shows viable human CM (pre-stained using PKH26: red) imaged after 24 h of culture within non-printed fibrin-gelatin gels, manually casted and cross-linked. Scale bar depicts 200  $\mu\text{m}$ .

## A.2 Image permits

***A.2.1 All the images used in Chapter 4 have been adopted with permission from "The applicability of furfuryl-gelatin as a novel bioink for tissue engineering applications." Journal of Biomedical Materials Research Part B: Applied Biomaterials 107, no. 2 (2019): 314-323.***



**The applicability of furfuryl-gelatin as a novel bioink for tissue engineering applications**

Author: Shweta AnilKumar, Shane C. Allen, Nishat Tasnim, et al  
 Publication: JOURNAL OF BIOMEDICAL MATERIALS RESEARCH PART A  
 Publisher: John Wiley and Sons  
 Date: Apr 15, 2018

© 2018 Wiley Periodicals, Inc.

---

**Order Completed**

Thank you for your order.

This Agreement between Shweta Anil ("You") and John Wiley and Sons ("John Wiley and Sons") consists of your license details and the terms and conditions provided by John Wiley and Sons and Copyright Clearance Center.

Your confirmation email will contain your order number for future reference.

License Number 4722740236123 [Printable Details](#)

License date Dec 05, 2019

**Order Details**

Type of use	Dissertation/Thesis
Requestor type	Author of this Wiley article
Format	Print and electronic
Portion	Full article
Will you be translating?	No

**Licensed Content**

Licensed Content Publisher	John Wiley and Sons
Licensed Content Publication	JOURNAL OF BIOMEDICAL MATERIALS RESEARCH PART A
Licensed Content Title	The applicability of furfuryl-gelatin as a novel bioink for tissue engineering applications
Licensed Content Author	Shweta AnilKumar, Shane C. Allen, Nishat Tasnim, et al
Licensed Content Date	Apr 15, 2018
Licensed Content Volume	107
Licensed Content Issue	2
Licensed Content Pages	10

**About Your Work**

Title of your thesis / dissertation	Exploration and optimization of biomaterials and cells required for the fabrication of a "cardiac patch"
Expected completion date	Dec 2019
Expected size (number of pages)	140

**Requestor Location**

Requestor Location	Shweta Anil 2401 N Oregon St  EL PASO, TX 79902 United States Attrn: Shweta Anil
--------------------	---

**Tax Details**

Publisher Tax ID	EU826007151
------------------	-------------

**Price**

Total	0.00 USD
-------	----------

Would you like to purchase the full text of this article? If so, please continue on to the content ordering system located here: [Purchase PDF](#)  
 If you click on the buttons below or close this window, you will not be able to return to the content ordering system.

**Total: 0.00 USD**

***A.2.2 All the images used in Chapter 5 have been adopted with permission from "A Comparative Study of a 3D Bioprinted Gelatin-Based Lattice and Rectangular-Sheet Structures." Gels 4, no. 3 (2018): 73. (open source article).***

© 2018 by the authors. Licensee MDPI, Basel, Switzerland. This article is an open access article distributed under the terms and conditions of the Creative Commons Attribution (CC BY) license (<http://creativecommons.org/licenses/by/4.0/>).

***A.2.3 All images used in Chapter 6 have been adopted with permission from "A Visible Light-Cross-Linkable, Fibrin–Gelatin-Based Bioprinted Construct with Human Cardiomyocytes and Fibroblasts." ACS Biomaterials Science & Engineering 5, no. 9 (2019): 4551-4563.***

---

A Visible Light-Cross-Linkable, Fibrin–Gelatin-Based Bioprinted Construct with Human Cardiomyocytes and Fibroblasts

Author: Shweta Anil Kumar, Matthew Alonzo, Shane C. Allen, et al

Publication: ACS Biomaterials Science & Engineering

Publisher: American Chemical Society

Date: Sep 1, 2019

Copyright © 2019, American Chemical Society

---

**PERMISSION/LICENSE IS GRANTED FOR YOUR ORDER AT NO CHARGE**

This type of permission/license, instead of the standard Terms & Conditions, is sent to you because no fee is being charged for your order. Please note the following:

- Permission is granted for your request in both print and electronic formats, and translations.
- If figures and/or tables were requested, they may be adapted or used in part.
- Please print this page for your records and send a copy of it to your publisher/graduate school.
- Appropriate credit for the requested material should be given as follows: "Reprinted (adapted) with permission from (COMPLETE REFERENCE CITATION). Copyright (YEAR) American Chemical Society." Insert appropriate information in place of the capitalized words.
- One-time permission is granted only for the use specified in your request. No additional uses are granted (such as derivative works or other editions). For any other uses, please submit a new request.

[BACK](#) [CLOSE WINDOW](#)

---

## **Vita**

Shweta Anil Kumar was born on August 6, 1994 in Kerala, India to Mr Anil Kumar, an electrical engineer and Dr. Bindu G Nair, an obstetrician/gynecologist. She completed her high school in the United Arab Emirates, following which she joined the National Institute of Technology, Calicut in 2012. She graduated in 2016 with a Bachelor's degree in Chemical Engineering. The same year, she started her doctoral program in Materials Science and Engineering at the University of Texas at El Paso under the guidance of Dr Binata Joddar. Shweta worked as a Research Assistant throughout the course of her PhD during which she made numerous publications both as the lead and coauthor. She is also an active member of numerous student organizations such as the Society for Biomaterials, UTEP chapter and Alpha Chi. She was presented with the Graduate Research Award in 2018 for outstanding work in Materials Science Research. She also had the opportunity to work as a PhD intern at the Pacific Northwest National Laboratory (PNNL) for a duration of 8 months under the mentorship of Drs. Nancy Washton and Eric Walter.

Contact Information: [shweta.anilkumar@yahoo.com](mailto:shweta.anilkumar@yahoo.com)